

APPLICATION OF DIRECT TENSION TESTING TO FIELD SAMPLES TO  
INVESTIGATE THE EFFECTS OF HMA AGING

A Dissertation

by

JAMES JEFFERIES LAWRENCE

Submitted to the Office of Graduate Studies of  
Texas A&M University  
in partial fulfillment of the requirements for the degree of

DOCTOR OF PHILOSOPHY

Approved by:

Chair of Committee,	Amy Epps Martin
Committee Members,	Charles J. Glover
	Dallas N. Little
	Robert L. Lytton
Head of Department,	John Niedzwecki

December 2012

Major Subject: Civil Engineering

Copyright 2012 James Jefferies Lawrence

## ABSTRACT

There are many factors which contribute to fatigue failure in HMA. While studies have been made with respect to binder aging, little has been done to investigate the effect of aging on the fatigue failure of asphalt mixtures. The lack of an effective and efficient method of testing field samples has contributed to this deficiency. This study focused on the development of a method for preparing and testing field samples in direct tension. This methodology was then be employed in combination with the VEC and RDT\* tests to investigate several factors that affect fatigue in HMA. Particular emphasis was placed on the role of aging in the fatigue process.

A method of testing field samples in direct tension was successfully developed. Results from the VEC and RDT\* tests performed on several field samples collected from across the state of Texas were analyzed. US 277 field sample results were compared to laboratory mixed and compacted (LMLC) sample results as well as results obtained from extracted binder testing. Findings show that oxidative aging has an impact on the stiffness and performance of HMA. Chip seal surface treatments can extend the life of the pavement, but their affects are found primarily at the surface.

Two additional field sites were tested, analyzed, and compared to LMLC results. These comparisons verified the effects of aging and show that a relationship between LMLC samples and field samples can be developed. Modulus values for one month of artificial aging of LMLC samples is equivalent to 10.5 months of aging in the field.

Finally, 21 Texas sites used for the study were analyzed and a multivariate linear regression was performed to determine the factors that play the most significant role in the aging process. A linear regression model was constructed to determine the number of loads to failure from fatigue cracking due, primarily, to aging.

## DEDICATION

This dissertation is dedicated first to my lovely wife, Melinda, who continued to encourage me to press forward, even though there were many days I wanted to quit. She found hope where I thought there was none to be had.

Second, to my boys, Isaac, David, and Joshua, who put up with "Angry Dad" far too many times while I worked through many challenges and frustrations. Their laughter and happiness always brought me back to earth. They kept me focused on the most important aspects of life. They are the lights in my life that lift my soul and make many of my burdens easy to bear.

Finally, to Michael. I'll never give up and will greet you some day knowing that I did everything I could to live my life to the fullest.

## ACKNOWLEDGEMENTS

I would first like to thank my advisor, Dr. Amy Epps Martin for sticking with me throughout this process. Her guidance and encouragement has helped me to keep going. She gave me the freedom to go in the direction I needed to, but was always there when I got stuck and needed the extra help.

Also, thanks to my committee, Dr. Charles Glover, Dr. Dallas Little, and Dr. Robert Lytton. They have been so accommodating, especially during the last couple of months of my work when my life and schedule got a little bit crazy. They have been supportive and encouraging.

I wouldn't be where I'm at if it weren't for the tremendous help from Jeff Perry and David Zeig. Their assistance, expertise, and knowledge of laboratory and testing procedures help me to keep on schedule and to solve many of the problems that inevitably arose during the process.

I also need to thank the many undergraduate and graduate students who helped to fabricate samples, collect data, and perform tests. Their contributions were ginormous!

Also, thanks to TxDOT and TTI for funding and supporting an exciting project. Without the funding, there would be no research.

Of course, I wouldn't be here without the love and support of my family. My wife, Melinda, and my sons, Isaac, David, and Joshua, have been helpful and supportive. They have been understanding during the long days and late nights when I had to be in

the office or was unavailable. They have always been there for me and have made home a safe place to land so that I could have some respite from the stress.

Finally, and most especially, I want to thank my Heavenly Father. He has heard my cries and answered my prayers. He has touched the stones I have forged and made them something I could not. His touch provided the light for a dark voyage across a wide ocean.

## TABLE OF CONTENTS

	Page
ABSTRACT .....	ii
DEDICATION .....	iv
ACKNOWLEDGEMENTS .....	v
TABLE OF CONTENTS .....	vii
LIST OF FIGURES.....	ix
LIST OF TABLES .....	xi
CHAPTER I INTRODUCTION .....	1
Fatigue Testing Background .....	2
Direct Tension Testing of LMLC Samples .....	4
Viscoelastic Characterization (VEC) Test .....	4
Modified Repeated Direct Tension (RDT*) Test.....	7
Motivation and Objectives .....	10
Outline.....	12
CHAPTER II DIRECT TENSION TESTING OF HOT MIX ASPHALT FIELD SAMPLES .....	14
Direct Tension Testing of Field Samples .....	14
Field Sample Selection .....	15
Sample Configuration and Preparation .....	17
Machine Modifications.....	20
Test Modifications.....	21
Analysis Modifications.....	22
Results .....	23
Summary .....	27
CHAPTER III INVESTIGATION OF AGING EFFECTS AT A SINGLE FIELD SITE USING DIRECT TENSION TESTING .....	29
Materials.....	30
Testing Methodology .....	31

	Page
Sample Preparation.....	31
HMA Mixture Testing.....	36
Binder Testing.....	39
Test Results.....	39
Extracted Binder Test Results.....	40
Field Sample Test Results.....	46
LMLC Sample Test Results.....	49
Comparison of Test Results.....	52
Summary.....	58
 CHAPTER IV COMPARISON OF AGING IN THE FIELD WITH ACCELERATED LABORATORY AGING.....	  60
Materials and Testing.....	60
Site Selection.....	61
LMLC Sample Preparation.....	62
Field Sample Preparation.....	63
Testing Procedures.....	65
LMLC Sample Test Results.....	67
Field Sample Test Results.....	69
Comparison of Field and LMLC Sample Results.....	74
Summary.....	77
 CHAPTER V INVESTIGATION OF FACTORS AFFECTING AGING OVER MULTIPLE FIELD SITES.....	  78
Material Selection.....	79
Multivariate Linear Regression Factors.....	81
Multivariate Linear Regressions.....	82
Combined Location Linear Regression.....	83
Wheel Path Linear Regression.....	85
Shoulder Linear Regression.....	87
Summary.....	90
 CHAPTER VI CONCLUSIONS.....	 92
 REFERENCES.....	 97
 APPENDIX A FIELD SITE INFORMATION.....	 101
 APPENDIX B STATISTICAL ANALYSIS DATA.....	 104



## LIST OF FIGURES

	Page
FIGURE 1 Strain response and stress input from the RDT* Test .....	9
FIGURE 2 Sample trimming procedures with ends (a) untrimmed and (b) trimmed.....	18
FIGURE 3 Vertical gluing jig (a) and horizontal magnetic gluing vice with three inch wide sample (b). .....	19
FIGURE 4 Three inch wide sample attached to ball and socket joint shown with movable base plate. ....	21
FIGURE 5 Vertical gluing jig (a) and test setup (b) for LMLC samples.....	34
FIGURE 6 Field sample testing configuration.....	35
FIGURE 7 Magnetic gluing vice for field samples.....	35
FIGURE 8 Field sample test setup with ball and socket joint at base. ....	37
FIGURE 9 CA of LMLC samples at optimum binder content. ....	41
FIGURE 10 CA of LMLC samples at medium AV.....	42
FIGURE 11 CA value with depth and years for US-277 shoulder. ....	43
FIGURE 12 CA value with depth and years for US-277 wheel path. ....	43
FIGURE 13 Average combined CA for all sections of US-277. ....	46
FIGURE 14 $E_{ve}$ for US 277 field samples.....	47
FIGURE 15 $N_f$ for US 277 field samples. ....	48
FIGURE 16 $E_{ve}$ for LMLC samples at differing AV. ....	50
FIGURE 17 $E_{ve}$ for LMLC samples at differing binder contents.....	51
FIGURE 18 Number of loads to fatigue failure for LMLC samples with medium AV and optimum binder content.....	52
FIGURE 19 Laboratory to field $E_{ve}$ comparison.....	54

	Page
FIGURE 20 $E_{ve}$ vs. CA for LMLC samples with different AV and increasing age. ....	55
FIGURE 21 $E_{ve}$ vs. CA for LMLC samples with different binder contents and increasing age. ....	56
FIGURE 22 $E_{ve}$ vs. CA of field samples for US 277 between 2008 and 2011. ....	58
FIGURE 23 Test setup for (a) LMLC and (b) field samples. ....	65
FIGURE 24 $E_{ve}$ trends for artificially laboratory aged LMLC samples. ....	68
FIGURE 25 $N_f$ trends for artificially laboratory aged LMLC samples. ....	69
FIGURE 26 $E_{ve}$ for field samples taken from the wheel path. ....	70
FIGURE 27 $E_{ve}$ for field samples taken from the shoulder. ....	72
FIGURE 28 $N_f$ for field samples taken from the wheel path. ....	73
FIGURE 29 $N_f$ for field samples taken from the shoulder. ....	74
FIGURE 30 LMLC and field sample combined $E_{ve}$ results. ....	76
FIGURE 31 LMLC and field sample combined $N_f$ results. ....	76

## LIST OF TABLES

	Page
TABLE 1 Field Sample Characteristics .....	16
TABLE 2 Field Sample VEC and RDT* Test Results .....	25
TABLE 3 D-Optimal Statistical Design for LMLC Samples .....	32
TABLE 4 Binder Content and Air Voids for US 277 Samples .....	33
TABLE 5 Field Sample Collection Sites .....	80
TABLE 6 Correlation Matrix for All Data.....	84
TABLE 7 Correlation Matrix for WP Data.....	86
TABLE 8 Correlation Matrix for SH Data.....	88

# CHAPTER I

## INTRODUCTION

In 1912 Carl G. Fisher developed the idea for the Coast to Coast Rock Highway, which would later become the Lincoln Highway. The Lincoln Highway was the first road in the United States to stretch from the Atlantic coast to the Pacific Coast. It would eventually connect New York City to San Francisco, California (1). One hundred years later, there are over 16,500 miles of Interstate highways across the United States (2). During a time when so much emphasis is placed on the deteriorating transportation system, it is important to remember the incredible progress that has been made in the past century. The future of transportation will be as bright as the past as new and improved methods of designing, constructing, and testing roads are developed.

This chapter includes a review of the background surrounding current methods of fatigue testing for hot mix asphalt (HMA) and some of their strengths and weaknesses. Two new tests developed at Texas A&M and used for direct tension testing are also described. These two tests will be used for calculating several values associated with fatigue in HMA. A brief discussion on the background of binder and mixture aging and their association with fatigue cracking follows along with a description of the need for this study. Finally, an outline of the dissertation is given, describing the contents of each of the following chapters.

## **Fatigue Testing Background**

Material testing to predict fatigue cracking is one area that has received, and continues to receive, a great deal of attention. Pavement design, construction, maintenance, and reconstruction can be improved by successfully predicting fatigue failure in HMA pavements. Over the years, several testing methods have been developed to determine the tensile properties of HMA, including diametral, simple and supported flexure, direct axial, triaxial, and wheel-track type tests (3). Each one comes with its own set of strengths and weaknesses.

The Indirect Tension (IDT) test has been one of the more commonly used and studied tests. This test is performed by applying a compressive load to the side of a disk shaped sample, causing the sample to fail in tension along the center axis. The IDT is simple to perform (3, 4). However, this test determines the material and fracture properties using a biaxial state of stress, has shown to provide lower fatigue lives than other testing methods, and is not a good representation of the stresses experienced in the field (3-8). Some of this reduction may be the result of permanent deformation occurring under the loading strips applied to the sample during testing (4, 5, 8).

The Flexural Bending (FB) test indirectly determines fatigue properties by loading a prismatic sample at the third points of its length, causing the sample to bend. This causes tension in the bottom of the sample. Material properties can then be calculated and the fatigue life determined. While this test is a good representation of material behavior in the field (3), samples are more difficult to obtain and conventional testing time is extensive (9).

The Semicircular Bending (SCB) Test is a relatively new test that is gaining momentum and popularity. Semicircular disks are taken from cores and tested by supporting the flat edge at two points at a specific spacing and applying a compressive load at the top of the arch. Samples are easy to obtain and the test is simple to perform, but requires indirect calculation of the tensile properties of the material (5). Permanent deformation under the load may also occur, which can change the stress distribution, but it's much less than that experienced in the IDT test (4, 5).

Other tests, like the Overlay Tester (10) and Fenix Test (11), have recently been used to determine HMA fatigue and tensile material properties, but these tests are early in development and require further investigation.

Direct tension testing has also been successfully applied to laboratory mixed, laboratory compacted (LMLC) samples. These tests measure material behavior in the sample where uniform stresses occur (3). They also make testing and analysis simpler, quicker, and less expensive than other methods (3). However, it has been suggested that field samples are too thin to be practically tested using this type of test (12).

This study found that direct tension testing of field samples is not only possible, but can also provide accurate and timely results. It investigates the successful application of two new direct tension testing methods to field samples. The Viscoelastic Characterization (VEC) test and the Modified Repeated Direct Tension (RDT\*) test were initially developed for application to LMLC samples. Through this study, modifications to the sample preparation, test setup, testing procedures, and analysis methodology were made and reported. Several samples from various sites throughout

Texas were tested, and the results reported indicate that these direct tension tests can be successfully applied to field samples in order to determine material properties associated with fatigue cracking.

### **Direct Tension Testing of LMLC Samples**

Common fatigue analysis methods use material properties such as the stiffness modulus, complex modulus, and phase angle to determine the number of loads to failure for a HMA pavement (12). Two new direct tension tests have been developed which can be used to calculate some of these important material properties.

#### *Viscoelastic Characterization (VEC) Test*

The VEC test was developed at Texas A&M University for determining the relaxation modulus and complex modulus of LMLC samples (13). This new test method efficiently models the viscoelastic characteristics of HMA without causing damage to the sample. Time dependent stress and strain determined from this test are used to calculate the relaxation modulus master curve and the relaxation rate. Using Laplace transforms, the data can also be used to calculate the complex modulus master curve (13).

The VEC test is performed by applying a monotonically increasing load to a 4 inch (101.6 mm) diameter by 4 inch (101.6 mm) high sample at a machine displacement rate of 0.01 inches per minute (0.254 mm/min.). The time of loading was controlled by monitoring three vertical linear variable differential transformers (LVDTs) placed equidistant around the sample. These LVDTs were monitored so that the strain

experienced by the sample did not exceed 100  $\mu\epsilon$ . It was assumed that under such a low strain level, the sample was undamaged and could be retested after allowing for recovery (13). The test was performed at 10°C (50°F), 20°C (68°F), and 30°C (86°F) with a 2 to 3 hour temperature conditioning period between temperatures. Resulting stress and strain data at each temperature is averaged and fit with the following time dependent functions for stresses and strains, respectively (13):

$$\sigma(t) = a_{\sigma}(1 - e^{-b_{\sigma}t}) \quad (1)$$

$$\epsilon(t) = a_{\epsilon}(1 - e^{-b_{\epsilon}t}) \quad (2)$$

where:

$\sigma(t)$  = time-dependent stress

$\epsilon(t)$  = time-dependent strain

$t$  = time

$e$  = the base of the natural logarithm

$a_{\sigma}$   $b_{\sigma}$   $a_{\epsilon}$   $b_{\epsilon}$  = fitting parameters

Using the calculated fitting parameters, the Laplace transforms of the stress and strain can be determined as:



$$\bar{\sigma}(s) = \frac{(a_{\sigma} b_{\sigma})}{s(s+b_{\varepsilon})} \quad (3)$$

$$\bar{\varepsilon}(s) = \frac{(a_{\varepsilon} b_{\varepsilon})}{s(s+b_{\varepsilon})} \quad (4)$$

where:

$s$  = Laplace transform variable.

Using equations 3 and 4, the relaxation modulus,  $E(t)$ , and complex modulus,  $E^*(\omega)$ , can then be determined as:

$$E(t) = \mathcal{L}^{-1} \left\{ \frac{\bar{\sigma}(s)}{s \times \bar{\varepsilon}(s)} \right\} = \frac{a_{\sigma}}{a_{\varepsilon}} \left( 1 + \frac{b_{\sigma} - b_{\varepsilon}}{b_{\varepsilon}} e^{-b_{\varepsilon} t} \right) \quad (5)$$

$$E^*(\omega) = i\omega \mathcal{L} \{ E(t) \}_{s=i\omega} = i\omega \left\{ \frac{\bar{\sigma}(s)}{s \bar{\varepsilon}(s)} \right\}_{s=i\omega} = \frac{a_{\sigma} b_{\sigma} (\omega^2 + b_{\varepsilon} b_{\sigma})}{a_{\varepsilon} b_{\varepsilon} (\omega^2 + b_{\sigma}^2)} + \frac{a_{\sigma} b_{\sigma} \omega (b_{\sigma} - b_{\varepsilon})}{a_{\varepsilon} b_{\varepsilon} (\omega^2 + b_{\sigma}^2)} i \quad (6)$$

where:

$\omega$  = Loading frequency

Luo and Lytton (2010) provide a more detailed description of the calculations involved (13). They have shown that the VEC test can be used for accurate and efficient

development of the relaxation modulus and complex modulus master curves (13). A sample can be tested at all three temperatures within 7 hours (13). If analysis of the collected data is automated, the entire process, including development of the master curves can be completed within one day (14). The VEC test also uses direct tension as opposed to traditional indirect tension tests, which may not accurately characterize the tensile properties of the material. Finally, the VEC test keeps the strain limit below 100  $\mu\epsilon$  which is assumed to be undamaging, allowing for further testing of the sample.

#### *Modified Repeated Direct Tension (RDT\*) Test*

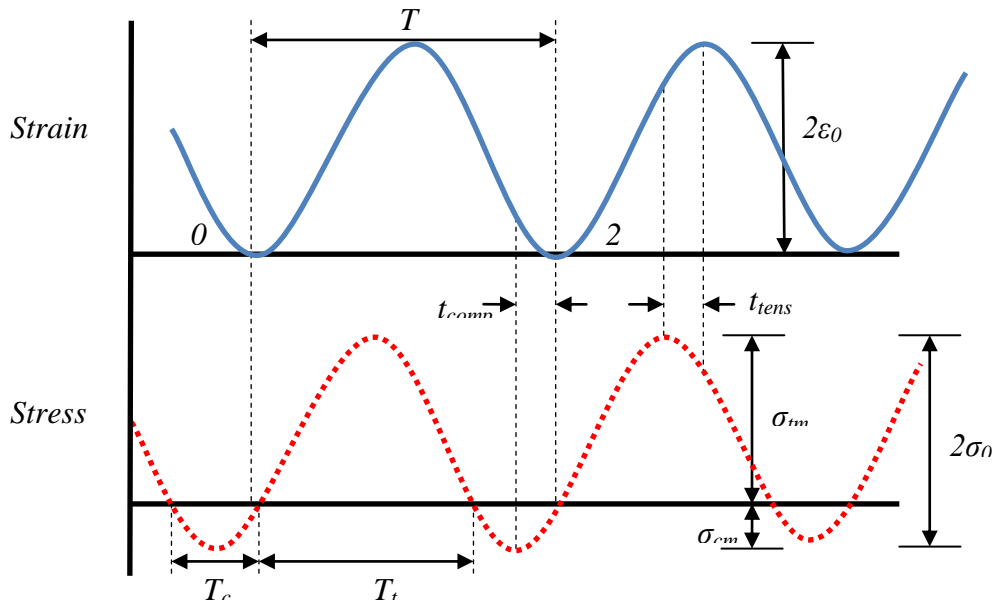
While the VEC test determines some of the undamaged properties of the material, it can be followed by the RDT\* test in order to verify the undamaged properties and determine the cumulative damaged properties of a mixture. The RDT\* test was also developed at Texas A&M in order to determine undamaged and damaged properties of LMLC samples (15). The resulting data could then be used to determine important properties such as Paris' fracture coefficient and exponent, the rate of crack growth and damage accumulation, and ultimately, the number of loads to fatigue failure (15).

The undamaged portion of the test was used in order to verify and validate the results of both the VEC and RDT\* tests for determining the undamaged properties of a mixture. While the undamaged portion of the test is described in the following paragraphs, Luo et al. (2008) provide a detailed description of the calculations used for determining the damaged mixture properties (15).

Determination of the undamaged properties of the mixture requires that a sample of the same dimensions as that used in the VEC test be preconditioned at a temperature of 20°C (68°F). The test is run in displacement control mode with load and deformation data collected every 0.005 seconds. The sample is exposed to a haversine loading with a maximum vertical strain level of 80  $\mu\epsilon$  for 500 cycles at a frequency of 1 Hz (6.28 radians/sec.). For 2 inch (51 mm) LVDT gauge length, 80  $\mu\epsilon$  is a change in LVDT length of approximately 0.00016 inches (0.004064 mm). No rest period is given between cycles. This portion of the test can be used to calculate the undamaged viscoelastic phase angle and the dynamic modulus of the material at a 1 Hz (6.28 radians/sec.) frequency. At the completion of the 500 cycles at 80  $\mu\epsilon$ , a 1000 cycle haversine loading is applied at a frequency of 1 Hz (6.28 radians/sec.) with a maximum strain level of 350  $\mu\epsilon$ . For 2 inch (51 mm) gauge length, 350  $\mu\epsilon$  is a change in LVDT length of approximately 0.0007 inches (0.01778 mm). Though visible cracks may not be apparent, at the completion of the test the sample is damaged and cannot be retested (15).

The RDT\* method, as developed by Luo et al. (15), separates the tension and compression components of the test and calculates their related material properties separately. In order to understand some of the variables used in the calculations, it is helpful to show an illustration of the stress response and strain input produced by the test. In FIGURE 1,  $T$  represents the period of the strain wave with a cycle of  $2\pi$  radians (360°).  $T_c$  is the portion of the stress period corresponding to compressive stresses being applied to the sample.  $T_t$  represents the portion of the stress period corresponding to tensile stress application. In viscoelastic materials the strain lags behind the stress. Also

the material responds differently when in tension than it does in compression (15). To account for these differences in response, the variables  $t_{tens}$  and  $t_{comp}$  (with corresponding lag angles of  $\varphi_t$  and  $\varphi_c$ , respectively) are used to represent the tensile and compressive lag times, respectively.  $\sigma_{tm}$  is the maximum tensile stress, while  $\sigma_{cm}$  is the maximum compressive stress applied to the sample for each phase. The amplitudes of the input and response waves are identified by  $\sigma_0$  and  $\varepsilon_0$ , respectively (15).



**FIGURE 1 Strain response and stress input from the RDT\* Test. Adapted from Luo et al. (15).**

The tensile phase angle,  $\varphi_t$ , in degrees, is calculated using equation 7 while the dynamic tensile modulus,  $E_{ve}$ , is calculated from equation 8 (15).

$$\varphi_t = \frac{2\pi t_{tens}}{T} \quad (7)$$

$$E_{ve} = \frac{\sigma_{0t}}{\varepsilon_0} \quad (8)$$

where,

$\sigma_{0t}$  = Amplitude of the tensile stress calculated using  $\sigma_{tm}$  and  $T_t$

Once the VEC and RDT\* test methods are validated, the damaged portion of the RDT\* test can then be used with the results of the undamaged VEC and RDT\* test results to calculate the number of loads to failure in fatigue ( $N_f$ ).

### **Motivation and Objectives**

Cracking failure of hot mix asphalt (HMA) due to fatigue by repetitive traffic loading has long been an important issue that affects the long-term performance of pavement systems. Understanding the material properties and environmental factors that affect fatigue cracking is an important part of understanding and predicting this mode of failure. While many of the past performance prediction models have been empirically based, concerted efforts have been underway to better predict this phenomenon using more mechanistic methodologies. At Texas A&M University, uniaxial, repeated load tests (VEC and RDT\* tests) and an associated analysis system were developed as the Modified Calibrated Mechanistic with Surface Energy (CMSE\*) method. Other models,

such as the Viscoelastic Continuum Damage (VECD) model, have also been developed. These models use measured mixture properties such as the relaxation and dynamic modulus, phase angle, and the rate of damage accumulation along with other damage properties to determine  $N_f$  for HMA (7, 15-18). The CMSE\* method also includes surface energies associated with binders and aggregates, Paris' Law fracture parameters, and calculated shift factors which incorporate the effects of mixture anisotropy, healing, and simplified aging using a multiplicative factor based on changes in binder properties (16, 19). While this effort to include aging as a shift factor is a step in the right direction, it is still empirical in nature. In order to move toward a more mechanistic method of quantification for HMA, aging needs to be better understood and further investigated.

While HMA mixture aging is not well quantified (20, 21), considerable effort has been made to characterize aging in neat binders. Tools, such as Fourier Transform Infrared Spectroscopy (FTIR) and the Dynamic Shear Rheometer (DSR), have been used to investigate changes in binder viscosity and its correlation with binder oxidation in the laboratory (22-24). Binders have been extracted from existing field pavements in order to examine the binder aging process and some of the factors which affect it (20, 21). But binder aging alone cannot be used to draw a complete picture of the effects of binder oxidation on fatigue in HMA mixtures. It is important to investigate binder properties in combination with the mixture properties determined from effective laboratory testing to better characterize the effect of aging on HMA performance.

This study focuses on the development of a method for preparing and testing field samples in direct tension. This methodology was then employed in combination

with the VEC and RDT\* tests to investigate several factors that may affect fatigue in HMA. Particular emphasis is placed on the role of aging in the fatigue process.

### **Outline**

In this dissertation, several chapters are used to describe the background, research, and findings associated with this study.

Chapter I included a summary of the literature associated with fatigue testing methods used previously as well as those to be used in this study. The background associated with binder and HMA aging was discussed along with the motivation for this study.

Chapter II discusses the application of direct tension testing to LMLC and field samples. A detailed description of the modifications necessary for successful direct tension field sample testing is discussed along with results which support the new methodology.

Chapter III takes the test procedures from Chapter II and applies them to one particular site in Texas. LMLC and field samples are tested and compared. Binder from corresponding field cores is extracted and tested. These results are also compared to the field sample test results. All comparisons are used to identify relationships between binder aging, LMLC sample aging, and HMA aging in the field.

Chapter IV expands upon Chapter III by examining the relationship between samples taken from three different Texas field sites and their corresponding laboratory artificially aged LMLC samples. Field samples were collected annually over four years.

All samples were tested using the VEC and RDT\* tests and the results analyzed. A comparison of  $E_{ve}$  and  $N_f$  between LMLC samples and field samples is made.

Chapter V is a statistical analysis of the factors that are influential in the aging process using stepwise linear regressions on the data collected from tests performed on over 200 field samples collected from throughout the state of Texas. Significant factors with combined two way effects are identified and a linear regression model for the calculation of age influenced  $N_f$  is provided.

Chapter VI discusses the findings and conclusions reached through this study.



## CHAPTER II

### DIRECT TENSION TESTING OF HOT MIX ASPHALT FIELD SAMPLES

A comparison can be made to validate the VEC and RDT\* tests by testing the same sample using both tests. The complex modulus at a frequency of 1 Hz (6.28 radians/sec.) can be pulled from the 20°C (68°F) master curve developed from VEC test data and compared with the dynamic modulus from the RDT\* test. If the two moduli are similar, then the tests were successful and can be confidently used to determine the undamaged properties of a mixture.

#### **Direct Tension Testing of Field Samples**

The RDT\* and VEC tests were originally designed for testing LMLC samples. It's much more of a challenge to test field samples and correctly characterize and compare the material properties. Field samples vary from site to site with respect to layer thickness, air voids, binder type, and aggregate type, among other factors. Even samples taken from the same site have variations from sample to sample. However, if these tests can be successfully applied to field samples, a comparison can be made between the VEC and RDT\* tests, validating the tests as viable options for direct tension testing of field samples. To make this possible, changes to the sample configuration had to be made in order to test the HMA layer of interest in the direct way that it experiences tension in the field. In addition, several modifications had to be made to the VEC and RDT\* test setup,

procedures, and analysis. Various field sites were selected in order to determine the factors that have the greatest impact on differences between VEC and RDT\* test results.

### *Field Sample Selection*

Seven field sites throughout Texas were selected from which to take samples for this study. Each site was selected based on differing factors such as sample thickness, composition, and climate. Sample thicknesses range from 1.5 inches (38.1 mm) to 3 inches (76.2 mm). Climates were selected based on geographical regions throughout Texas and include dry-warm (DW), dry-cold (DC), wet-warm (WW), and wet-cold (WC). For six of the seven sites, four cores were taken from each site with two cores from the wheel path (WP) and two cores from the shoulder (SH). For the remaining site, only cores from the shoulder were collected. The defining characteristics of each site are shown in TABLE 1.

Texas Department of Transportation (TxDOT) mixtures Type C and Type D can be found in TxDOT Standard Specification 340 while the CMHB-F mixture is found in TxDOT Standard Specification 344 (25). The 25 mm SFHMAC mixture was a special TxDOT specification, SS3248, prepared for perpetual pavement sections.

**TABLE 1 Field Sample Characteristics**

Route Name	Construction Year	Climate <sup>1</sup>	Mixture Type	Aggregate	Binder	Sample Size (in)	WP/ SH <sup>2</sup>	Air Voids (%)
Interstate Highway 20	2001	WC	12 mm SP <sup>3</sup>	Sandstone	PG 76-22	1.5	WP	9.6
							SH	8.8
Interstate Highway 35	2007	DW	25 mm SFHMAC <sup>4</sup>	Traprock/ River Gravel	PG 76-22	3	WP	10.1
							SH	11.1
US Route 277	2008	DW	TxDOT Type C	Limestone	PG 70-22	2	WP	14.1
							SH	7.4
US Route 82	2008	DC	CMHB-F <sup>5</sup>	Limestone	PG 70-28	1.5	WP	7.2
							SH	7.2
US Route 83	2008	DC	TxDOT Type D	Granite	PG 70-28	1.5	WP	8.6
							SH	10.1
State Highway 36	2006	WW	TxDOT Type D	Limestone	PG 64-22	1.5	WP	5.8
							SH	9.8
Farm to Market 2994	2002	DW	TxDOT Type D	River Gravel	PG 70-22	2	WP	9.1
							SH	11.0
State Highway 36	2006	WW	TxDOT Type D	Limestone	PG 64-22	1.5	WP	4.1
							SH	3.0
Farm to Market 2994	2002	DW	TxDOT Type D	River Gravel	PG 70-22	2	WP	5.3
							SH	6.8
Farm to Market 2994	2002	DW	TxDOT Type D	River Gravel	PG 70-22	2	WP	6.6
							SH	5.6
Farm to Market 2994	2002	DW	TxDOT Type D	River Gravel	PG 70-22	2	WP	8.3
							SH	8.1

<sup>1</sup> WC = Wet Cold, DW = Dry Warm, DC = Dry Cold, WW = Wet Warm

<sup>2</sup> WP = Wheel Path, SH = Shoulder

<sup>3</sup> 12 mm Superpave mix

<sup>4</sup> TxDOT Stone Filled Hot Mix Asphalt Concrete

<sup>5</sup> TxDOT Type F Course Mix-High Binder Mixture

### *Sample Configuration and Preparation*

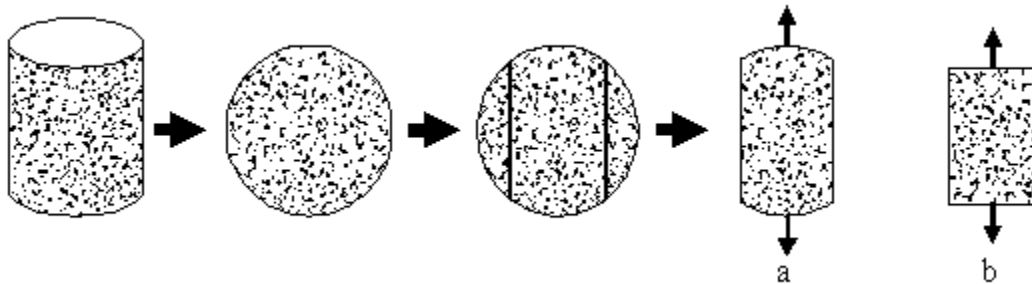
The cylindrical shape used to test LMLC samples for the VEC and RDT\* tests was not conducive to testing field samples. A new sample shape as well as a procedure for gluing the samples to the test platens had to be developed for the testing of field samples.

#### **Sample Cutting**

Testing field samples in direct tension requires some modifications to the samples taken from the field. Cores in their original configuration do not lend themselves to direct tension testing in the direction of interest. In order to facilitate this type of testing on field materials collected as cores, they must be trimmed and oriented so that the layer in question can be pulled in the direction for which the tensile properties of the material are sought. In order to determine the tensile properties associated with fatigue failure, collected cores are trimmed to leave only the layer of interest. The resulting circular disk of thickness varying from 1.5” to 3” is trimmed into a rectangular shape. Preliminary attempts were made to test the samples without trimming the ends of the sample as shown in FIGURE 2(a). However, this proved to be problematic. If the initial lengthwise cuts were not well centered, platens glued to the sample for testing would not align properly causing unwanted moments and occasional failure at the sample/platen interface. In order to address these issues, the rounded ends were removed and the rectangular shape shown in FIGURE 2(b) was adopted.

Fatigue failure is most often associated with longitudinal cracking which runs parallel to the direction of traffic; therefore the length of the prism runs perpendicular to

the traffic direction. For a 6” diameter core, this results in a prism with a length of approximately 4” and a width of 3” as shown in FIGURE 2(b). The depth of the prism is dependent on the thickness of the layer under investigation.

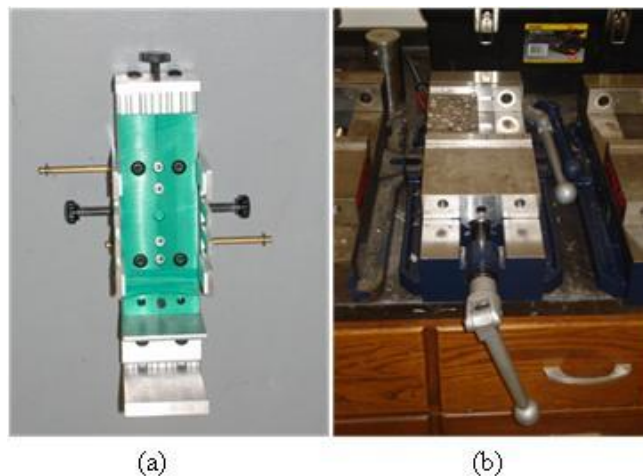


**FIGURE 2 Sample trimming procedures with ends (a) untrimmed and (b) trimmed.**

### **Sample Gluing**

Initial attempts at gluing platens to the sample for testing were made on the vertical gluing jig shown in FIGURE 3(a). While this method of gluing centered the sample on the platens with respect to width, it failed to center it with respect to depth. It also failed to properly align the top and bottom platens. Improperly centered samples and misaligned platens tend to cause unwanted moments in the testing process which introduce high variability and unreliability in the test results. In some cases, the moments placed on the sample prevented the test from running to completion due to the platens being peeled from the sample or the sample failing in bending.

In order to better center the samples between platens, a horizontal, magnetic gluing vice, shown in FIGURE 3(b), was employed. Thickness and width of the samples were carefully measured at each end and at the midpoint of the sample. The platen dimensions were also measured. The sample measurements were then averaged and divided by two. Gauge metal of appropriate thicknesses was inserted below and beside the sample to position the sample in the center of the platens. Platens were placed flush against the side and bottom of the vice, then brought together to ensure proper alignment with each other. The vice was then reopened and the sample inserted between the platens with the appropriate gauge metal pieces in place. Platens and sample ends were cleaned and a 2 ton (17.8 kN) epoxy was applied to each end of the sample. The vice was then tightened until complete contact was made with the platens and the epoxy. Care was taken to not over tighten the vice, allowing the platens to remain aligned with each other rather than aligning with the sample ends.



**FIGURE 3 Vertical gluing jig (a) and horizontal magnetic gluing vice with three inch wide sample (b).**

Unwanted moments were minimized by properly preparing the sample, ensuring proper platen alignment, and centering the sample between the platens.

In order to measure displacement of the sample during testing, LVDTs were centered, vertically, on each of the four sides of the sample with a 2 inch (50.8 mm) gauge length. The data collected from these LVDTs was averaged to obtain the approximate sample displacement near the center of the sample.

#### *Machine Modifications*

While careful preparation of the field samples greatly reduced the potential for moments during testing, some changes also had to be made to the servo hydraulic testing machine in order to reduce eccentricity. Initial tests used a fixed-fixed connection, where both platens were directly bolted, on both ends, into the testing machine. This tended to exaggerate the small eccentricities inherent in the samples. To remedy this problem, a fixed-pinned connection was used which incorporated a ball and socket joint on one end of the sample, as shown in FIGURE 4. This allowed the sample to move more freely during testing. The socket base plate was also adjusted horizontally for each test to ensure that the ball was not forced into the joint, causing unwanted bending in the sample. As a result, the ball fit directly into the joint without the application of any horizontal forces. This modification to the servo hydraulic testing machine further reduced the potential for error in testing caused by eccentric loading and applied moments.



**FIGURE 4 Three inch wide sample attached to ball and socket joint shown with movable base plate.**

In addition to the mechanical modifications made to the machine, a program was added to the testing system which would automatically detect when one of the measuring LVDT's for the VEC test reached the 100  $\mu\epsilon$  limit. At this point, the test would automatically terminate, reducing the possibility of human error caused by attempting to stop the test manually.

#### *Test Modifications*

With adjustments made to sample preparation and the testing machine, modifications could then be made to the tests themselves. VEC test cycles were completed in approximately 5 to 15 seconds at the original rate of 0.01 inches/min. (0.254 mm/min.). This limited amount of data proved to be insufficient for proper analysis and development of the relaxation modulus and complex modulus master curves. In order to



provide more test data from the VEC test, the loading rate was adjusted from 0.01 inches/min. (0.254 mm/min.) to 0.004 inches/min. (0.102 mm/min) and finally to 0.002 inches/min. (0.051 mm/min). This provided a minimum of 20 seconds worth of data for most cases.

The RDT\* test was adjusted to separate the undamaged and damaged cycles. Other adjustments were also necessary to eliminate the possibility of damaging the samples during the undamaged cycles due to excessive strain. The controlled strain limit for the undamaged cycles was changed from 80  $\mu\epsilon$  to 30  $\mu\epsilon$  in order to accomplish this. The reduction in this limit made it more difficult for the testing machine to control the test, increasing the amount of noise in the resulting data. However, it prevented the sample from experiencing damaging strains. The number of undamaged cycles was also reduced from 500 to 50. 500 cycles was unnecessary when 50 cycles provided sufficient data to perform the necessary analysis. The damaged strain limit was also reduced from 350  $\mu\epsilon$  to 175  $\mu\epsilon$ . This allowed for collection of sufficient data to calculate the damaged properties while preventing sample failure or failure at the sample/platen interface.

#### *Analysis Modifications*

As mentioned in the previous section, the decrease in strain limits for the undamaged cycles of the RDT\* test caused an increase in the noise observed in the recorded data. The analysis of the RDT\* data requires that the peaks and valleys of the stress and strain be located. Automation of this process resulted in picking the peaks and valleys of the noise rather than the actual response. Manual identification of these points proved to be

far too time consuming and inefficient for adequate and timely analysis. It was observed that the recorded noise occurred at a much higher frequency than the 1 Hz (6.28 radians/sec.) loading frequency. This made it possible to apply a low pass frequency filter to the collected data, removing the unwanted noise occurring at frequencies above 1 Hz (6.28 radians/sec). The result was a much smoother data set that allowed for automated peak picking of the stress and strain curves.

## **Results**

With sample, machine, test, and analysis modifications made, the VEC and RDT\* tests could be applied to field samples. The data was collected and test results analyzed for the selected sites listed in TABLE 1. The results from these tests can be seen in TABLE 2, which include  $E^*$  and  $E_{ve}$  as well as the absolute percent difference between  $E^*$  and  $E_{ve}$  for each sample.

A careful inspection of the results from the individual LVDT's indicates that a stiffness gradient occurs between the pavement surface and the bottom of the layer being tested. While further analysis of this gradient is ongoing, it is beyond the scope of this particular study. However, the average response of the four LVDT's was sufficient to give an overall view of the material behavior and performance needed for test comparisons and practical application.

Of the 26 samples tested, only three appeared as outliers in a statistical analysis. These included a sample from US Route 83 located in the wheel path and two from State Highway 36, one in the wheel path and one in the shoulder. After reviewing the notes

and results associated with US Route 83, it appears that the unusually large percent differences between  $E^*$  and  $E_{ve}$  could be the result of poor sample preparation and handling which resulted in eccentric loading during testing. State Highway 36, however, is a very stiff mixture. This high level of stiffness may have influenced the results of the VEC test. Mixtures of this level of stiffness may require a higher strain limit than the prescribed  $100 \mu\epsilon$  in order for the VEC test to produce viable results. This warrants further evaluation using several samples of high stiffness.

For the remaining 23 samples, the absolute percent difference between  $E^*$  and  $E_{ve}$  follow a normal distribution with a mean of 5.4% and a standard deviation of 3.72%, indicating that the results from the VEC and RDT\* tests were similar. A study by L. K. Huang suggested that differences between stiffness moduli from SCB and FB test of about 10% or less were acceptable (26). Thus, the VEC and RDT\* tests are viable direct tension tests for determining the undamaged moduli of a HMA field sample.

**TABLE 2 Field Sample VEC and RDT\* Test Results**

Route Name	Wheel Path /Shoulder	Percent Air Voids	$E_{ve}$ Average (MPa)	$E^*(1)$ (MPa)	$E_{ve}$ (MPa)	Absolute % Difference
Interstate Highway 20	Wheel Path	9.6%	6631	6356	6538	2.8%
		8.8%		8313	7793	6.7%
	Shoulder	10.1%		6240	6072	2.8%
		11.1%		6396	6121	4.5%
Interstate Highway 35	Shoulder	3.3%	3883	3475	3575	2.8%
		3.6%		3952	4191	5.7%
US Route 277	Wheel Path	14.1%	4564	4020	4407	8.8%
		7.4%		4589	4928	6.9%
	Shoulder	7.2%		4323	4459	3.0%
		7.2%		4367	4462	2.1%
US Route 82	Wheel Path	8.6%	6054	5027	4826	4.2%
		10.1%		5496	6190	11.2%
	Shoulder	8.8%		7744	6900	12.2%
		7.6%		7101	6300	12.7%
US Route 83	Wheel Path	5.8%	1989 <sup>6</sup>	1921	3000	<b>36.0%</b>
		9.8%		1887	1800	4.8%
	Shoulder	9.1%		2004	1999	0.2%
		11.0%		1981	2169	8.7%
State Highway 36	Wheel Path	4.1%	8923	8567	9419	9.0%
		3.0%		6254	9061	<b>31.0%</b>
	Shoulder	5.3%		7870	8426	6.6%
		6.8%		4682	6962	<b>32.8%</b>
Farm to Market 2994	Wheel Path	6.6%	4719	4899	5040	2.8%
		5.6%		5093	5097	0.1%
	Shoulder	8.3%		3966	4140	4.2%
		8.1%		4566	4597	0.7%

<sup>6</sup> Value does not include outlier value of 3000 MPa.

It is also important to consider the effects of the different properties of each individual sample. This is necessary in order to determine if the two tests can be applied over a broad range of field samples, or if the test results are limited based on the individual properties of the sample. Differences between  $E^*$  and  $E_{ve}$  were examined based on air void content, binder content, sample thickness, age, and climate conditions to determine what correlations, if any, could be drawn from the results. In each case, correlations were weak, with age having the greatest correlation coefficient of 0.4311, indicating a slight increase in  $E^*$  and  $E_{ve}$  differences with respect to aging. Binder content and sample thickness appeared to have the next greatest correlations, though they were also weak, with values of 0.3289 and -0.3068, respectively. Climate conditions and air voids tend to have little effect on  $E^*$  and  $E_{ve}$  differences, both having correlation coefficients less than 0.18.

A mixed stepwise regression was also run for the above mentioned effects to determine their level of significance. At a 95% level of significance, only the age of the sample and sample thickness were shown to have a significant effect on the absolute difference between  $E^*$  and  $E_{ve}$ . Respective p-values for these effects were 0.014 and 0.045, respectively. It can, therefore, be stated that thicker samples taken early in the life of the pavement minimize the difference between  $E^*$  and  $E_{ve}$ . As a result, it is important to use as much of the layer in question as possible when using the VEC and RDT\* tests for determining field sample properties. As the sample ages, careful evaluation should be made with respect to the change in modulus, in order to ensure that the test results are of sufficient quality for accurate pavement evaluation.

Further evidence for the viability of the VEC and RDT\* tests can be seen by examining the resulting modulus values at each individual site. Noting that variability can be found from location to location within a site, the average values of  $E_{ve}$  for each site in TABLE 2 Field Sample VEC and RDT\* Test Results are relatively close to the actual measured values for each individual sample. Standard deviations for the study sites range from 185 MPa (26,800 psi) for US Route 83 to 876 MPa (127,000 psi) for US Route 82 with 75% of the individual values falling within 10% of their respective site mean. The variation that is found can be attributed to factors such as different air void contents, binder contents, and traffic loading rates, among others. The similarities between samples provide some confidence in the consistency of the tests for any given site.

### **Summary**

By comparing VEC and RDT\* test results from the same sample as well as the results from different samples taken from the same site, it can be seen that these two tests can be successfully applied to field samples. The VEC and RDT\* tests provide a quick and accurate method of determining the material properties necessary to assess fatigue under field conditions. Streamlining of the test preparation and further automation of the analysis will further make the VEC and RDT\* tests practical methods for determining the material properties of samples obtained from the field.

Researchers will be able to separate and assess the effects of aging and trafficking on the number of loads to fatigue failure by examining VEC and RDT\* test

results from the wheel path and shoulder of any given pavement over time. This, in turn, will allow for more accurate development of mechanistic models which incorporate accurate aging prediction and correctly characterize fatigue. Current and future models can be compared and analyzed for accuracy by testing field samples throughout the life of the pavement and comparing the test results to those obtained from the models.

Over the past 100 years, significant progress has been made in the development of an efficient and effective transportation system. The direct tension testing of field samples using the VEC and RDT\* tests will help propel the industry forward into the next 100 years of success by allowing for the quick, accurate, and direct determination of the material properties of HMA pavements. As these results are applied, agencies will be better able to determine pavement life and plan for the maintenance, rehabilitation, and reconstruction of the transportation system.

CHAPTER III  
INVESTIGATION OF AGING EFFECTS AT A SINGLE FIELD SITE USING  
DIRECT TENSION TESTING

In this portion of the study, field samples acquired from a site in south Texas were investigated over time to see if relationships existed between the oxidative aging of the binder and the performance of the mixture. Cores were taken four times, at construction and then at intervals of approximately one year. Laboratory aged mixtures were also compared to the field samples. Raw materials collected from the same site in south Texas were used to prepare laboratory mixed, laboratory compacted (LMLC) samples that were artificially aged and tested to determine their material properties. Binder extracted from the LMLC and field samples was also examined.

This chapter discusses materials collected for the study are identified followed by a description of the sample preparation methods and test methodologies used to obtain the material properties of the aged and initial condition samples from the laboratory as well as the field. Binder extraction and test methods are also described. Material properties were then used to estimate  $N_f$  using the CMSE\* method, without the application of shift factors. Results from the binder tests, field sample tests, and LMLC sample tests are reported followed by a cross-comparison of all of the results. From each of these tests, conclusions were made with respect to the effects of aging on the selected HMA mixture.



## **Materials**

Materials for this study were selected from US Route 277 in the Laredo District of the Texas Department of Transportation (TxDOT). At the time of construction, raw materials from the site were collected for the fabrication of LMLC samples. Field cores were taken immediately following construction and thereafter at approximately one year intervals for a total of four sampling times. Binder used specifically for testing was extracted from selected field cores.

US Route 277 was constructed in 2008. Aggregates for this mixture consisted of a blend of four different aggregates to create a TxDOT Type C mixture (25). Three of the aggregates consist of limestone from the South Texas Aggregates Inc., Sabinal Quarry located in Uvalde County, Texas. They include a coarse limestone aggregate, a blend of Type D and Type F limestone aggregates, and manufactured sand. The fourth aggregate used in the blend is manufactured sand from the Vulcan Materials Company, Knippa Quarry, also located in Uvalde County, Texas.

Binder for the US Route 277 mixture consisted of a PG 70-22 Valero Asphalt binder with an optimum asphalt content of 4.5% by weight of mixture using the Superpave volumetric mixture design method.

Twelve cores were taken from the field in 2008; six from the wheel path, and six from the shoulder. Air void content (AV) for all twelve field samples was determined. Two cores from the wheel path and two from the shoulder were used for mixture testing. One field core from the wheel path and one from the shoulder were used for binder extraction. The remaining cores were retained as alternates.

A portion of the test section was treated with a chip seal following the initial core extraction. In 2009, six more field samples were taken from the untreated wheel path and six more from the shoulder with six additional field samples taken from the treated wheel path. This sampling process was repeated in 2010 and 2011. Field samples were selected from the treated and untreated sections for mixture and binder testing as described for the 2008 samples. The 2011 field wheel path samples all had a chip seal, which was placed on the pavement surface approximately nine months prior to coring.

### **Testing Methodology**

Two uniaxial tension tests developed at Texas A&M University were used to determine the material and fatigue properties of the samples. These include the Viscoelastic Characterization (VEC) test (13) and the Modified Repeated Direct Tension (RDT\*) test (15). Asphalt binder was extracted from selected field samples and analyzed using a Fourier Transform Infrared Spectrometer (FTIR) to determine the degree of binder oxidation.

### *Sample Preparation*

LMLC and field samples were prepared for uniaxial tension testing in order to minimize eccentricities and to reduce moments during testing. Binders were extracted from selected field cores.

## LMLC Samples

LMLC samples used in this study were fabricated based on a D-optimal statistical design which incorporated several combinations of binder contents and AV with 0, 6, 9, and 12 month aging periods in a 60 C accelerated aging room. TABLE 3 includes the D-optimal design combinations. Ranges used for binder contents and AV are shown in TABLE 4.

**TABLE 3 D-Optimal Statistical Design for LMLC Samples**

Run	Aging	Binder Content	Air Void
1	0 months	Opt -0.5%	Low
2			High
3		Opt +0.5%	Medium
4			High
5			Low
6		Optimum	Medium
7			High
8	6 months	Opt -0.5%	High
9			Medium
10		Opt +0.5%	Low
11			Medium
12			High
13		Optimum	Low
14			Medium
15	9 months	Opt -0.5%	High
16			Medium
17		Opt +0.5%	Medium
18			Low
19			High
20		Optimum	Medium
21		12 months	Opt -0.5%
22	Low		
23	Opt +0.5%		Low
24			High
25			Low
26	Optimum		High
27			Medium

**TABLE 4 Binder Content and Air Voids for US 277 Samples**

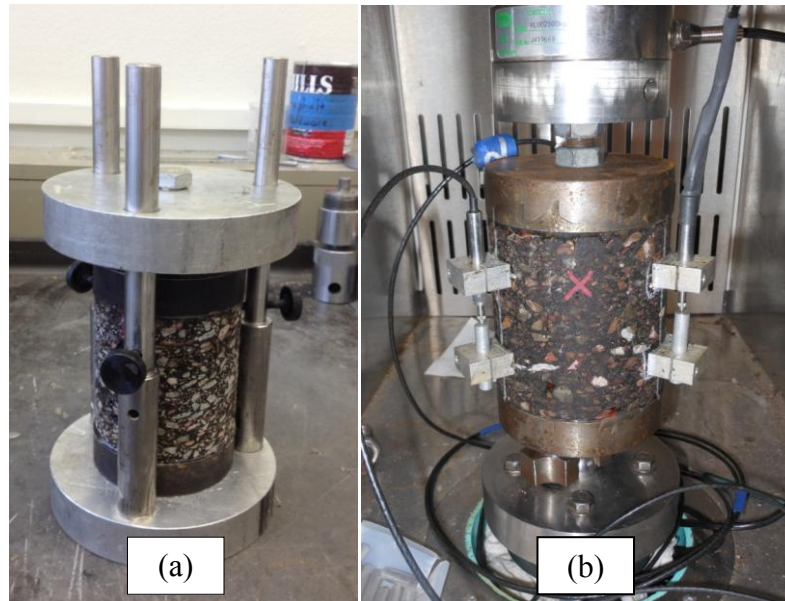
	<b>Binder Content</b>		<b>Air Voids</b>
<b>Low</b>	Optimum -0.5 %	(4.0 %)	< 5%
<b>Medium</b>	Optimum	(4.5 %)	5% - 7%
<b>High</b>	Optimum +0.5 %	(5.0 %)	> 7%

Aggregates used for the LMLC samples were placed in an oven at the mixing temperature of 149° C and were left overnight in order to remove any moisture. The binder was also heated to the same mixing temperature for 2 hours just prior to mixing. The mixture was then short-term oven aged at the compaction temperature of 135°C for four hours as prescribed by AASHTO R30 for performance testing.

Samples were molded using the Super Gyrotory Compactor (SGC) to 152 mm diameter by 152 mm height in order to meet the specified target AV content. The initial AV content found in the 152 mm diameter by 152 mm high samples was slightly higher than the values shown in TABLE 4 due to the conditions imposed by the SGC mold (27). To obtain a more uniform AV distribution, representative of the typical air void distributions encountered in field samples, LMLC samples were compacted at a higher AV content and then cored to a 102 mm diameter. The samples then had 25 mm trimmed from each end to produce the final 102 mm diameter by 102 mm high sample with the appropriate target low, medium, or high AV content.

The prepared LMLC samples were next placed in vertical gluing jigs (FIGURE 5a) so that 102 mm diameter steel platens could be affixed to each end. The gluing jigs provided a method of aligning the platens to minimize eccentricities during the tension

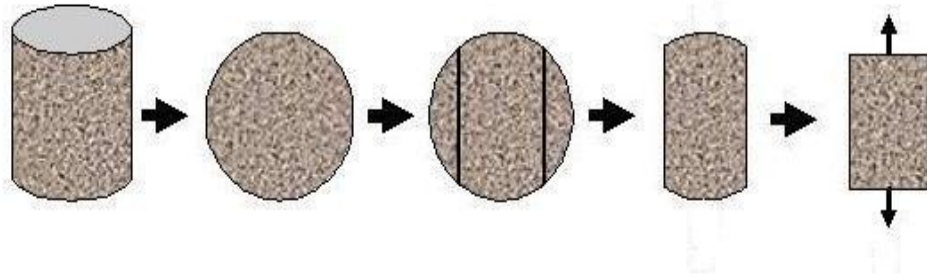
testing process. Following sufficient drying time, three linear variable displacement transducers (LVDTs) were placed vertically and equidistant around the sample (Figure 1b). The LVDT gauge length was 51 mm.



**FIGURE 5** Vertical gluing jig (a) and test setup (b) for LMLC samples

### **Field Samples**

Field cores were trimmed into a prismatic shape as shown in FIGURE 6. This allowed the samples to be tested in the same direction that they would experience tension forces in the field. Special care was taken during cutting to ensure that the sample sides were as close to parallel as possible.



**FIGURE 6 Field sample testing configuration**

A horizontal magnetic gluing vice (FIGURE 7) was used to affix steel platens to each end of the field samples. The magnetic vice ensured that the platens remained aligned with each other, regardless of any small discrepancies in the sample, which may have occurred during the cutting process.



**FIGURE 7 Magnetic gluing vice for field samples.**

LVDTs were placed at 51 mm gauge length on each of the long sides of the sample to measure the vertical displacement induced during testing.

### **Binder Extraction**

The binder extraction process for the field samples was executed by first separating any applied chip seals from the sample by knife. Field samples were then cut by electric saw into several layers, from top to bottom, with each layer being approximately 12.7 mm thick. These layers were then broken into small pieces.

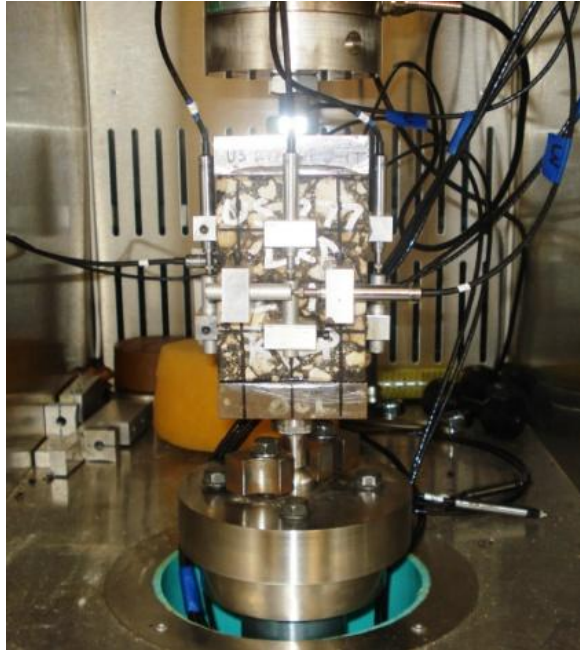
The extraction used three successive washes of a mixture of 15% ethanol plus 85% toluene by volume. After the extraction, the solvent was centrifuged and filtered to remove all the aggregate particles from the binder solution.

The asphalt binder was recovered from the solvent with a Büchi RE111 Rotovap. Nitrogen was used to carry off the solvent and prevent further oxidation. During solvent removal, the bath temperature was kept at 100° C to avoid hardening or softening of the asphalt in dilute solution. To ensure total solvent removal, the temperature was increased to 174° C for 45 min after the condensing solvent could no longer be detected visually.

### *HMA Mixture Testing*

In order to calculate the fatigue properties of LMLC and field samples, both the VEC and RDT\* tests were performed. VEC and RDT\* tests were performed using a servo-hydraulic testing machine. A ball and socket joint was used to further minimize the effects of sample eccentricity and undesirable moments for both LMLC and field

samples. FIGURE 8 shows the field sample test setup with LVDT placement and the ball and socket joint.



**FIGURE 8** Field sample test setup with ball and socket joint at base.

### **VEC Test**

The original VEC test and analysis was developed at Texas A&M University for application to LMLC samples (13, 15). Modifications were later made to this test for application to field samples as described in Chapter II.

The VEC test was performed by applying a monotonically increasing tensile load to a sample at a strain rate of  $50.8 \mu\text{m}$  per minute. The test continued at this rate until one of the measuring LVDT's reached a strain level of  $100 \mu\epsilon$ . It is assumed that at this small strain level, no damage occurs and the sample can be used in further testing (13).



The sample was initially conditioned and tested at 10° C. Once the test was completed, the sample was reconditioned for a minimum of 2 hours and retested at 20° C and 30° C using the same procedure.

Recorded load and displacement data from the LVDTs for each temperature were used to calculate stress and strain. These values were averaged and defined using a fitting curve at each temperature. Fitting parameters from these curves were then used, in conjunction with Laplace transformations and calculated shift factors, to determine the relaxation modulus ( $E_t$ ) master curve and the complex modulus ( $E^*$ ) master curve at 20°C.

### **RDT\* Test**

The RDT\* test was developed by X. Luo et al. at Texas A&M University (15). This test was also further refined for application to field samples as described in Chapter II

The RDT\* test was performed on a sample preconditioned at 20°C. The sample was exposed to a Haversine load in displacement control mode with a maximum vertical strain level of 30  $\mu\epsilon$  for 50 cycles at a frequency of 1 Hz. For a 51 mm LVDT gauge length, 30  $\mu\epsilon$  is a change in gauge length of approximately 1.5  $\mu\text{m}$ . This portion of the test was used to calculate the undamaged viscoelastic phase angle and the undamaged dynamic modulus of the mixture.

Following the 50 cycles at 30  $\mu\epsilon$ , a 1000 cycle Haversine loading was applied at a frequency of 1 Hz with a maximum strain level of 175  $\mu\epsilon$ . For a 51 mm LVDT gauge

length, 175  $\mu\epsilon$  is a change in gauge length of approximately 8.9  $\mu\text{m}$ . At the completion of the test the sample was damaged and could not be retested.

Data obtained from the RDT\* test were averaged and filtered using a low pass filter. The filter removed machine noise from the data, allowing for automated data processing.

The damaged portion of the RDT\* test (175  $\mu\epsilon$  level) was used in combination with the results of the undamaged portion of the test to determine fracture properties, such as Paris' law fracture coefficient,  $A$ , Paris' law exponent,  $n$ , and the rate of damage accumulation,  $b$ . These were then used in the CMSE\* model to calculate  $N_f$  (15, 16).

### *Binder Testing*

Extracted binders from field cores and LMLC samples were analyzed using FTIR to determine the degree of oxidation. A Nicolet 6700 FTIR spectrometer with an attenuated total reflectance zinc selenide prism was used to determine the degree of binder oxidation, by measuring carbonyl area (CA). CA is the area under the absorbance peak from 1650-1820 $\text{cm}^{-1}$ , in arbitrary units, which provides a direct measurement of the oxidation progress in asphalt binder. This property is also strongly correlated to rheological properties measured in the Dynamic Shear Rheometer (23).

### **Test Results**

Mixture and fracture properties for LMLC samples and field samples were calculated using the data obtained from both the VEC and RDT\* tests. Binder properties were also

determined. The results of these calculations were evaluated and compared as a way of validating the VEC and RDT\* testing methods. LMLC and field mixture results and binder results were also evaluated individually and combined in order to provide a preliminary evaluation of the effects of aging and maintenance treatments on HMA mixtures.

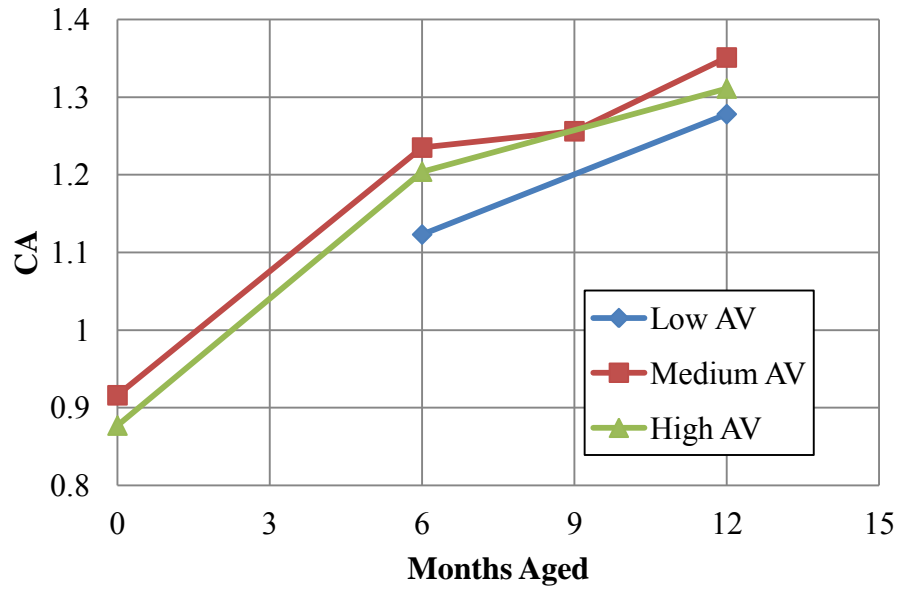
#### *Extracted Binder Test Results*

Following the testing of the LMLC samples, the binders were extracted and tested using FTIR to determine its chemical properties. Due to the nature of the D-optimal statistical design used in the sample fabrication determination, a full factorial set of data is not available. However, the overall trends can still be observed from the test results.

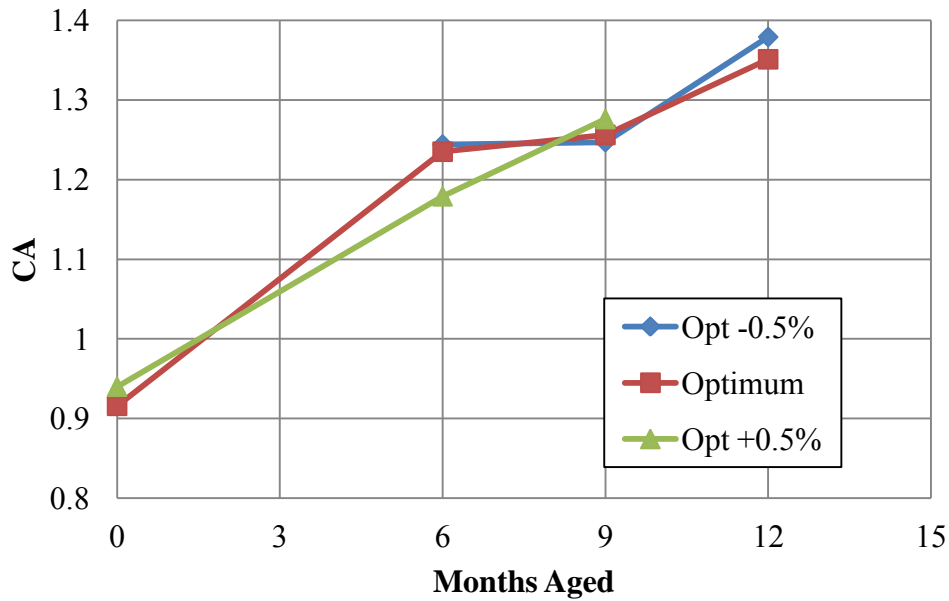
FIGURE 9 shows the CA of the samples which had optimum binder content with each series representing different AV contents. From FIGURE 9 it can be seen that as the samples age in the laboratory, the CA increases. However, the Low AV samples show less oxidation (lower CA values) as a result of less exposure to oxygen within the sample. The Medium AV and High AV samples appear to experience similar changes in CA as the sample ages. This indicates that there may be a threshold AV content at which the diffusion of oxygen into the binder becomes constant.

In FIGURE 10 the AV content is held constant at Medium AV with each series representing different binder contents. FIGURE 10 shows that the change in binder content appears to have little effect on the change in CA.

While it appears that a change in AV content has a greater impact as compared to a change in binder content, the binder from the LMLC samples is aging in a measurable way and trends are as expected, with CA increasing with time.



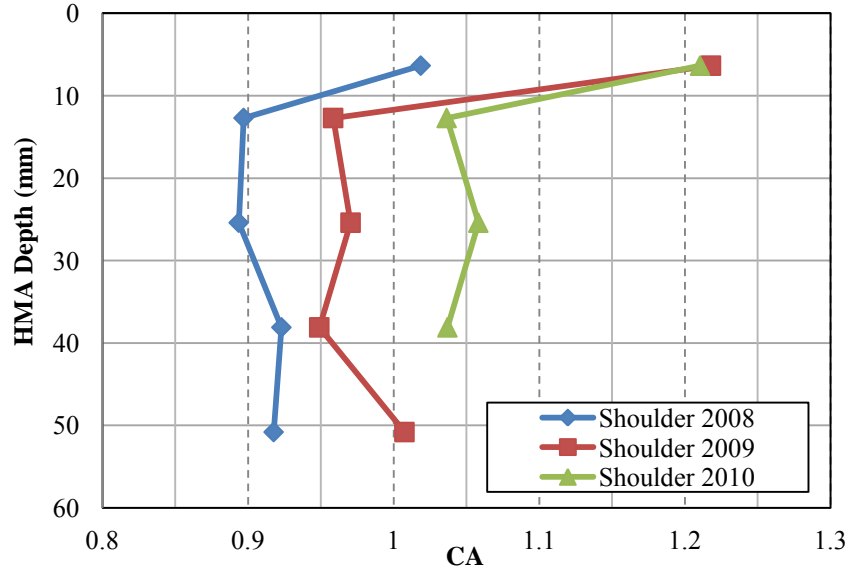
**FIGURE 9 CA of LMLC samples at optimum binder content.**



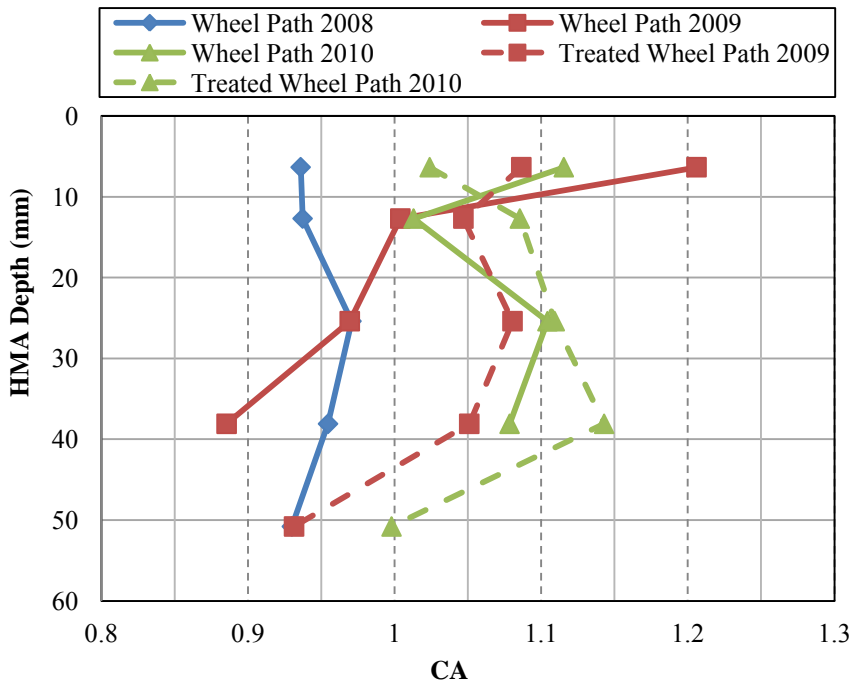
**FIGURE 10 CA of LMLC samples at medium AV.**

With respect to the field cores, after extraction and recovery, the binder for each layer was tested and its chemical properties determined by FTIR. Binder CA growth rates were measured from samples obtained from the wheel path and shoulder for each of the four years from 2008 to 2011.

FIGURE 11 and FIGURE 12 show the CA with depth for the shoulder and wheel path sections, respectively.



**FIGURE 11 CA value with depth and years for US-277 shoulder.**



**FIGURE 12 CA value with depth and years for US-277 wheel path.**

In FIGURE 11, for the samples taken from the shoulder, there was no chip seal treatment on the surface, indicating that the data represents the natural aging process of the road without traffic. The CA values of the first layer for all of the samples are considerably higher than those for the underlying layers. The 2008 sample was collected three months after construction. The CA value of the first layer for this sample was already over 0.1 higher than the average value for layers 2 through 5 which have a standard deviation of 0.015. This is likely due to direct exposure to oxygen during paving in combination with the three month service period. For the 2009 shoulder sample, the CA values of all the layers had increased as expected. Furthermore, the CA for the first layer, which increased 0.2 compared to 0.08 for the deeper layers, has a much faster aging rate between 2008 and 2009. The CA difference between the top layer and the underlying layers rose to about 0.25. The reason for this phenomenon may be the oxygen diffusion resistance, which plays an important role in field aging. The oxygen diffusion resistance for the surface layer is negligible due to the direct exposure to the air. These conclusions agree with observations made in previous studies (28).

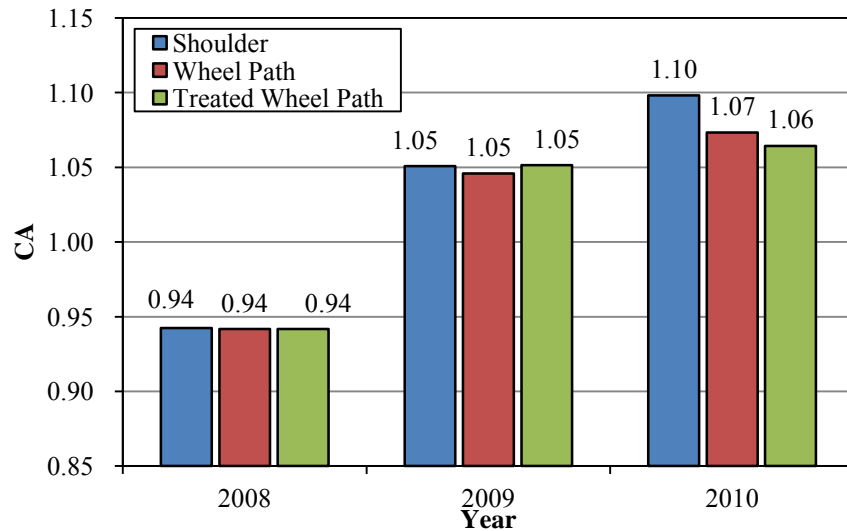
Similar results were found from the CA data for the wheel path as shown in FIGURE 12. As previously mentioned, some of the wheel path sections had a chip seal surface treatment placed on the pavement surface after three months of use; just after the 2008 core collection. The purpose of the chip seal was to protect the HMA from oxidative aging by cutting off the contact between the air and pavement. It is also thought to rejuvenate the binder directly beneath the treatment.

The CA for the chip seal treated wheel path samples had a much lower value for the first layer when compared with the untreated sample from the same year. This is a good indication that the first layer aged much less under the chip seal treatment. However, it is not clear whether this was due to cutting off oxygen flow, binder rejuvenation, or a combination of the two factors. The CA value for the chip seal binder, which was not included in FIGURE 11 and FIGURE 12, was approximately 1.5 to 1.6, which is extremely high. This could be due to direct exposure to air or from high UV radiation and high temperatures that result from the darker exposed area associated with chip seals. With the exception of layer 1, the untreated core in 2009 did not behave as expected when compared with the core in 2008. For layer 4 (about 38 mm beneath the surface) the CA of the 2009 core turned out to be less than the CA for the 2008 core. This may be due to the variability of the cores or materials, especially when considering that AV content for the 2009 core was approximately 1% less than the core from 2008. The results shown in FIGURE 12 also give the impression that the chip seal accelerated the aging beneath the surface, which is not as expected.

FIGURE 13 shows the average CA results for the shoulder, untreated wheel path, and treated wheel path combined. While there is a difference between results from year to year, there is no evident difference between the wheel path and shoulder until 2010. In 2010, the oxidation occurring in the untreated wheel path is slightly less than that occurring in the shoulder. The treated section's oxidation is less than both the shoulder and untreated wheel path. From these results it appears that the average pavement oxidation is eventually affected by both traffic and maintenance treatments. Also note



that the CA increased for all three locations by about 0.07 during the first year, indicating that much of the aging occurs during the first year of the life of the pavement.



**FIGURE 13 Average combined CA for all sections of US-277.**

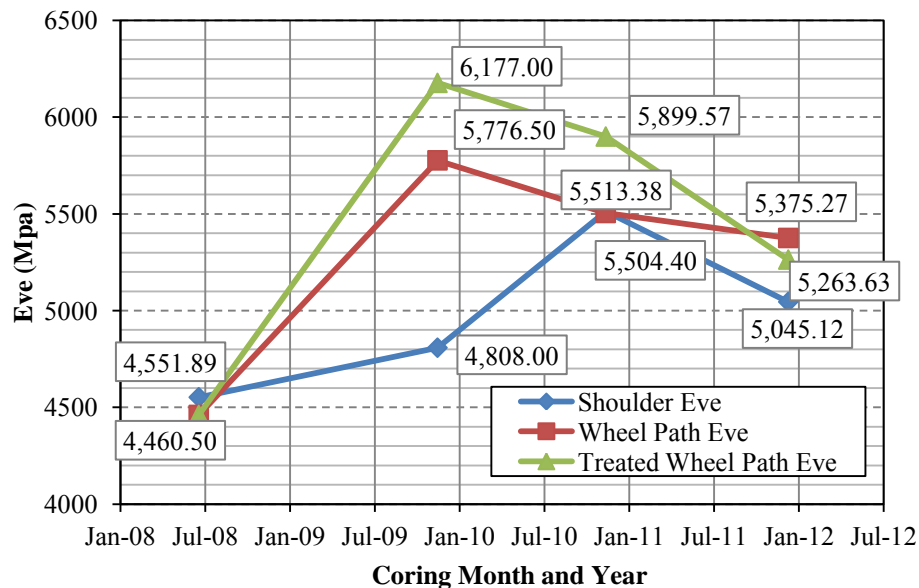
#### *Field Sample Test Results*

Results of the VEC and RDT\* tests for the field samples were first used to compare the moduli of the various samples taken from the wheel path, treated wheel path, and shoulder from 2008 to 2011.

FIGURE 14 shows the dynamic modulus ( $E_{ve}$ ) values obtained from the RDT\* test. These values correlate well with the complex modulus ( $E^*$ ) values from the VEC test which had results that were within 10% of  $E_{ve}$  (26). From the results shown in FIGURE 14, it can be seen that the  $E_{ve}$  of the shoulder continues to increase as the pavement ages with the exception of the 2011 sample (Jan-12 in FIGURE 14), which

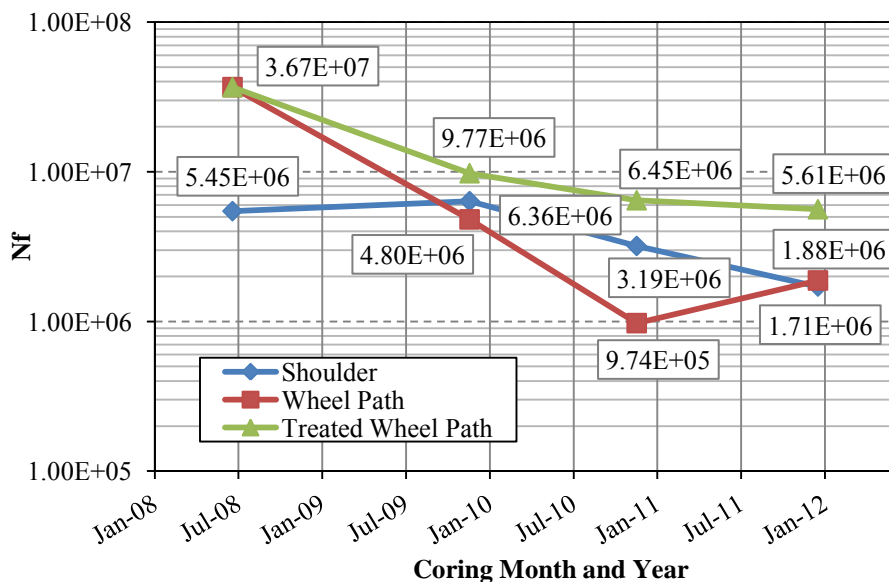
had a chip seal placed on it shortly after the 2010 sample was collected. The shoulder experiences effectively no traffic, therefore, this result is primarily due to the aging of the HMA.

Both the treated and untreated wheel path experience an initial increase in  $E_{ve}$  between 2008 and 2009, however, contrary to the shoulder trend, the modulus then begins to decline for the following three years. From 2008 to 2009, the modulus increases as the pavement ages and is exposed to traffic loading. However, after only the first year, the HMA begins to accumulate damage in the form of fatigue cracking and the modulus declines. Also note that the rate of decline for the untreated wheel path slightly decreased between 2010 and 2011. Again, this may be due to the placement of a chip seal on the surface of the pavement shortly after collection of the 2010 samples.



**FIGURE 14**  $E_{ve}$  for US 277 field samples.

Some other interesting trends can be seen by examining the  $N_f$  values calculated for these same samples.  $N_f$  values were calculated using the VEC and RDT\* results in the CMSE\* model. Calculated  $N_f$  values are shown in FIGURE 15. Notice that the  $N_f$  values for the shoulder remain relatively flat with a slight decline in  $N_f$  values as it ages. The wheel path sections, however, have an initial sharp decline with the rate of change in  $N_f$  values slowing as time progresses. Once again, there was a slight increase in  $N_f$  for the 2011 wheel path samples, which had the chip seal applied in 2010. It is also important to note that for the treated wheel path section, the  $N_f$  values remain at a higher level than the untreated section, suggesting that the chip seal has a positive effect in extending the life of a pavement. It also appears that the placement of a chip seal later in the life of a pavement can also positively affect the pavement life.



**FIGURE 15**  $N_f$  for US 277 field samples.

Based on these results, the HMA stiffens with aging, which plays a role in the fatigue failure of pavements. It can also be concluded that a chip seal placed as a maintenance treatment can extend the life of a pavement. However, these results are specific to this particular site. Additional research is recommended using mixtures from other sites in order to determine if these trends are typical of all HMA and if the trends can be predicted.

#### *LMLC Sample Test Results*

The VEC and RDT\* tests were also performed on LMLC samples. Test data collected allowed for a comparison of the material properties and performance of the LMLC samples at different AV and binder contents for the initial condition and aged samples. An Analysis of Variance (ANOVA) test concluded that there are statistically significant effects of aging level, binder content, and air voids on  $E_{ve}$  while there are no statistically significant interaction effects among them (i.e., the rate of change in  $E_{ve}$  over different aging levels are not statistically different over different AV or over different binder contents). A Tukey HSD statistical test confirmed that  $E_{ve}$  was statistically different at each aging level. As seen in the field samples, it is safe to conclude that  $E_{ve}$  increases with age. FIGURE 16 shows how  $E_{ve}$  changes over time with low, medium, and high AV contents. As expected, the modulus increases as the sample ages. Low AV samples had a higher  $E_{ve}$  value, followed by that for the medium and high AV samples. While the medium and high AV samples appeared to have very similar  $E_{ve}$ 's at 6 months, the Tukey HSD analysis for the effect of AV indicated  $E_{ve}$  was significantly different

overall among all three AV contents. Also, notice that the rate of change in  $E_{ve}$  over time is similar for all three AV contents as expected from the insignificant interaction effect test results between aging levels and AV contents.

FIGURE 17 shows the change in the  $E_{ve}$  values for three different binder contents: optimum, optimum -0.5%, and optimum +0.5%. From FIGURE 17 the rate of change in  $E_{ve}$  appears approximately the same for the optimum and optimum -0.5% binder contents, but is slightly slower for the optimum +0.5% binder content. However, as mentioned above, the ANOVA test on the interaction effect between binder contents and aging levels indicated that the rate of change in  $E_{ve}$  across three binder contents was not statistically significantly different. Tukey HSD analysis on the main effect of binder content indicated that overall there was no significant difference in  $E_{ve}$  based on binder content for optimum and optimum +0.5% while a significant difference did exist between these two and the optimum -0.5%.

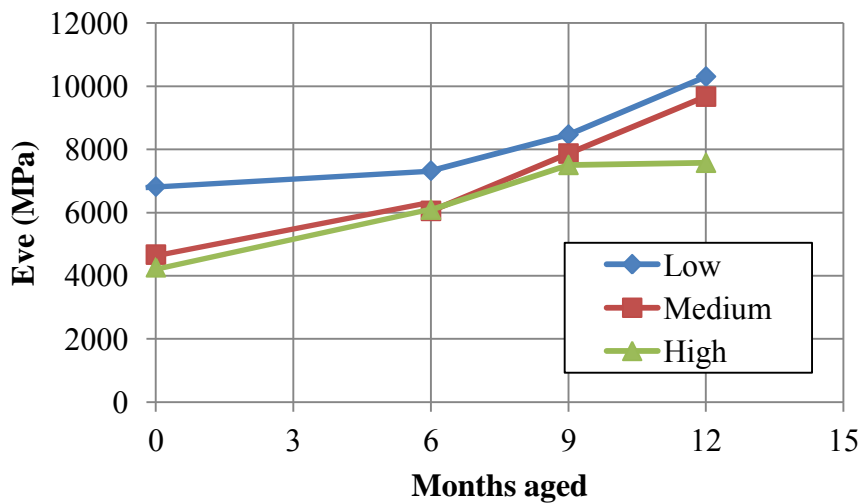
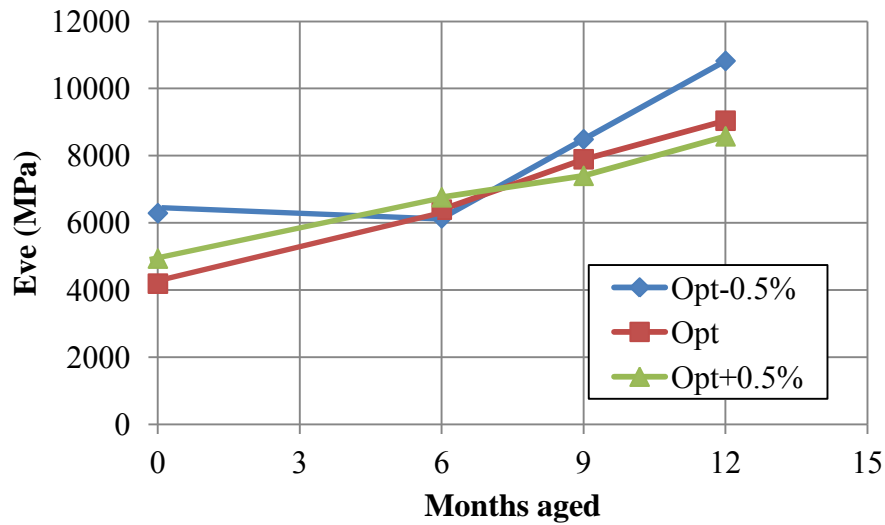


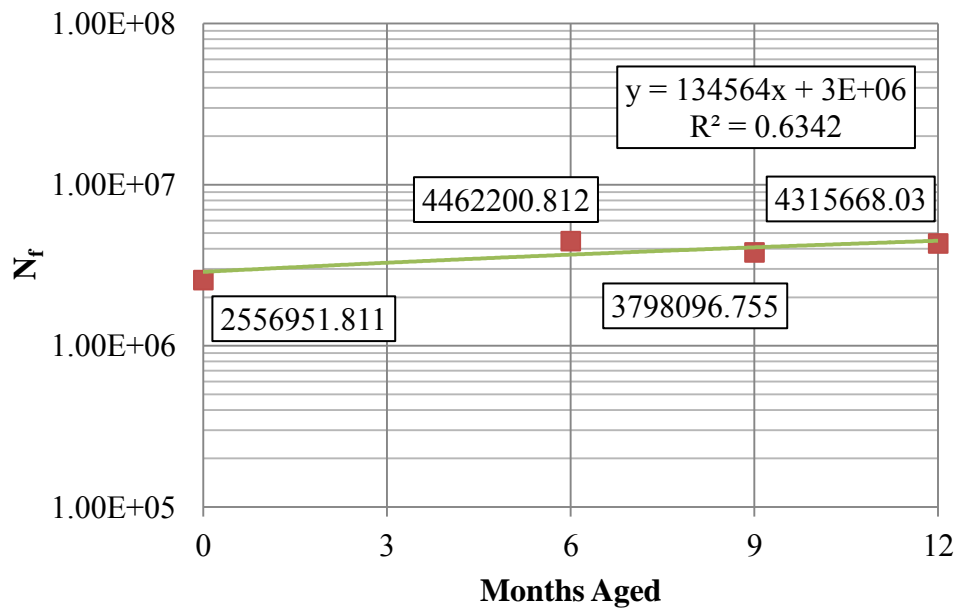
FIGURE 16  $E_{ve}$  for LMLC samples at differing AV.



**FIGURE 17**  $E_{ve}$  for LMLC samples at differing binder contents.

Finally, FIGURE 18 shows  $N_f$  for the LMLC samples prepared and tested at the optimum binder content and medium AV. As the samples age and stiffen,  $N_f$  slightly increases, indicating that aging is affecting the mixture performance, though its effect is small. A linear fit of the data indicates that  $N_f$  changes at a rate of approximately 180,500 loads per month of artificial aging. While this may seem significant, it must be remembered that this is associated with accelerated aging, meaning that one month in the laboratory aging room could be equivalent to several months in the field. One study of nine different binders found that one month of laboratory aging was equivalent to a range of 13 to 19 months in the field (29). However, that relationship was developed with respect to binders under different aging conditions and cannot be directly compared to the mixture aging conducted in this study. Nevertheless, the  $E_{ve}$  and  $N_f$  values

collected for both LMLC and field samples allowed for some relationships to be developed, as discussed in the subsequent section.



**FIGURE 18** Number of loads to fatigue failure for LMLC samples with medium AV and optimum binder content.

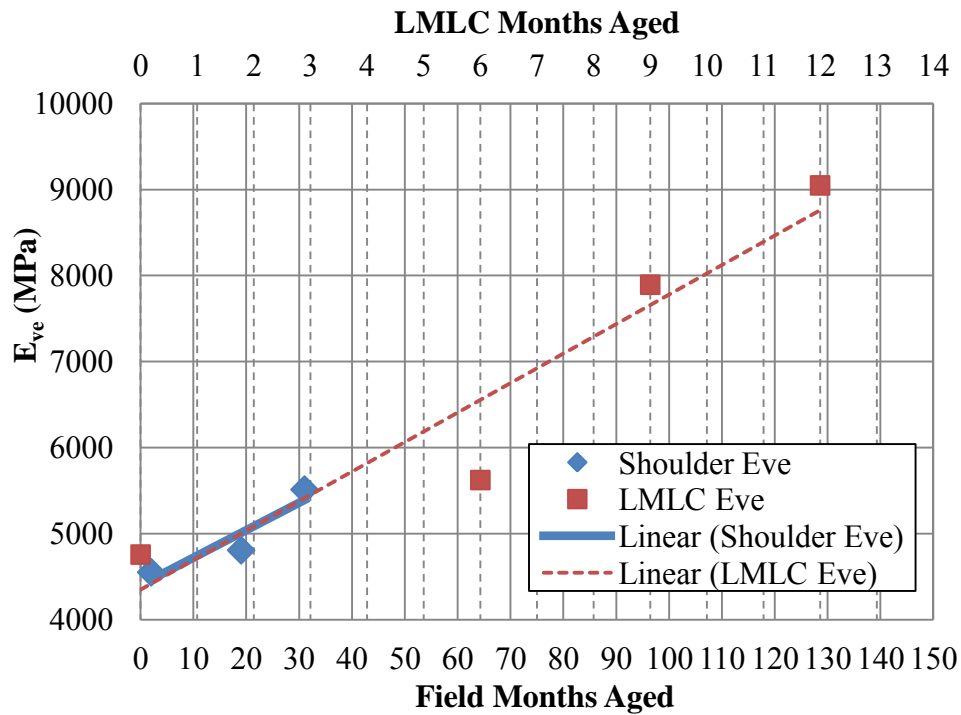
#### *Comparison of Test Results*

With testing and analysis results obtained for binders, field samples, and LMLC samples, it is possible to make some comparisons between the results. A connection between binder aging and field performance along with a correlation between field and LMLC mixture performance may provide the information required to predict the effects of aging on the performance of HMA in the field.

### **LMLC vs. Field Samples**

LMLC samples were only exposed to accelerated laboratory aging and experienced no traffic loading prior to testing. In order to make an equivalent comparison to performance in the field, it is important to compare the LMLC sample results with field results from samples which had minimal exposure to traffic loading. To accomplish this, a comparison was made between the LMLC samples and the field samples taken from the shoulder of US 277. FIGURE 19 shows this comparison of  $E_{ve}$  values. The 2011 field sample is not shown because the chip seal placement altered the resulting  $E_{ve}$  value, making it incompatible. By plotting the two lines representing the linear fit of  $E_{ve}$  for the LMLC and field samples on the same graph, the relationship between field and LMLC samples can be easily seen. With the age of the LMLC samples in months listed at the top of the graph and the number of months that spanned between field samples acquisition listed at the bottom, it can be determined that one month of aging in the laboratory is equivalent to approximately 10.5 months in the field for US 277. This is less than the 13 to 19 months found in previous studies (29), but the Laredo climate is a case of extreme heat which may have affected the rate of aging.





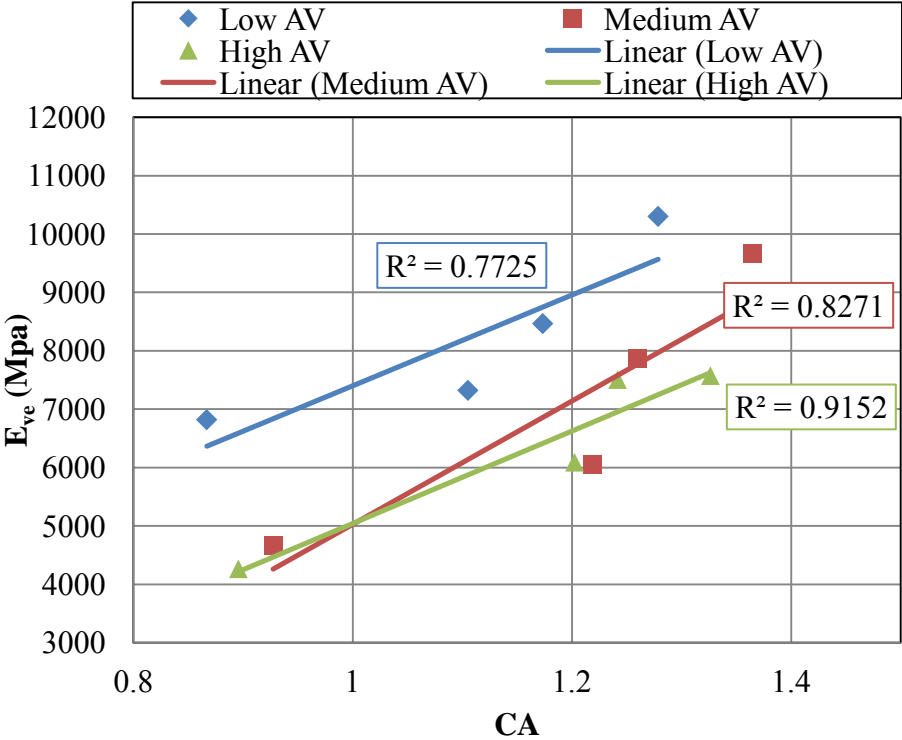
**FIGURE 19 Laboratory to field  $E_{ve}$  comparison.**

### LMLC Samples vs. Extracted Binder

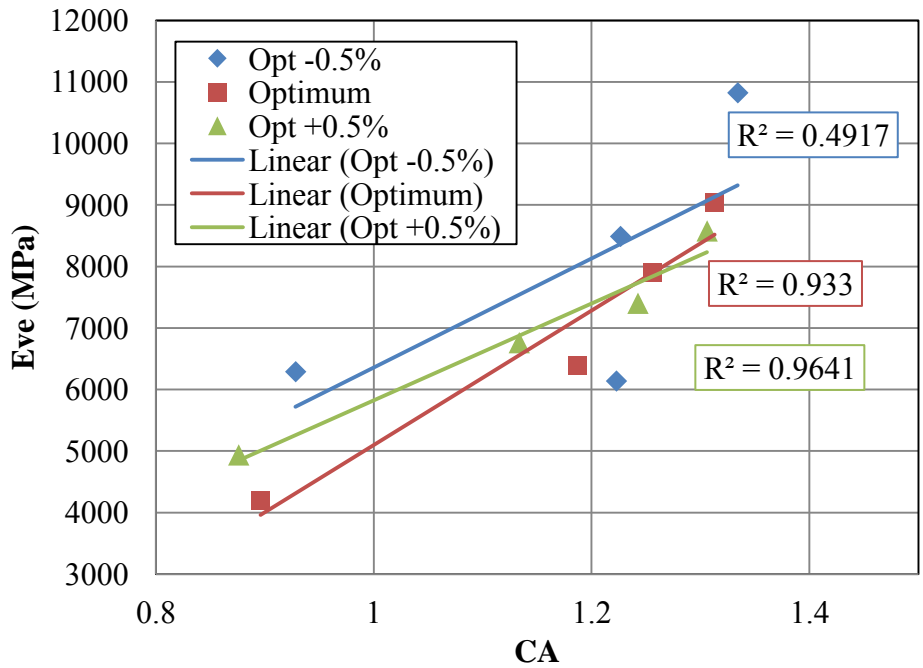
Comparing the  $E_{ve}$  values of the LMLC samples versus the corresponding CA from their respective extracted binders it can be seen that the two properties are related (FIGURE 20 and FIGURE 21). FIGURE 20 shows the relationship between  $E_{ve}$  and CA for the LMLC samples at low, medium, and high AV. All three sets of samples show that a correlation exists between CA and  $E_{ve}$  for mixtures, with a strong correlation for the high AV samples.

The same can be said when viewing the LMLC samples at optimum, optimum - 0.5%, and optimum +0.5% binder contents as seen in FIGURE 21. Optimum, optimum +0.5% binder contents appear to show an acceptable correlation between CA and  $E_{ve}$ ,

with the higher binder content having a much stronger correlation. Thus, it can be stated that there is a strong relationship between binder oxidation, resulting binder stiffening, and ultimate mixture stiffening with aging.



**FIGURE 20** E<sub>ve</sub> vs. CA for LMLC samples with different AV and increasing age.



**FIGURE 21**  $E_{ve}$  vs. CA for LMLC samples with different binder contents and increasing age.

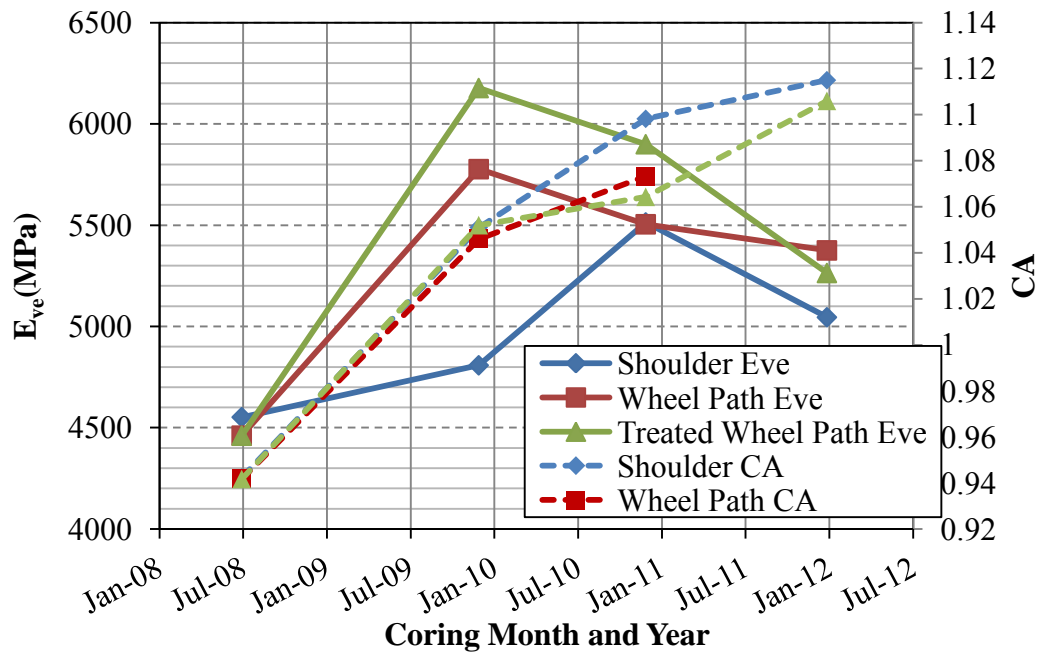
### Field Samples vs. Extracted Binders

It has been shown that as a LMLC mixture ages, it stiffens, which will ultimately affect pavement performance. The next step is to be able to predict the role of aging on pavement performance in the field. The effects of aging on HMA field mixtures can also be viewed by taking the CA results from the binders extracted from the field cores and comparing them with the  $E_{ve}$  results obtained from the field samples.

The stiffness of a mixture is affected by much more than just the aging process. Traffic, AV content, aggregate type, and climate, among other things, all play a role in how a mixture will change stiffness and, ultimately, how the pavement will perform. With so many factors playing a role in field performance, the correlation between  $E_{ve}$

and CA for field samples cannot be made. Some generalized conclusions, however, can be made.

FIGURE 22 is a combined plot of  $E_{ve}$  and CA with respect to the month the sample was obtained, with  $E_{ve}$  shown on the left axis and CA on the right.  $E_{ve}$  trends are represented by solid lines, while CA results are shown as dashed lines. Based on this comparison, the oxidation of the binder, as represented by CA of the corresponding extracted binder, plays a role in the stiffness of the mixture. This is especially apparent when viewing the response of the shoulder, which has little or no exposure to traffic loading. With the exception of the 2011 sample, which, as stated previously, had a chip seal placed on it, the shoulder's mixture stiffness continues to increase over time as the CA increases. In the case of the treated and untreated wheel path, this phenomenon is apparent between 2008 and 2009, but the mixture loses stiffness as it begins to experience damage and cracks begin to accumulate throughout the HMA. This is also shown by the fact that  $N_f$  continues to decrease with time as was seen in FIGURE 15.



**FIGURE 22  $E_{ve}$  vs. CA of field samples for US 277 between 2008 and 2011.**

### Summary

The laboratory test results from LMLC and field samples and corresponding extracted binders lead to the following important conclusions regarding HMA aging as well as the effects of chip seals on pavement performance:

- Aging does play a role in the fatigue failure of HMA as evidenced by the performance of field samples, taken over time, from the shoulder. The stiffening of a mixture also coordinates well with an increase in oxidation, represented by CA development in corresponding extracted binders.
- While both AV and binder content play a role in mixture aging, AV plays a much more significant role.

- For US-277, much of the HMA aging occurs during the first year. In general, the rate of aging for US-277 decreases over time.
- Chip seals appear to slow HMA aging, and, as a result, slow the rate of damage accumulation due to fatigue. However, this effect takes place primarily at the surface of the HMA where the chip seal is placed.
- It is possible to develop a relationship between binder aging and mixture aging. A relationship can also be drawn between *artificially* aged LMLC samples and *realistically* aged field samples.

These generalized conclusions are an important first step in moving toward mechanistic models which incorporate and quantify aging. A relationship between binders and LMLC samples, and between LMLC samples and field samples, lends itself to the potential development of prediction models which incorporate aging. The next step in this development requires a deeper investigation into other field sites with different mixture and environmental conditions. While the findings in this chapter are a good starting point, a quality fatigue failure prediction model must be applicable to a wide range of HMA mixtures in all types of climates and conditions.

CHAPTER IV  
COMPARISON OF AGING IN THE FIELD WITH ACCELERATED LABORATORY  
AGING

This chapter examines HMA mixture aging at three different sites across Texas based on the properties of field samples cut from cores and corresponding LMLC samples made from raw materials used during construction. A description of the materials collected from each site is included along with a brief description of the test methods used to determine the mixture properties of the samples. The CMSE\* method (15, 19) was used to determine the loads to failure in fatigue for both the LMLC and field samples. The results associated with the LMLC samples are discussed. Next, the field sample test results are presented followed by an examination of the relationships between the LMLC, artificially laboratory aged samples, and the naturally aged field samples.

**Materials and Testing**

Materials were collected from three Texas sites where HMA was utilized in the construction of new pavement surface layers. Enough binder and aggregate was collected for LMLC samples to be fabricated and tested. Field cores were also collected immediately after construction and then three more times at approximately one, two, and three years after construction.

### *Site Selection*

Each of the sites selected had different characteristics which distinguished it from the others, such as climate, aggregate type, and binder type. This allowed for a more broad study. A description of each site follows.

#### **US 277 Laredo District**

US Route 277 is located in the Laredo District of TxDOT and is in the southernmost part of the state. The climate is dry and warm (DW) with an annual average of the high temperatures of 86.3°F (30.2°C) and 21.5 inches (545 mm) of average annual precipitation (30). The mixture was a TxDOT Type C mixture (25) with a PG 70-22 binder. The optimum binder content was 4.5% by weight of the mixture. The aggregate consisted of a well graded blend of limestone and manufactured sand from Uvalde County, Texas.

#### **US 83 Childress District**

US Route 83 is located in the Childress District of TxDOT and is located in the northernmost part of the state. The climate is dry and cool (DC) with an annual average of the high temperatures of 74.3°F (23.5°C) and 22.7 inches (576 mm) of average annual precipitation (30). The mixture consisted of a TxDOT Type D mixture (25) with a PG 70-28 binder. The optimum binder content was 5.3% by weight of the mixture. The aggregate consisted of a well graded granite material from Snyder, OK.



## **SH 24 Paris District**

State Highway (SH) 24 is located in the Paris District of TxDOT and is located in the northeastern portion of the state. The climate is wet and cool (WC) with an annual average of the high temperatures of 74.0°F (23.4°C) and 47.8 inches (1214 mm) of average annual precipitation (30). The mixture consisted of a TxDOT Type D mixture (25) with a PG 64-22 binder. The optimum binder content was 5.4% by weight of the mixture. The aggregate consisted of a well graded sandstone material from Sawyer, OK.

### *LMLC Sample Preparation*

LMLC samples were fabricated using the Super Gyrotory Compactor (SGC). A blended aggregate gradation was used, and a mixture design was prepared in accordance with Superpave requirements. HMA mixture designs included the materials described in the preceding section. The aggregates used for the samples were heated to a temperature of 300°F (149°C) and left overnight to remove any moisture. The binder was also heated to the same temperature for two hours before mixing. The mixture was then short term oven aged at the molding temperature of 275°F (135°C) for four hours. This short term aging is intended to capture the aging that takes place during mixing, transport, and placement of HMA in the field.

The samples were compacted into cylinders of 6 inch (152 mm) height by 6 inch (152 mm) diameter to the required AV content in the SGC. The initial AV content in these compacted samples was measured to be higher than the specified content due to the conditions imposed by the mold. To remedy this problem, the samples were molded

at a higher AV content and then cored to a 4 inch (102 mm) diameter. The sample had 1 inch (25 mm) trimmed from each end to produce the final 4 inch (102 mm) diameter by 4 inch (102 mm) high sample with the specified range of AV. The coring and trimming of the LMLC samples provided samples with a more uniform distribution of AV, similar to what would be found in the field (27). The AV content used for each of the three mixtures had an average AV content of 5-7%. Optimum binder content, as described in the preceding section for each site, was used in this study.

Prior to laboratory testing, the samples were subjected to artificial laboratory aging for periods of 6, 9, and 12 months at a constant temperature of 140°F (60°C) in an environmental room. Samples tested immediately after fabrication represent the initial aging condition and approximate the pavement condition at the time of placement. After artificial laboratory aging, the sample was centered and glued to steel platens using a vertical gluing jig with high strength 2-ton epoxy glue. The freshly glued sample was left in the jig for a minimum of four hours to ensure complete setting of the glue. Three linear variable displacement transducers (LVDTs) were attached at 120° from each other along the sample diameter.

#### *Field Sample Preparation*

In order to obtain a good representation of HMA mixture behavior under varying conditions and ages, field cores were taken from the wheel path, shoulder, and, where possible, from adjoining wheel path and shoulder sections which had been treated with a chip seal. Field cores were taken from each site at approximately one year intervals

following an initial coring shortly after construction for the purpose of examining the effects of aging.

For US 277, field cores were taken from the wheel path, shoulder, and treated wheel path in July 2008, December 2009, December 2010, and January 2012. The initial coring in 2008 took place just prior to the placement of the chip seal and did not include a treated field core. It is assumed that the treated section would exhibit the same properties as the untreated section at the time of chip seal treatment.

US 83 field cores were collected from the wheel path and shoulder in 2008 with subsequent coring from the wheel path, shoulder, treated wheel path, and treated shoulder in 2009, 2010, and 2011.

SH 24 field cores were collected from the shoulder and wheel path in 2009, 2010, and 2011. This site did not include a treated section.

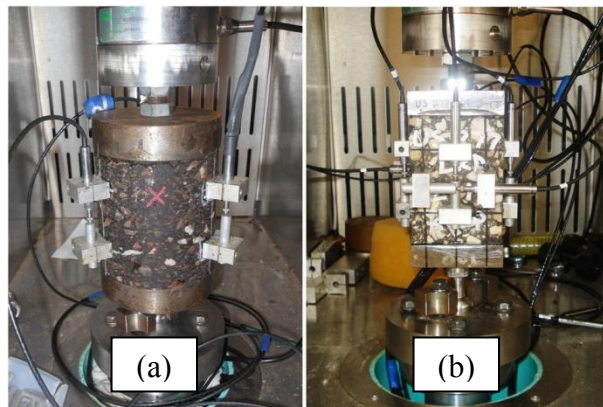
All collected field cores were photographed, catalogued, and trimmed to obtain the surface layer of HMA. The AV content for the surface layer from each core was determined. The layers were then trimmed to the sample shape shown in FIGURE 6. This allowed the samples to be tested in direct tension perpendicular to the direction of traffic, in the same manner they experienced tension in the field under traffic loading.

Following trimming, the samples were placed in a magnetic gluing vice and steel platens were affixed to each end. Imperfections in the trimming process produced samples with ends which were not always perfectly parallel. The magnetic vice provided a way to ensure that the platens were aligned with each other, and not with the imperfectly trimmed samples. This helped to eliminate eccentricities in the testing

process and minimized undesirable moments. Finally, LVDTs were affixed to each side of the sample with a 2 inch (50.8 mm) gauge spacing for a total of four LVDTs.

### *Testing Procedures*

LMLC and field samples were tested following the same procedure. Samples were placed in a servo-hydraulic testing machine with a fixed connection at the top of the sample. A pinned connection, by way of a ball and socket joint, was used for the bottom of the sample to help align the sample in the testing machine and further minimize undesired moments during testing. The test setup for both LMLC and field samples is shown in FIGURE 23, which also shows the LVDT placement.



**FIGURE 23 Test setup for (a) LMLC and (b) field samples.**

The samples were tested using two uniaxial test methods developed at Texas A&M University. These include the Viscoelastic Characterization (VEC) test (13) and the Modified Repeated Direct Tension (RDT\*) Test (15).

For the VEC test, a monotonically increasing load is applied to the sample at a machine displacement rate of 0.002 inches per minute (50.8  $\mu\text{m}$  per minute). This continued until one of the measuring LVDTs recorded a displacement of 100  $\mu\epsilon$ . It was assumed that at 100  $\mu\epsilon$  the sample is not damaged and can subsequently be retested (13). Each sample was tested with load and displacement data collected at 50° F (10° C), 68° F (20° C), and 86° F (30° C). The load and displacement data were used to calculate the respective stresses and strains.

Stresses and strains calculated from the VEC test were then processed using fitting parameters and Laplace transformations to create relaxation and complex modulus master curves at 68° F (20° C) (13).

Following the VEC tests, the samples were reconditioned to 68° F (20° C) and tested using the RDT\* test. For the RDT\* test, the samples were subjected to repeated, strain controlled loading. Strain levels were controlled by one of the sample-mounted LVDTs.

Initially, the samples were subjected to a tensile load resulting in an undamaging strain level of 30  $\mu\epsilon$ . The sample was then compressed back to its original configuration. This haversine loading cycle was repeated for 50 cycles at a frequency of 1 Hz in order to obtain the undamaged properties of the mixture, including the dynamic modulus ( $E_{ve}$ ). The results of this portion of the test were also used to verify the results of the VEC test.

Following a short resting period of 5 to 10 minutes, the samples were then subjected to 1000 cycles of a 175  $\mu\epsilon$  strain level at a frequency of 1 Hz. These cycles were used to capture the damaged behavior of the mixture.

By using both the undamaged mixture properties and the results of the damaged portion of the uniaxial repeated load test, the dissipated pseudo-strain energy (DPSE) associated with fracture was calculated. The DPSE associated with fracture, AV contents, and binder film thicknesses (based on aggregate gradation and binder content) were then used to calculate damage parameters such as Paris' Law fracture coefficient ( $A$ ) and exponent ( $n$ ) (15).

All of these mixture properties were then used in the CMSE\* performance prediction model (15, 19) to calculate  $N_f$ .

### **LMLC Sample Test Results**

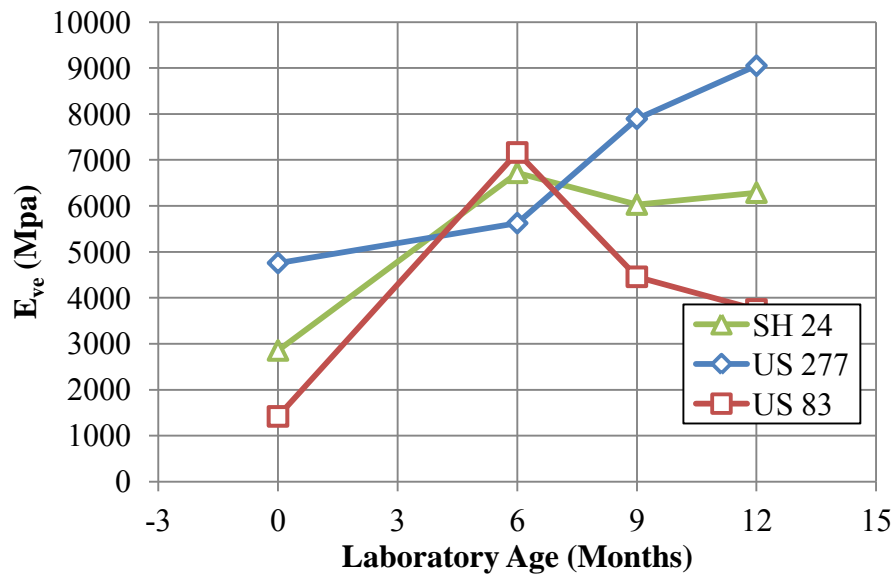
VEC and RDT\* tests were carried out on LMLC samples at different AV and binder content combinations selected by a D-optimal statistical design. The design aimed at evaluating the effects of these two mixture parameters on mixture properties and performance.

FIGURE 24 shows the  $E_{ve}$  values for the three different sites at optimum binder content and medium AV.  $E_{ve}$  increases considerably with age confirming that the mixture becomes stiffer with time. US 277 was the stiffest of the three sites, while US 83 had the lowest stiffness. Also, US 277 continued to show an increase in the modulus after nine months while the other two sites start to level off.

An Analysis of Variance (ANOVA) test of the data showed that AV, binder content, and aging level had statistically significant effects on  $E_{ve}$  with no statistically significant interaction effects among them. A Tukey Honest Significant Differences

(HSD) analysis for each of significant factors was also performed, which confirmed that the overall  $E_{ve}$  was statistically different for all three AV contents. Mixtures with low AV (<4%) exhibited higher  $E_{ve}$  values than those with medium (5-7%) and high (>7%) AV. The insignificant interaction effects between AV and aging level is evidenced by the similar rate of change in  $E_{ve}$  over time.

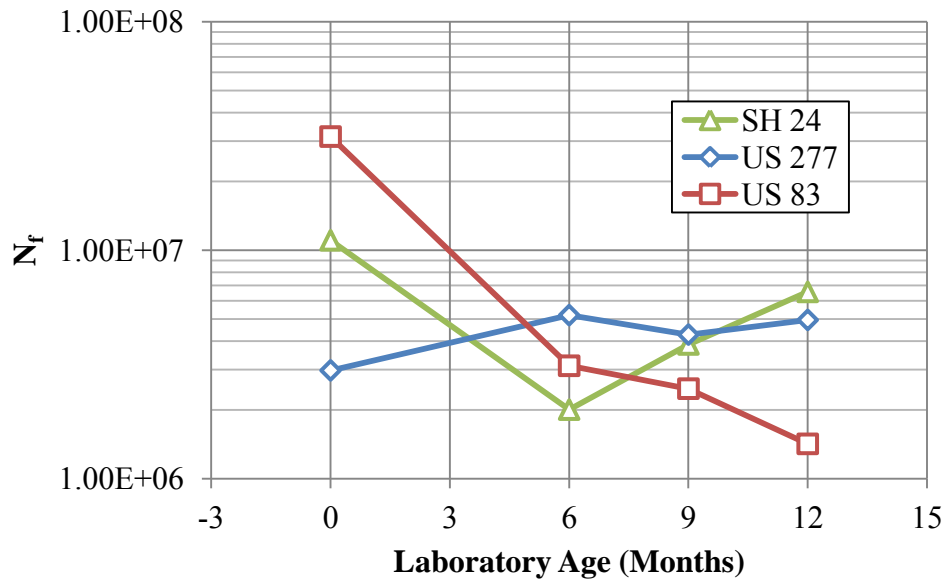
A Tukey HSD analysis of binder content showed that there was no statistically significant difference between optimum and optimum +0.5%. However, a significant difference was found between optimum -0.5% and optimum as well as between optimum -0.5% and optimum +0.5%.



**FIGURE 24**  $E_{ve}$  trends for artificially laboratory aged LMLC samples.

FIGURE 25 shows the  $N_f$  for the three mixtures at optimum binder content and medium AV.  $N_f$  for US 83 decreases with age which is consistent with the observation

that the mixture stiffens with age and becomes more susceptible to failure. US 277 and SH 24 show slight increases in  $N_f$  with time; however, the overall trends are relatively stable when compared with that for US 83. Based on these results, the US 83 mixture is more sensitive to the effects of aging.



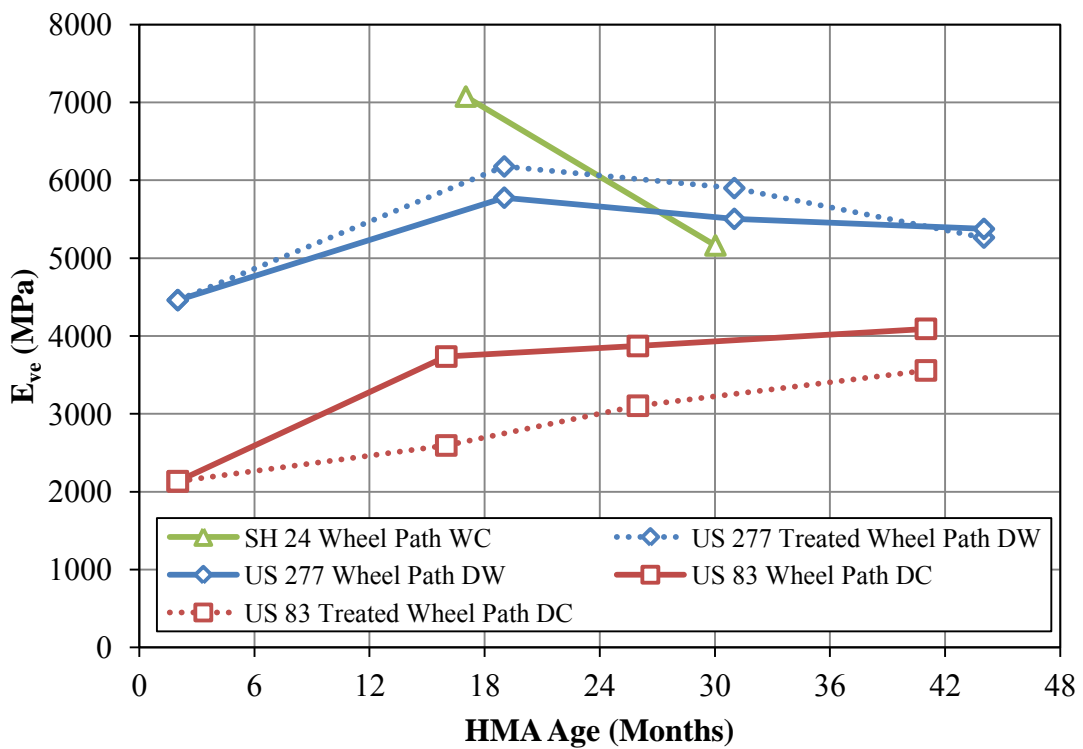
**FIGURE 25**  $N_f$  trends for artificially laboratory aged LMLC samples.

### Field Sample Test Results

Data collected from the tests performed on the field samples for US 277, US 83, and SH 24 were analyzed and evaluated. Results from both the wheel path and shoulder were examined. FIGURE 26 shows the  $E_{ve}$  values for the treated and untreated wheel path sections. As with the LMLC samples, the  $E_{ve}$  values for US 83 continue to increase with age. However, the  $E_{ve}$  values for US 277 exhibit a sharp increase followed by a gradual



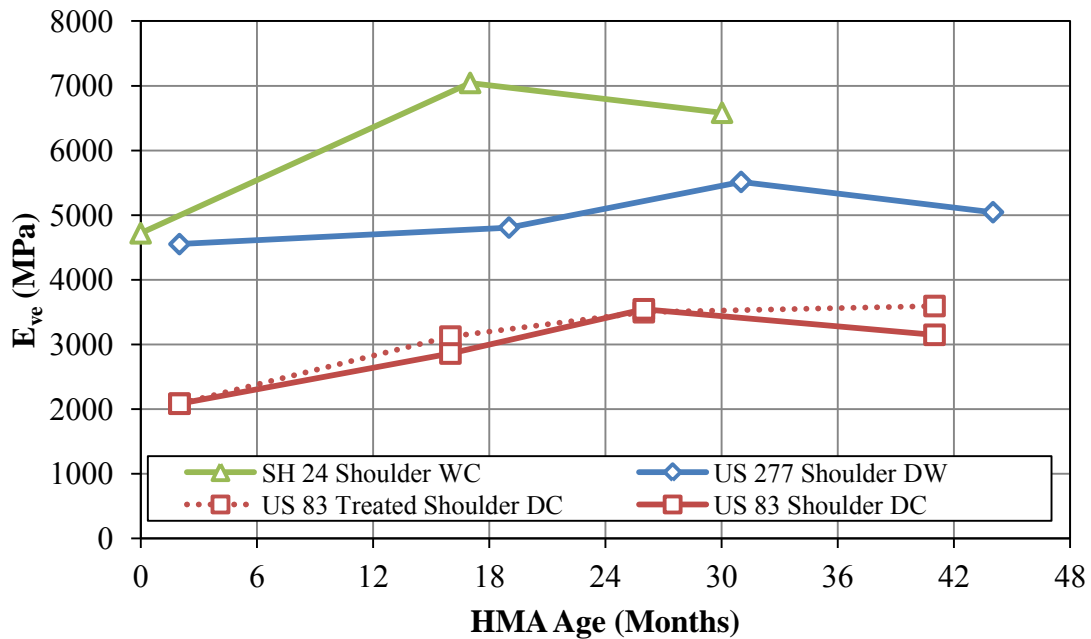
decrease. This may be a result of the formation of micro cracks in the trafficked wheel path, which are resulting in a weakening of the layer. The same can be said for the results of the  $E_{ve}$  values for the SH 24 samples. Note that the treated wheel path  $E_{ve}$  values for US 277 are similar to those found in the untreated wheel path, indicating that the treatment had minimal effect on the overall stiffness of the HMA layer. However, there appears to be a significant benefit from the chip seal treatment on the trafficked wheel path section of US 83, which is located in a cooler climate than US 277.



**FIGURE 26**  $E_{ve}$  for field samples taken from the wheel path.

In order to more directly examine the effects of aging without the confounding effects of traffic, the shoulder samples were analyzed and evaluated. FIGURE 27 shows  $E_{ve}$  for the shoulders of US 277, US 83, and SH 24. Each site shows an initial increase in  $E_{ve}$  to a maximum value followed by a slight decrease. This minimal change in  $E_{ve}$  after the initial jump may be associated with a more steady, level trend which continues in the future and is similar to previous results found in aged binder testing (31, 32). Also note that the treatment placed on the shoulder of US 83 appears to have no major effect on the overall  $E_{ve}$  of the HMA layer. For both the wheel path and shoulder, there is a sharp increase in  $E_{ve}$  over the first 18 months. For the US 277 and US 83 shoulder samples, this upward trend continues past 24 months. While some of this increase may be due to the impact of traffic loading on the wheel path samples, the increase in  $E_{ve}$  for the shoulder samples can be attributed more directly to mixture aging.

While the  $E_{ve}$  value provides an indication of the HMA mixture response to oxidative aging of the binder, which also plays a role in the fatigue failure of HMA, it is important to examine the  $N_f$  values calculated from the CMSE\* method.  $N_f$  includes other influential factors such as binder film thickness, AV content, binder content, and pavement structure as well as damage properties including Paris' Law fracture coefficient and exponent and the rate of fracture damage accumulation. FIGURE 28 shows the calculated values of  $N_f$  for the wheel paths of US 277, US 83, and SH 24. Boxes near the data points indicate the AV content of the HMA layer in the field.

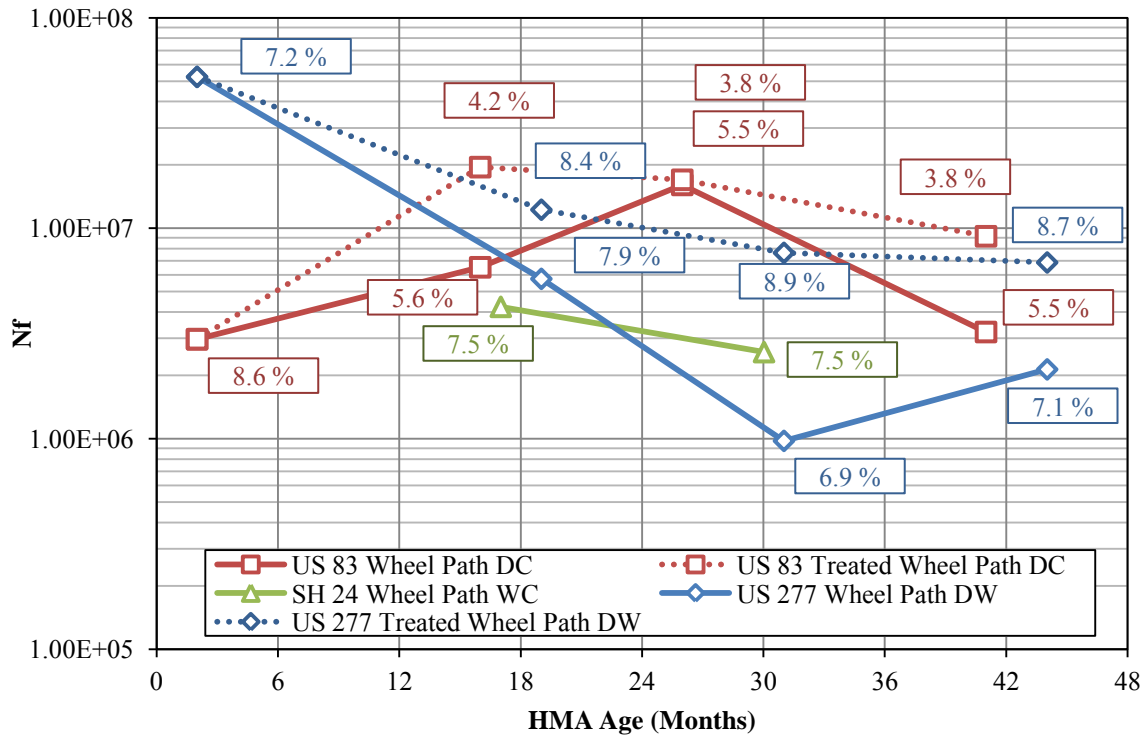


**FIGURE 27**  $E_{ve}$  for field samples taken from the shoulder.

As expected, US 277 and SH 24 show a continued decrease in  $N_f$  values as the pavement ages and is subjected to traffic. For both of these cases, the AV content in the field remains relatively constant. Following the collection of the third core, the US 277  $N_f$  values increase slightly. This may be attributed to the placement of a chip seal shortly after the third core collection, indicating a small benefit from a treatment placed a few years after the pavement is constructed. The  $N_f$  values for the treated section of US 277 decrease at a slower rate than those for the untreated section, indicating that the chip seal slows the rate of damage to the pavement due to fatigue.

US 83 shows an increase in  $N_f$  over the first couple years of cores. Note, however, that the AV content decreases considerably from the first year. As the HMA was exposed to traffic, further compaction occurred, causing the mixture to further

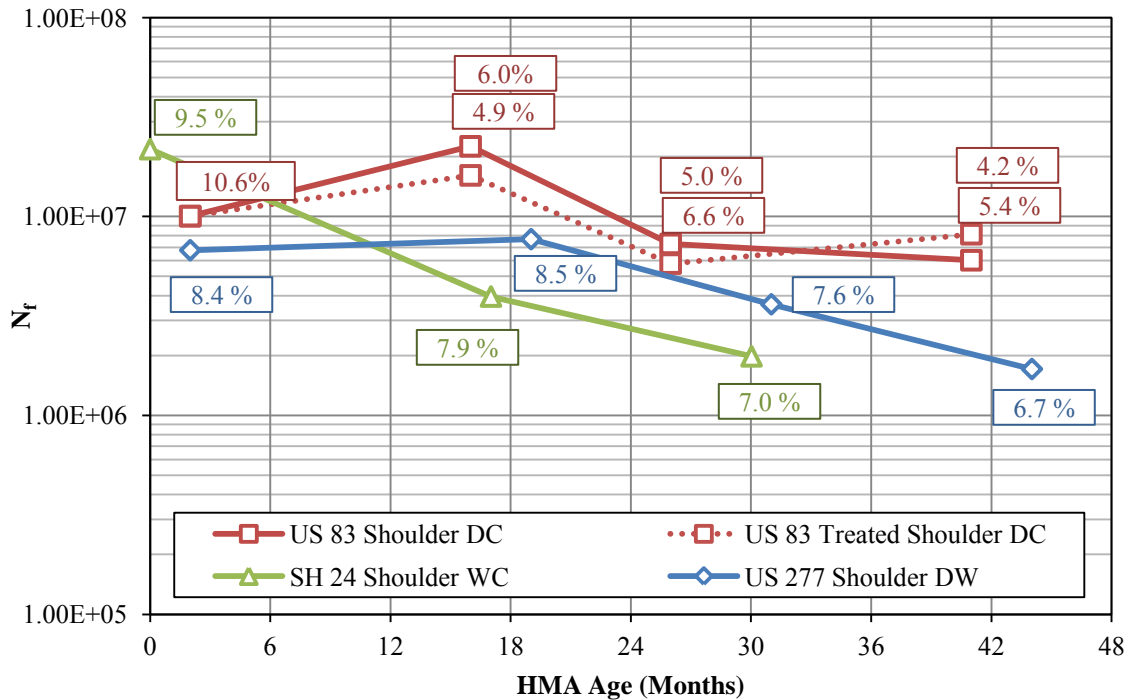
stiffen, which resulted in an extension of the pavement life. In other words,  $N_f$  increased with further compaction and lower AV.



**FIGURE 28**  $N_f$  for field samples taken from the wheel path.

Shoulder  $N_f$  values for US 277, US 83, and SH 24 are shown in FIGURE 29. As previously mentioned, the shoulder values provide more focus on the effects of aging by eliminating the effects due to traffic. Once again,  $N_f$  decreases as the HMA ages, but at a slower rate than for the wheel path samples subjected to traffic. The US 83 values see an increase in  $N_f$  in the early stages (higher AV in the first cores than in the following years), but then follow the slowly decreasing trend exhibited by US 277 and SH 24. The

chip seal placed on the shoulder of US 83 seems to have little effect on extending the pavement life. While the downward trend on the shoulders is less than that for the wheel paths, it is still significant, indicating that HMA aging does have a significant impact on fatigue failure in HMA.



**FIGURE 29**  $N_f$  for field samples taken from the shoulder.

### Comparison of Field and LMLC Sample Results

With both LMLC and field sample data analyzed and examined separately, an evaluation of the combined results was made in order to determine if relationships can be seen between artificially laboratory aged samples and naturally aged field cores.

FIGURE 30 shows the combined results of the LMLC and field sample  $E_{ve}$  values. The top axis represents the artificial aging period for the LMLC samples while the bottom axis is the actual age of the HMA layer in the field. By adjusting the axes to fit the field  $E_{ve}$  to the LMLC  $E_{ve}$ , it was determined that one month of aging in the laboratory was equivalent to 10.5 months of aging in the field for both US 277 and US 83. SH 24 data could not be aligned without a vertical shift in the LMLC results; however, the trends between laboratory and field with the 1:10.5 comparison are similar.

The combined graphical results for  $N_f$  are not as easily interpreted as the  $E_{ve}$  results. While all of the combined  $N_f$  results shown in FIGURE 31 either decrease or remain relatively constant, as expected, any correlations between LMLC and field sample results could not be made directly. This may be due to the number of factors which play a role in the calculation of  $N_f$ . In order to relate the LMLC sample  $N_f$  results to the field  $N_f$  results, a more complex model needs to be developed.

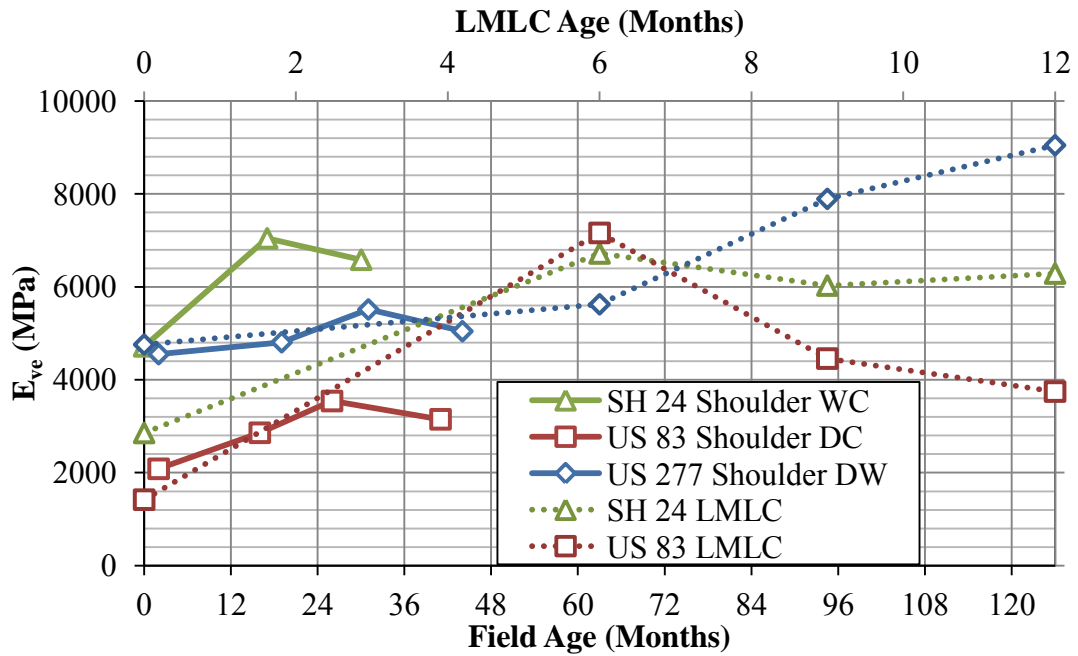


FIGURE 30 LMLC and field sample combined  $E_{ve}$  results.

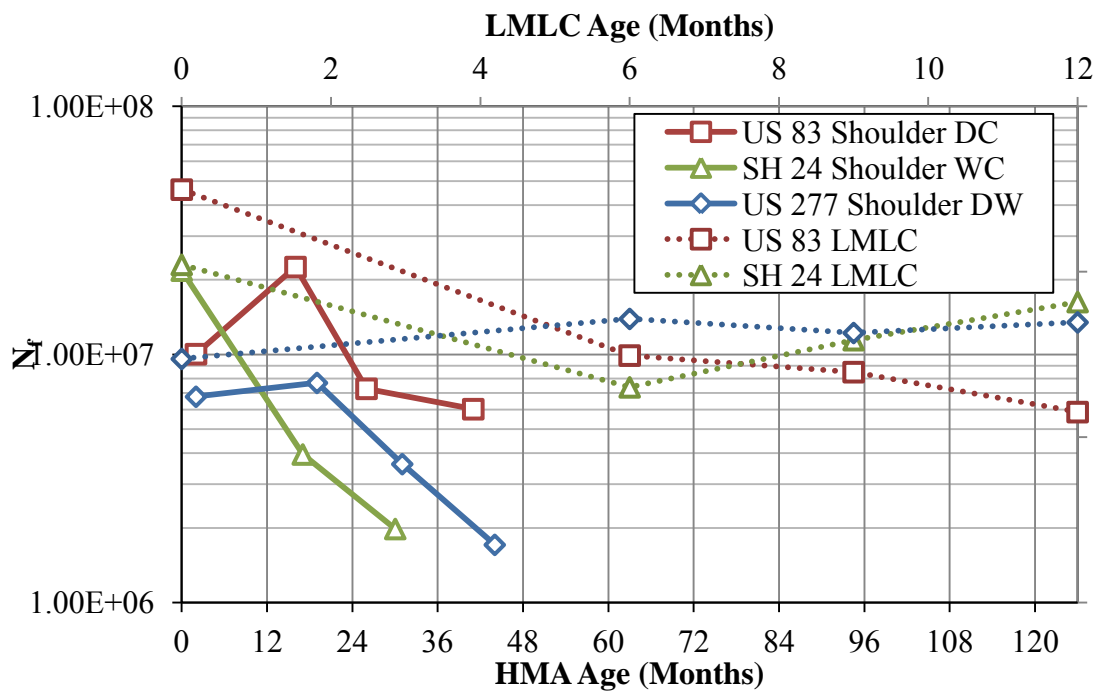


FIGURE 31 LMLC and field sample combined  $N_f$  results.

## Summary

Characterizing the role of aging in the development of fatigue failure in HMA mixtures is not a simple task. There are many factors which play a role, not only in fatigue cracking as a whole, but also in the aging process. In order to effectively characterize and predict HMA aging in the field, aging in LMLC mixtures must be understood and correlated with actual field performance.

This chapter shows that HMA aging through binder oxidation not only occurs, but plays a significant role in the development of fatigue failure. A comparison can be made between artificially laboratory aged LMLC samples and naturally aged field cores taken from the shoulder, where minimal trafficking has occurred. For the sites in Texas included in this study, when comparing  $E_{ve}$ , one month of artificial aging in the laboratory is equivalent to 10.5 months in the field.

Future studies should include the further development of a more mechanistic model to predict  $N_f$  in the field from mixture data collected from unaged LMLC samples available during mixture design and collected unaged binder data, in combination with accelerated laboratory aged binder data or aged binder data calculated using existing models (32). This can be accomplished by developing the relationship between artificially laboratory aged LMLC  $N_f$  values and  $N_f$  values obtained from naturally aged field samples. By developing this relationship with field cores taken from the shoulder, the impact of aging without the confounding effects of traffic can be better understood and predicted. With these components, a pavement prediction model that accounts for aging and its impact on  $N_f$  in the field can be fully developed.



CHAPTER V  
INVESTIGATION OF FACTORS AFFECTING AGING OVER MULTIPLE FIELD  
SITES

In order to move toward a more mechanistic model which includes aging for predicting  $N_f$ , it's necessary to determine which factors have the greatest affect on fatigue cracking, particularly, those factors related to aging.

In this chapter, the data collected from 21 sites across the state of Texas are used. Three of the sites are US 277, US 83, and SH 24, which were described in the preceding chapter. A description of the 18 additional sites is also given. Cores from these sites were trimmed and analyzed in the same fashion as those from the preceding chapters. Factors which affect the calculation of  $N_f$  will be listed as well as additional factors which may contribute to the aging affects. A multivariate linear regression analysis of all sites, including samples from both the wheel path and shoulder, was made. Factors found to be influential in the regression are listed. Another multivariate linear regression analysis was made from the data collected from only the wheel path samples. The factors influencing  $N_f$  for these sites are also listed. A final multivariate linear regression analysis on the shoulder samples is also discussed. The factors identified from the shoulder only analysis are those factors which are influential in aging. Finally, a linear regression model is included for prediction of  $N_f$  on the shoulder, which includes the factors that have been shown to be influential in the aging process.

## Material Selection

Twenty-one sites across Texas were used in this part of the study. Sites were selected from five different climate zones which include DW, DC, WW, WC, and moderate (M). Each site had different characteristics, such as aggregate type, binder type, binder content, and layer of interest. All binders were classified as Superpave Performance Grade (PG) binders. Cores were taken from the shoulder, wheel path, treated and untreated shoulder and wheel path where possible. Each site and its associated characteristics are listed in TABLE A-1 of Appendix A. An abbreviated list showing location, climate, construction date, and binder type is shown in TABLE 5.

Testing and subsequent data collection for several cores collected from US Route 190 was not possible due to the stiffness of the samples. The high modulus values (ranging from 7500 to 11,000 MPa) discovered during the non-damaging tests caused the samples to fail prematurely during the damaging portions of testing, leaving an incomplete data set for this site. A similar situation occurred for US Route 54. This site was constructed in 1998 resulting in samples which were extremely brittle. Again, failure occurred during the damaging portion of the RDT\* test, resulting in an incomplete data set. State Highway 59 and US Route 69 had similar problems with a few samples, but not to the same degree as US Route 190 and US Route 54. However, of the 218 samples tested from the shoulder and wheel path of the listed sites, 191 ran to completion and provided enough data to calculate  $N_f$ .

**TABLE 5 Field Sample Collection Sites**

<b>TxDOT District</b>	<b>Location</b>	<b>Climate</b>	<b>Construction Date</b>	<b>Binder Type</b>	<b>TxDOT District</b>	<b>Location</b>	<b>Climate</b>	<b>Construction Date</b>	<b>Binder Type</b>
Bryan	US Route 290	M	2002	PG 64-22	Lubbock	US Route 84	DC	2009	PG 70-22
Atlanta	Interstate Highway 20	WC	2001	PG 76-22	Childress	US Route 83	DC	2008	PG 70-28
Waco	Interstate Highway 35 Layer #5	M	2002	PG 70-22	Yoakum	State Highway 36	WW	2006	PG 64-22
Wichita Falls	State Highway 59	DC	2007	PG 70-22	Atlanta	US Route 259	WC	2005	PG 76-22
Laredo	Interstate Highway 35 Layer #3	DW	2007	PG 76-22	Paris	State Highway 24	WC	2009	PG 64-22
Laredo	Interstate Highway 35 Layer #4	DW	2007	PG 70-22	Odessa	Farm to Market 1936	DW	2002	PG 70-22
Lufkin	US Route 69	WW	2003	PG 70-22	Pharr	Farm to Market 2994	DW	2002	PG 70-22
Laredo	Farm to Market 649	DW	2006	PG 76-22	Amarillo	US Route 54	DC	1998	PG 70-28
Laredo	US Route 277	DW	2008	PG 70-22	Paris	State Highway 19/24	WC	2000	?
Tyler	US Route 259	WC	2007	PG 70-22	Bryan	State Highway 6	M	2000	?
Lubbock	US Route 82	DC	2008	PG 76-22					

## Multivariate Linear Regression Factors

There are several factors which contribute to the calculation of  $N_f$  as well as other factors which are influential in evaluating pavement performance in the field. For this study, nine factors were selected which were assumed to have an impact on or are influenced by the aging of HMA pavements. Some of these factors are included in the calculation of  $N_f$  while others are not.

The factors associated with  $N_f$  are percent binder content by weight of mixture (AC), AV content, rate of accumulation of dissipated pseudo strain energy ( $b$ ), maximum design shear strain located at the edge of a loaded tire at the top of the layer of interest ( $\gamma$ ), and  $E_{ve}$  (16).

Additional factors which were assumed to influence (or are influenced by) the aging of HMA included the age of the HMA layer of interest in years, climate conditions (DW, DC, WW, WC, and M), location of the HMA sample whether WP or SH, and the crack ratio ( $c_{1000}/c_0$ ). For the statistical analysis, climate conditions of DW, DC, WW, WC, and M were numbered 1, -1, 2, -2, and 0, respectively, with WP represented with 1 and SH represented with 0.

$c_{1000}/c_0$  is a ratio of the size of an average crack in the field sample after 1000 loading cycles in the RDT\* test to the original crack size before testing.  $c_{1000}$  and  $c_0$  are both values which can be calculated based on the sample cross sectional area, AV content, and the response in repeated load testing (33).

## Multivariate Linear Regressions

With these nine factors selected, linear regression analysis was performed. In order to get a full view of the impact of these factors on aging and the calculation of  $N_f$ , a linear regression was performed first on all of the collected data, regardless of WP or SH location, followed by a linear regression on just the wheel path sample data, and finally on the data collected from the shoulder samples. Shoulder samples experience an insignificant amount of traffic, and so it can be assumed that any change in  $N_f$  is associated with the aging of the HMA mixture. If the factors selected are influential in the aging process, then a linear regression should create a linear model which fits the collected data relatively well. The linear regressions for the combined and wheel path data would be expected to produce models with a poor fit, since the wheel path sections experience traffic loading and would have additional factors which contribute to  $N_f$ .

For all three scenarios, a stepwise, mixed mode (forward and backward), linear regression was performed. This was first done with no interactions between terms, then with two way interactions between all terms. The stepwise linear regression starts with a basic linear model which includes a dependant variable ( $y$ ), and intercept term ( $\beta_0$ ) and an error term ( $\varepsilon$ ) as seen in Equation 9.

$$y = \beta_0 + \varepsilon \tag{9}$$

Each factor is then added, one independent variable at a time based on an  $F$ -test. The factor which provides the largest  $F$  value for the regression is added to the model.

For the second step, the two factors which provide the largest  $F$  values for the two factor model are added. In this case, the first factor may not be included in the model that includes the best two factors. Each  $F$  value is calculated as shown in Equation 10. This calculated value must be greater than  $F_\alpha$ , which is the  $F$ -test statistic for a predetermined level of significance,  $\alpha$ . Factors continue to be added until an individual factors  $F$  value is less than  $F_\alpha$  (34). For this study, an  $\alpha$  of 0.25 was used.

$$F_j = \frac{SSR_j - SSR}{MSR} \quad j = 1, 2, \dots \quad (10)$$

where,

- $F_j$  =  $F$  value for the  $j^{\text{th}}$  factor
- $SSR_j$  = sum of squares residuals for model containing all but  $j^{\text{th}}$  factor
- $SSR$  = sum of squares residual for the complete model
- $MSR$  = mean square error for the complete model.

#### *Combined Location Linear Regression*

A linear regression was first performed on the complete data set, which included samples from all sites in both the shoulder and the wheel path. In order to confirm that there were no collinear factors included in the model, a multivariate correlation matrix was created and is shown in TABLE 6 for the full data set. Any correlations over 0.9 indicate that two variables are highly correlated and may cause problems in the analysis

(34). In this particular case, there are no strong correlations between any of the factors.

In fact, the strongest correlation is found between  $E_{ve}$  and  $N_f$  with a correlation value of -0.40.

**TABLE 6 Correlation Matrix for All Data**

	Age	AC	AV	$E_{ve}$	$B$	$\gamma$	$N_f$	$c_{1000}/c_0$	Climate	Location
Age	1.00	0.08	0.31	0.18	-0.04	0.07	-0.17	0.05	0.08	-0.08
AC	0.08	1.00	-0.20	-0.08	0.02	-0.05	-0.02	0.09	-0.20	-0.04
AV	0.31	-0.20	1.00	0.18	-0.08	0.10	-0.39	0.14	0.00	-0.27
$E_{ve}$	0.18	-0.08	0.18	1.00	0.07	-0.17	-0.40	0.21	0.08	0.08
$b$	-0.04	0.02	-0.08	0.07	1.00	0.20	0.16	-0.12	-0.05	-0.12
$\gamma$	0.07	-0.05	0.10	-0.17	0.20	1.00	-0.08	-0.06	0.09	0.00
$N_f$	-0.17	-0.02	-0.39	-0.40	0.16	-0.08	1.00	-0.17	-0.02	-0.07
$c_{1000}/c_0$	0.05	0.09	0.14	0.21	-0.12	-0.06	-0.17	1.00	-0.01	0.06
Climate	0.08	-0.20	0.00	0.08	-0.05	0.09	-0.02	-0.01	1.00	0.05
Location	-0.08	-0.04	-0.27	0.08	-0.12	0.00	-0.07	0.06	0.05	1.00

The first regression analysis included only the individual factors with no interactions between them. This model included the following terms in order of significance:

- $E_{ve}$
- AV
- $b$
- AC
- $\gamma$
- Location

Climate, Age, and  $c_{1000}/c_0$  were all eliminated from the model. However, this model had a coefficient of variation ( $R^2$ ) value of 0.34, indicating that the model is a poor predictor of actual performance.

In an attempt to create a better model, the stepwise linear regression was re-evaluated to include two way interactions. For this scenario, all of the factors from the first model were included along with 14 additional individual and combined factors. The  $R^2$  value improved to 0.60. All factors were represented in this scenario as either individual or combined factors except for  $c_{1000}/c_0$ .

To further refine the model, the data were separated based on whether or not the field cores were taken from SH or WP. A stepwise linear regression was then performed on each. It was expected that the WP model would not create a quality model because the  $N_f$  values for these samples are dependent on other factors, such as traffic and healing, in addition to those that influence aging.

#### *Wheel Path Linear Regression*

It was expected that the WP model would not create a quality model because the  $N_f$  values for these samples are dependent on other factors, such as traffic and healing, in addition to those that influence aging. However, by running the regression on both the SH and WP, it provides a method of showing that the factors selected are effective for predicting  $N_f$  where  $N_f$  is influenced primarily by aging. If the model for SH is a good fit, then the factors included are sufficient. As stated previously, it is known that there are other factors influencing  $N_f$  in the wheel path, so if the model for the WP also fits with a similar  $R^2$  value as found for the SH, then the model for both WP and SH are flawed. If the model for the WP doesn't fit well, then it simply confirms that there are other factors that must be included in the WP model.



In order to confirm that there were no collinear factors included in the model, a multivariate correlation matrix was created and is shown in TABLE 7 for the WP data set. There are no strong correlations between any of the factors. The strongest correlation is found between AV and  $N_f$  with a correlation value of -0.43.

**TABLE 7 Correlation Matrix for WP Data**

	Age	AC	AV	$E_{ve}$	B	$\gamma$	$N_f$	$c_{1000}/c_0$	Climate
Age	1.00	0.20	0.21	0.04	0.03	0.18	0.01	0.04	0.13
AC	0.20	1.00	-0.23	-0.05	-0.04	-0.17	0.14	0.18	-0.29
AV	0.21	-0.23	1.00	0.14	-0.06	0.42	-0.44	0.00	0.13
$E_{ve}$	0.04	-0.05	0.14	1.00	0.19	-0.11	-0.38	0.10	0.09
b	0.03	-0.04	-0.06	0.19	1.00	-0.11	0.15	-0.11	-0.08
$\gamma$	0.18	-0.17	0.42	-0.11	-0.11	1.00	-0.09	-0.03	0.05
$N_f$	0.01	0.14	-0.44	-0.38	0.15	-0.09	1.00	-0.13	-0.03
$c_{1000}/c_0$	0.04	0.18	0.00	0.10	-0.11	-0.03	-0.13	1.00	-0.06
Climate	0.13	-0.29	0.13	0.09	-0.08	0.05	-0.03	-0.06	1.00

The first regression analysis for the WP included only the individual factors with no interactions between them. This model only included the following terms in order of significance:

- AV
- $E_{ve}$
- b

Climate, Age, AC,  $\gamma$ , and  $c_{1000}/c_0$  were all eliminated from the model. This model had an  $R^2$  value of 0.33, which is slightly lower than the  $R^2$  value for the full data set. This also indicates that the model is a poor predictor of actual performance. However, with the full data set, a better regression was obtained by including 2 way interactions

between factors. The same was done for the WP data in order to create a better model. However, the 2 way interaction model for WP only yielded an  $R^2$  value of 0.46. Only 6 additional terms were added to the model indicating that many of the selected factors or their interaction effects did not have a significant impact on the development of  $N_f$ .

These results confirm that the WP  $N_f$  cannot be well predicted with factors selected to model aging. Additional factors, such as traffic, would need to be added to obtain a more accurate linear regression model. This also does not show whether or not the factors selected for modeling are sufficient to characterize aging, but it is a step in the right direction. In order to determine which factors are significant in the effect of aging on  $N_f$ , a linear regression model for the SH must be created.

#### *Shoulder Linear Regression*

If the factors selected to characterize aging are sufficient, then the models for the SH should have a relatively high  $R^2$  value. As with the full data and WP analysis, the first step in the process is to confirm that there are no collinear effects between factors. The correlation matrix for the SH data is shown in TABLE 8. Once again, there are no strong correlations between factors with the highest correlations occurring between  $N_f$  and  $E_{ve}$  with a correlation value of -0.43 and between  $N_f$  and AV with a correlation value of -0.41. Thus, collinear effects are not a concern.

**TABLE 8 Correlation Matrix for SH Data**

	Age	AC	AV	$E_{ve}$	$b$	$\gamma$	$N_f$	$c_{1000}/c_0$	Climate
Age	1.00	-0.07	0.37	0.31	-0.09	0.09	-0.29	-0.04	0.03
AC	-0.07	1.00	-0.24	-0.09	0.07	-0.10	-0.14	0.11	-0.09
AV	0.37	-0.24	1.00	0.26	-0.15	0.01	-0.41	0.01	-0.08
$E_{ve}$	0.31	-0.09	0.26	1.00	-0.02	-0.03	-0.43	0.13	0.05
$b$	-0.09	0.07	-0.15	-0.02	1.00	0.37	0.15	0.00	-0.03
$\gamma$	0.09	-0.10	0.01	-0.03	0.37	1.00	-0.06	-0.01	0.05
$N_f$	-0.29	-0.14	-0.41	-0.43	0.15	-0.06	1.00	-0.07	0.00
$c_{1000}/c_0$	-0.04	0.11	0.01	0.13	0.00	-0.01	-0.07	1.00	-0.03
Climate	0.03	-0.09	-0.08	0.05	-0.03	0.05	0.00	-0.03	1.00

The first regression analysis for the SH included only the individual factors with no interactions between them. This model included the following terms in order of significance:

- AV
- AC
- $E_{ve}$
- Age

Climate,  $b$ ,  $\gamma$ , and  $c_{1000}/c_0$  were eliminated from the model. This model had an  $R^2$  value of 0.37, which is slightly lower than the  $R^2$  value for the full data set. This is slightly higher than both the full data set and WP  $R^2$  values, but it still does not indicate a quality model. A much higher  $R^2$  value is necessary to provide an acceptable level of confidence in the model. This also shows that a successful model cannot be made without including interaction effects between factors.

To create a better model and to identify the factors and interactions that are significant to the aging process, a linear regression model was made which included two

way interactions for the SH data. There are 14 terms which were included in the model. These terms, or factors, with the exception of the intercept term, in order of significance, are:

- Age and  $\gamma$
- Age
- $\gamma$
- AC and  $\gamma$
- AV
- AC
- $E_{ve}$
- Age and AV
- Age and  $E_{ve}$
- $b$
- AV and  $b$
- AV and  $E_{ve}$
- AC and  $b$

Climate and  $c_{1000}/c_0$  were eliminated from the model, indicating that their contribution to the aging model was insignificant. The  $R^2$  value was 0.76, which is considerably better than the 0.46  $R^2$  value for the WP and the 0.60  $R^2$  value for the full data set.

The linear regression model for  $N_f$  in the SH, as produced by the statistical analysis software, is shown in Equation 11.

$$\begin{aligned}
N_f = & -237676549 + 19403569 * \text{Age} + 5422172743 * \text{AC} - 5012173 * \text{AV} - 6906 * E_{ve} & (11) \\
& + 134333010 * b - 96921553487 * \gamma \\
& + (\text{Age} - 2.57) * \left[ \begin{aligned} & (2008549 * (\text{AV} - 8.02)) + (2123 * (E_{ve} - 5674)) \\ & + (104341948133 * (\gamma - 0.000468)) \end{aligned} \right] \\
& + (\text{AC} - 0.0533) * \left[ \begin{aligned} & (-10859954160 * (b - 0.08236)) \\ & + (26241653875302 * (\gamma - 0.000468)) \end{aligned} \right] \\
& + (\text{AV} - 8.02) * \left[ \begin{aligned} & (977.8 * (E_{ve} - 5673.72)) \\ & + (-48793007 * (b - 0.0824)) \end{aligned} \right]
\end{aligned}$$

By eliminating the Location factor through the removal of the WP data from the analysis, a much better model of the effects of aging was obtained. The difference in  $R^2$  value for the SH from the other two analysis confirm that the factors used to evaluate the shoulder were the correct factors to use and were significant in the aging process. It also confirms that aging plays a significant role in the lowering of  $N_f$  with time.

### Summary

While the linear regression of the SH data provided a good fit with the measured data, the model provided is simply a means to an end. The regression provides a good look at which factors play a significant role in aging, but further work is required to determine the type of model which these factors should be used in. A linear fit may not be the best option for moving towards a more mechanistic prediction model.

Future research should include an evaluation of several different model types using the factors identified in this chapter. Also, it is a concern that the linear regression model eliminated the Climate factor. Much of the accelerated aging work done on binders involves increasing the temperature to which it is exposed to speed up the aging process (31, 35). A more defined climate number may prove to be more influential in the aging process than a climate value based solely on five different climate zones. Perhaps the use of an average annual high temperature and an average high humidity value, separated into two different factors, would change the outcome of the linear regression and provide an even better fitting model. Regardless of the influence of the Climate factor, the other factors identified play a significant role and should be included in future modeling efforts.

## CHAPTER VI

### CONCLUSIONS

As 100 years of transcontinental highway construction approaches, it is important to investigate and evaluate the methods currently used to predict the performance of HMA pavements. New testing methods and a better understanding of all the factors which play a role in pavement performance are necessary for finding an economic, lasting solution for the next 100 years.

This study has examined a new way of testing field samples in direct tension. The results of tests performed on over 200 samples using this new methodology have been analyzed and evaluated to investigate the effects of aging on HMA fatigue cracking. The factors which play the most prominent role in the aging phenomenon have been identified using the data collected.

By comparing VEC and RDT\* test results from the same sample as well as the results from different samples taken from the same site, it can be seen that these two tests can be successfully applied to field samples. The VEC and RDT\* tests provide a quick and accurate method of determining the material properties necessary to assess fatigue under field conditions. Streamlining of the test preparation and further automation of the analysis will make the VEC and RDT\* tests even more practical methods for determining the material properties of samples obtained from the field.

Researchers will be able to separate and assess the effects of aging and trafficking on the number of loads to fatigue failure by examining VEC and RDT\* test

results from the wheel path and shoulder of any given pavement over time. This, in turn, will allow for more accurate development of mechanistic models which incorporate accurate aging prediction and correctly characterize fatigue. Current and future models can be compared and analyzed for accuracy by testing field samples throughout the life of the pavement and comparing the test results to those obtained from the models.

In order to move towards new models which include the effects of aging, a comparison between LMLC sample test results, field sample test results, and extracted binder test results was made for one field site. The laboratory test results from LMLC and field samples and corresponding extracted binders lead to the following important conclusions regarding HMA aging as well as the effects of chip seals on pavement performance:

- Aging does play a role in the fatigue failure of HMA as evidenced by the performance of field samples, taken over time, from the shoulder. The stiffening of a mixture also coordinates well with an increase in oxidation, represented by CA development in corresponding extracted binders.
- While both AV and binder content play a role in mixture aging, AV plays a much more significant role.
- In general, the rate of aging decreases over time.
- Chip seals appear to slow HMA aging, and, as a result, slow the rate of damage accumulation due to fatigue. However, this effect takes place primarily at the surface of the HMA where the chip seal is placed.



- It is possible to develop a relationship between binder aging and mixture aging. A relationship can also be drawn between *artificially* aged LMLC samples and *realistically* aged field samples.

These generalized conclusions are an important first step in moving toward mechanistic models which incorporate and quantify aging. A relationship between binders and LMLC samples, and between LMLC samples and field samples, lends itself to the potential development of prediction models which incorporate aging. While these findings are a good starting point, a quality fatigue failure prediction model must be applicable to a wide range of HMA mixtures in all types of climates and conditions.

A deeper investigation including three separate field sites shows that HMA aging through binder oxidation not only occurs, but plays a significant role in the development of fatigue failure. A comparison can be made between artificially laboratory aged LMLC samples and naturally aged field cores taken from the shoulder, where minimal trafficking has occurred. For the three sites in Texas included in this study, when comparing  $E_{ve}$ , one month of artificial aging in the laboratory is equivalent to 10.5 months in the field.

While this comparison shows that a relationship exists between LMLC samples and field samples, a more important, and more difficult relationship to develop is the relationship between the LMLC sample  $N_f$  and the field sample  $N_f$ .

In order to move toward the development of this relationship, the factors which play a role in the aging of HMA in the field had to be identified. This was accomplished

using the test results of field cores from 21 sites taken from the shoulder, where the impact of aging without the confounding effects of traffic could be investigated. The field sample test results were used in combination with pre-selected factors in a stepwise linear regression analysis. The linear regression analysis was performed on the total data set, as well as on the data collected from WP samples and SH samples. As expected, the SH samples with two way interactions between factors provided the best linear fit with an  $R^2$  value of 0.76. The following factors and combination of factors were identified as those that play a significant role in the aging of HMA pavements:

- Age and maximum design shear strain located at the edge of a loaded tire at the top of the layer of interest ( $\gamma$ )
- Age
- $\gamma$
- AC and  $\gamma$
- AV
- AC
- $E_{ve}$
- Age and AV
- Age and  $E_{ve}$
- rate of accumulation of dissipated pseudo strain energy ( $b$ )
- AV and  $b$
- AV and  $E_{ve}$
- AC and  $b$ .

While the linear regression of the SH data provided a good fit with the measured data, the model provided is simply a means to an end. The regression provides a good look at which factors play a significant role in aging, but further work is required to determine the type of model which these factors should be used in. A linear fit may not be the best option for moving towards a more mechanistic prediction model.

Future research should include an evaluation of several different model types using the factors identified in this study. Also, it is a concern that the linear regression model eliminated the Climate factor. A more defined climate number, such as an average annual high temperature and an average annual high humidity value, may prove to be more influential in the aging process than a climate value based solely on five different climate zones. Regardless of the influence of the Climate factor, the other factors identified do play a significant role and should be included in future modeling efforts. Additional factors which may play a role, but were not included in the scope of this study are film thickness, which is a representation of aggregate gradation, and binder type. These factors should also be included in future studies.

Future studies should also include the further development of a more mechanistic model to predict  $N_f$  in the field from mixture data collected from unaged LMLC samples available during mixture design and collected unaged binder data, in combination with accelerated laboratory aged binder data or aged binder data calculated using existing models (32).

## REFERENCES

1. U.S. Department of Transportation, Federal Highway Administration. *America's Highways 1776-1976: A History of the Federal-Aid Program*. U.S. Government Printing Office, Washington, D.C., 1976.
2. ———. Highway Statistics 2008, Table HM 220 - Highway Statistics 2008 - FHWA. April 4, 2011. <http://www.fhwa.dot.gov/policyinformation/statistics/2008/hm220.cfm>, Accessed 6/22, 2011.
3. Matthews, J. M., C. L. Monismith, and J. Craus. Investigation of Laboratory Fatigue Testing Procedures for Asphalt Aggregate Mixtures. *Journal of Transportation Engineering*, Vol. 119, No. 4, 1993, pp. 634-654.
4. Arabani, M., and B. Ferdowsi. Laboratory Evaluating and Comparison of the SCB Test Results with Other Common Tests for HMA Mixtures. *Advanced Characterisation of Pavement Soil Engineering Materials, Vols 1 and 2*, 2007, pp. 151-164.
5. Huang, B., X. Shu, and Y. Tang. Comparison of Semi-Circular Bending and Indirect Tensile Strength Tests for HMA Mixtures. In *Advances in Pavement Engineering*, ASCE, 2005, pp. 14.
6. Wen, H. Investigation of Effects of Testing Methods on Characterization of Asphalt Concrete. *ASTM Journal of Testing and Evaluation*, Vol. 31, No. 6, 2003, pp. 7.
7. Wen, H. F. Simple Performance Test for Fatigue Cracking and Validation with WesTrack Mixtures. *Bituminous Paving Mixtures 2002*, No. 1789, 2002, pp. 66-72.
8. Khalid, H. A. Evaluation of Asphalt Fatigue Properties in the Laboratory. *Proceedings of the Institution of Civil Engineers-Transport*, Vol. 141, No. 4, 2000, pp. 171-178.
9. Tayebali, A., J. Deacon, and C. Monismith. Development and Evaluation of Dynamic Flexural Beam Fatigue Test System. *Transportation Research Record*, Vol. 1545, No. - 1, 1996, pp. 89-97.
10. Zhou, F. J. Overlay Tester - Simple Performance Test for Fatigue Cracking. *Transportation Research Record*, No. 2001, 2007, pp. 1-8.
11. Perez-Jimenez, F. Fenix Test Development of a New Test Procedure for Evaluating Cracking Resistance in Bituminous Mixtures. *Transportation Research Record*, No. 2181, 2010, pp. 36-43.

12. Way, G. B. Observations on Current Performance Tests and Prediction Models for Asphalt Concrete Mixes. *Advanced Characterisation of Pavement Soil Engineering Materials, Vols 1 and 2*, 2007, pp. 255-269.
13. Luo, R., and R. L. Lytton. Characterization of the Tensile Viscoelastic Properties of an Undamaged Asphalt Mixture. *Journal of Transportation Engineering*, Vol. 136, No. 3, 2010, pp. 173-180.
14. Lawrence, J. J. Advanced Tools for Characterizing HMA Fatigue Resistance. , 2009.
15. Luo, X., A. E. Martin, R. Luo, R. L. Lytton, and C. J. Glover. *Aging Experiment Design Including Revised CMSE\* Testing Protocols and Analysis to Characterize Mixture Fatigue Resistance*. FHWA-DTFH61-07H-0009, U.S. Department of Transportation Federal Highway Administration, McLean, VA, 2008.
16. Walubita, L. F., A. E. Martin, C. Glover, S. H. Jung, G. Cleveland, and R. L. Lytton. Fatigue Characterization of HMAC Mixtures using Mechanistic Empirical and Calibrated Mechanistic Approaches Including the Effects of Aging. In *Asphalt Concrete: Simulation, Modeling, and Experimental Characterization*, ASCE, 2005, pp. 11.
17. Kutay, M. E. Conventional and Viscoelastic Continuum Damage (VECD) - Based Fatigue Analysis of Polymer Modified Asphalt Pavements. *2008 Journal of the Association of Asphalt Paving Technologists*, Vol. 77, 2008, pp. 395-433.
18. Arambula, E., and M. E. Kutay. Tension-Compression Fatigue Test Evaluation using Fracture Mechanics and Field Data. *Road Materials and Pavement Design*, Vol. 10, No. 1, 2009, pp. 83-108.
19. Walubita, L. F., A. Epps Martin, S. H. Jung, C. J. Glover, and E. S. Park. *Application of Calibrated Mechanistic Fatigue Analysis with Aging Effects*. FHWA/TX-06/0-4468-3, Texas Transportation Institute, College Station, TX, 2006.
20. Baek, C., B. S. Underwood, and Y. R. Kim. Effects of Oxidative Aging on Asphalt Mixture Properties. In *Transportation Research Board 91st Annual Meeting*, Washington D. C., 2012.
21. Al-Azri, N. A., S. H. Jung, K. M. Lunsford, A. Ferry, J. A. Bullin, R. R. Davison, and C. J. Glover. Binder Oxidative Aging in Texas Pavements: Hardening Rates, Hardening Susceptibilities, and Impact of Pavement Depth. *Transportation Research Record*, No. 1962, 2006, pp. pp 12-20.
22. Petersen, J. C., J. F. Branthaver, R. E. Robertson, P. M. Harnsberger, J. J. Duvall, and E. K. Ensley. Effects of Physiochemical Factors on Asphalt Oxidation Kinetics. *Transportation Research Record*, No. 1391, 1993, pp. p. 1-10.

23. Martin, K. L., R. R. Davison, C. J. Glover, and J. A. Bullin. Asphalt Aging in Texas Roads and Test Sections. *Transportation Research Record*, No. 1269, 1990, pp. p. 9-19.
24. Ruan, Y., R. R. Davison, and C. J. Glover. An Investigation of Asphalt Durability: Relationships between Ductility and Rheological Properties for Unmodified Asphalts. *Petroleum Science and Technology*, Vol. 21, No. 1-2, 2003, pp. 231-254.
25. TxDOT. *Texas Department of Transportation Standard Specifications for Construction and Maintenance of Highways, Streets, and Bridges.* , Austin, TX, 2004.
26. Huang, L. K. Evaluation of Semicircular Bending Test for Determining Tensile Strength and Stiffness Modulus of Asphalt Mixtures. *Journal of Testing and Evaluation*, Vol. 37, No. 2, 2009, pp. 122-128.
27. Masad, E., B. Muhunthan, N. Shashidhar, and T. Harman. Internal Structure Characterization of Asphalt Concrete using Image Analysis. *Journal of Computing in Civil Engineering*, Vol. 13, No. 2, 1999, pp. 88-95.
28. Domke, C., M. Liu, R. Davison, J. Bullin, and C. Glover. Study of Strategic Highway Research Program Pressure Aging Vessel Procedure using Long-Term, Low-Temperature Aging Experiments and Asphalt Kinetics. *Transportation Research Record*, Vol. 1586, No. -1, 1997, pp. 10-15.
29. Woo, W. J., E. Ofori-Abebbese, A. Chowdhury, J. Hilbrich, Z. Kraus, A. Epps Martin, and C. J. Glover. *Polymer Modified Asphalt Durability in Pavements*. FHWA/TX-07/0-4688-1, Texas Transportation Institute, College Station, TX, 2007.
30. Belsoft and Styleshout. U.S. Climate Data, Temperature-Precipitation-Sunshine. July 3, 2012. <http://www.usclimatedata.com/>, Accessed July 3, 2012.
31. Glover, C. J., R. R. Davison, C. H. Domke, Y. Ruan, P. Juristyarini, D. B. Knorr, and S. H. Jung. *Development of a New Method for Assessing Asphalt Binder Durability with Field Validation*. FHWA/TX-05/1872-2, U. S. Department of Transportation, Federal Highway Administration, Springfield, VA, 2005.
32. Jin, X., R. Han, Y. Cui, and C. J. Glover. Fast-Rate-Constant-Rate Oxidation Kinetics Model for Asphalt Binders. *Industrial & Engineering Chemistry Research*, Vol. 50, No. 23, 2011, pp. 13373-13379.
33. Luo, X. Characterization of Fatigue Cracking and Healing of Asphalt Mixtures. , 2012.
34. Ott, L., and M. Longnecker. *Introduction to Statistical Methods and Data Analysis*. Brooks/Cole Cengage Learning, Australia ; United States, 2010.

35. Juristyarini, P., R. Davison, and C. J. Glover. Development of an Asphalt Aging Procedure to Assess Long-Term Binder Performance. *Petroleum Science and Technology*, Vol. 29, No. 21, 2011, pp. 2258-2268.

APPENDIX A  
FIELD SITE INFORMATION

**TABLE A- 1 Field Site Information**

<b>TxDOT District</b>	<b>Location</b>	<b>Climate</b>	<b>Construction Date</b>	<b>Binder Type</b>	<b>AC (% of mix by wt.)</b>	<b>Mix Type</b>	<b>Aggregate Type</b>	<b>Layer of Interest Location</b>
Bryan	US Route 290	M	2002	PG 64-22	4.4	Type C	Limestone	Under CMHB Layer
Atlanta	Interstate Highway 20	WC	2001	PG 76-22	5.1	12.5 mm Sp	Sandstone	Below Microseal
Waco	Interstate Highway 35 Layer #5	M	2002	PG 70-22	5.3	19 mm Sp	Igneous / LS	Below 14-15 inch HMA layers
Wichita Falls	State Highway 59	DC	2007	PG 70-22	4.8	Type D	Limestone	Surface Layer
Laredo	Interstate Highway 35 Layer #3	DW	2007	PG 76-22	4.4	25 mm SFHMAC	Traprock/River Gravel	Under two HMA Layers, 4.25 in below surface



**TABLE A- 2 Continued**

<b>TxDOT District</b>	<b>Location</b>	<b>Climate</b>	<b>Construction Date</b>	<b>Binder Type</b>	<b>AC (% of mix by wt.)</b>	<b>Mix Type</b>	<b>Aggregate Type</b>	<b>Layer of Interest Location</b>
Laredo	Interstate Highway 35 Layer #5	DW	2007	PG 70-22	5.9	12.5 mm Sp	River Gravel	Under four HMA Layers, 13 inch below surface
Lufkin	US Route 69	WW	2003	PG 70-22	4.3	Type C	River Gravel	Surface Layer
Tyler	US Route 259	WC	2007	PG 70-22	4.3	Type C	Sandstone / Limestone	Surface Layer
Lubbock	US Route 82	DC	2008	PG 76-22	6.2	CMHB-F	Limestone	Surface Layer
Lubbock	US Route 84	DC	2009	PG 70-22	4.8	CMHB-C	River Gravel / Limestone	Surface Layer
Childress	US Route 83	DC	2008	PG 70-28	5.3	Type D	Granite	Surface Layer
Yokum	State Highway 36	WW	2006	PG 64-22	4.9	Type D	Limestone	Surface Layer
Atlanta	US Route 259	WC	2005	PG 76-22	5.6	Type D	River Gravel	Surface Layer

**TABLE A- 3 Continued**

<b>TxDOT District</b>	<b>Location</b>	<b>Climate</b>	<b>Construction Date</b>	<b>Binder Type</b>	<b>AC (% of mix by wt.)</b>	<b>Mix Type</b>	<b>Aggregate Type</b>	<b>Layer of Interest Location</b>
Paris	State Highway 24	WC	2009	PG 64-22	6	Type D	Sandstone	Surface Layer
Odessa	Farm to Market 1936	DW	2002	PG 70-22	7.3	CMHB-F	Rhyolite	Surface Layer
Pharr	Farm to Market 2994	DW	2002	PG 70-22	5.5	Type D	River Gravel	Surface Layer
Amarillo	US Route 54	DC	1998	PG 70-28	?	Type D	River Gravel	Below Seal Coat
Paris	State Highway 19/24	WC	2000	?	?	Type D	?	Surface Layer
Bryan	State Highway 6	M	2000	?	?	?	?	Surface Layer

## APPENDIX B

### STATISTICAL ANALYSIS DATA

This appendix contains the statistical data tables from all linear regression analysis, including full, WP, and SH analysis.

#### Full Data Set Analysis

This section contains the output for the statistical analysis of the full testing data set from the JMP statistical analysis program.

#### *Stepwise Regression No Interactions*

**TABLE B- 1 Stopping Rule for Full No Interactions**

Prob to Enter	0.25
Prob to Leave	0.25

**TABLE B- 2 Regression Statistics for Full No Interactions**

SSE	DFE	RMSE	RSquare	RSquare Adj	Cp	P	AICc	BIC
1.862e+17	169	33195604	0.3429	0.3196	4.1911597	7	6605.096	6629.598

**TABLE B- 3 Current Estimates for Full No Interactions**

Lock	Entered	Parameter	Estimate	nDF	SS	"F Ratio"	"Prob>F"
X	X	Intercept	150458474	1	0	0.000	1
		Age	0	1	9.61e+12	0.009	0.92594
	X	% Binder	-750754532	1	5.48e+15	4.969	0.02713
	X	% AV	-5566955.7	1	3.14e+16	28.481	3.01e-7
	X	Eve	-7591.12	1	3.31e+16	30.059	1.5e-7
	X	b	110951494	1	6.25e+15	5.674	0.01833
	X	shear	-2.146e+10	1	4.55e+15	4.131	0.04366
		C1000/C0	0	1	8024910	0.000	0.99993
		Climate #	0	1	1.75e+14	0.158	0.69147
	X	Location #	-9729255.8	1	3.66e+15	3.323	0.07007

**TABLE B- 4 Step History for Full No Interactions**

Step	Parameter	Action	"Sig Prob"	Seq SS	RSquare	Cp	p	AICc	BIC
1	% AV	Entered	0.0000	4.77e+16	0.1682	38.391	2	6635.88	6645.25
2	Eve	Entered	0.0000	3.03e+16	0.2750	13.387	3	6613.8	6626.24
3	b	Entered	0.0275	5.74e+15	0.2952	10.262	4	6610.93	6626.43
4	shear	Entered	0.0350	5.14e+15	0.3134	7.6754	5	6608.48	6627.01
5	% Binder	Entered	0.0413	4.72e+15	0.3300	5.4593	6	6606.33	6627.85
6	Location #	Entered	0.0701	3.66e+15	0.3429	4.1912	7	6605.1	6629.6

**TABLE B- 5 Summary of Fit for Full No Interactions**

RSquare	0.342947
RSquare Adj	0.31962
Root Mean Square Error	33195604
Mean of Response	23444113
Observations (or Sum Wgts)	176







**TABLE B- 6 Analysis of Variance for Full No Interactions**

Source	DF	Sum of Squares	Mean Square	F Ratio
Model	6	9.7202e+16	1.62e+16	14.7015
Error	169	1.8623e+17	1.102e+15	<b>Prob &gt; F</b>
C. Total	175	2.8343e+17		<.0001*

**TABLE B- 7 Parameter Estimates for Full No Interactions**

Term	Estimate	Std Error	t Ratio	Prob> t
Intercept	150458474	22971866	6.55	<.0001*
% Binder	-7.508e+8	3.368e+8	-2.23	0.0271*
% AV	-5566956	1043140	-5.34	<.0001*
Eve	-7591.12	1384.591	-5.48	<.0001*
b	110951494	46577118	2.38	0.0183*
shear	-2.15e+10	1.06e+10	-2.03	0.0437*
Location #	-9729256	5336903	-1.82	0.0701

**TABLE B- 8 Sorted Parameter Estimates for Full No Interactions**

Term	Estimate	Std Error	t Ratio	t Ratio	Prob> t
Eve	-7591.12	1384.591	-5.48		<.0001*
% AV	-5566956	1043140	-5.34		<.0001*
b	110951494	46577118	2.38		0.0183*
% Binder	-7.508e+8	3.368e+8	-2.23		0.0271*
shear	-2.15e+10	1.06e+10	-2.03		0.0437*
Location #	-9729256	5336903	-1.82		0.0701

*Stepwise Regression Two Way Interactions*

**TABLE B- 9 Stopping Rule for Full Two Way Interactions**

Prob to Enter	0.25
Prob to Leave	0.25

**TABLE B- 10 Regression Statistics for Full Two Way Interactions**

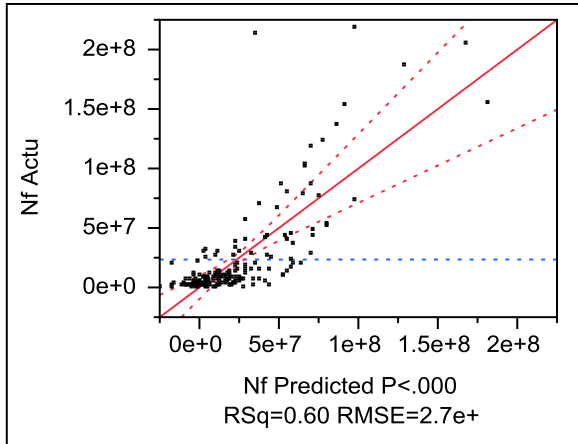
SSE	DFE	RMSE	RSquare	RSquare Adj	Cp	p	AICc	BIC
1.127e+17	155	26967122	0.6023	0.5510	10.280487	21	6550.484	6613.62

**TABLE B- 11 Current Estimates for Full Two Way Interactions**

Entered	Parameter	Estimate	nDF	SS	"F Ratio"	"Prob>F"
X	Intercept	94024309.8	1	0	0.000	1
X	Age	-309885	3	1.56e+16	7.162	0.00016
X	% Binder	184285200	4	1.88e+16	6.480	7.56e-5
X	% AV	-2258837.1	4	3.99e+16	13.725	1.33e-9
X	Eve	-8204.5456	5	6.44e+16	17.710	7.4e-14
X	b	143980207	4	2.12e+16	7.302	0.00002
X	shear	-1.214e+11	5	5.34e+16	14.681	8.9e-12
X	Climate #	1755096.83	2	4.32e+15	2.969	0.0543
X	Location #	-6627094.3	5	1.86e+16	5.112	0.00023
X	(Age-2.64773)*(Eve-5814.88)	1678.91844	1	6.88e+15	9.454	0.00249
X	(Age-2.64773)*(shear-0.00025)	5.1628e+10	1	1.03e+16	14.143	0.00024
X	(% Binder-0.05286)*(b-0.07438)	-8.0203e+9	1	1.55e+15	2.136	0.14588
X	(% Binder-0.05286)*(shear-0.00025)	2.4958e+13	1	1.21e+16	16.610	7.31e-5
X	(% Binder-0.05286)*(Location #-0.52841)	2034874971	1	9.01e+15	12.386	0.00057
X	(% AV-7.33624)*(Eve-5814.88)	1836.70152	1	1.39e+16	19.097	2.27e-5
X	(% AV-7.33624)*(b-0.07438)	-43578362	1	3.06e+15	4.208	0.04191
X	(% AV-7.33624)*(shear-0.00025)	3.9098e+10	1	7.7e+15	10.594	0.00139
X	(Eve-5814.88)*(b-0.07438)	-63327.191	1	5.27e+15	7.242	0.00791
X	(Eve-5814.88)*(Location #-0.52841)	4883.15125	1	2.53e+15	3.481	0.06397
X	(shear-0.00025)*(Location #-0.52841)	-1.177e+11	1	3.2e+15	4.404	0.03748
X	Climate #*(Location #-0.52841)	7908895.37	1	3.93e+15	5.405	0.02138
	C1000/C0	0	1	4.27e+14	0.586	0.44525
	(Age-2.64773)*(% Binder-0.05286)	0	1	1.1e+12	0.001	0.96919
	(Age-2.64773)*(% AV-7.33624)	0	1	4.09e+14	0.561	0.45483
	(Age-2.64773)*(b-0.07438)	0	1	2.91e+14	0.398	0.52888
	(Age-2.64773)*(C1000/C0-56026.6)	0	2	4.29e+14	0.293	0.74675
	(Age-2.64773)*Climate #	0	1	4.6e+13	0.063	0.80245
	(Age-2.64773)*(Location #-0.52841)	0	1	3.75e+14	0.514	0.47451
	(% Binder-0.05286)*(% AV-7.33624)	0	1	4.12e+14	0.565	0.45348
	(% Binder-0.05286)*(Eve-5814.88)	0	1	2.03e+13	0.028	0.86782
	(% Binder-0.05286)*(C1000/C0-56026.6)	0	2	1.08e+15	0.739	0.47943
	(% Binder-0.05286)*Climate #	0	1	3.73e+13	0.051	0.82166
	(% AV-7.33624)*(C1000/C0-56026.6)	0	2	1.39e+15	0.957	0.38615
	(% AV-7.33624)*Climate #	0	1	3.42e+14	0.469	0.49453
	(% AV-7.33624)*(Location #-0.52841)	0	1	5.95e+14	0.817	0.36751
	(Eve-5814.88)*(shear-0.00025)	0	1	9.75e+13	0.133	0.71552
	(Eve-5814.88)*(C1000/C0-56026.6)	0	2	9.36e+14	0.640	0.52847
	(Eve-5814.88)*Climate #	0	1	1.34e+14	0.183	0.66898
	(b-0.07438)*(shear-0.00025)	0	1	9.03e+12	0.012	0.91169
	(b-0.07438)*(C1000/C0-56026.6)	0	2	7.03e+14	0.480	0.61981
	(b-0.07438)*Climate #	0	1	1.13e+12	0.002	0.9687
	(b-0.07438)*(Location #-0.52841)	0	1	3.68e+14	0.504	0.47877
	(shear-0.00025)*(C1000/C0-56026.6)	0	2	8.48e+14	0.580	0.56135
	(shear-0.00025)*Climate #	0	1	5.04e+14	0.692	0.40667
	Climate #*(C1000/C0-56026.6)	0	2	1.49e+15	1.024	0.3616
	(Location #-0.52841)*(C1000/C0-56026.6)	0	2	9.34e+14	0.639	0.52897

**TABLE B- 12 Step History for Full Two Way Interactions**

Step	Parameter	Action	"Sig Prob"	Seq SS	RSquare	Cp	p	AICc	BIC
1	(% AV-7.33624)*(Eve-5814.88)	Entered	0.0000	9.26e+16	0.3268	76.212	4	6602.85	6618.35
2	(% AV-7.33624)*(shear-0.00025)	Entered	0.0041	1.2e+16	0.3690	64.902	6	6595.77	6617.29
3	(% AV-7.33624)*(b-0.07438)	Entered	0.0001	1.83e+16	0.4337	45.431	8	6581.14	6608.59
4	(Eve-5814.88)*(Location #-0.52841)	Entered	0.0008	1.32e+16	0.4805	32.486	10	6570.52	6603.78
5	(% Binder-0.05286)*(Location #-0.52841)	Entered	0.0225	6.66e+15	0.5039	27.967	12	6567.02	6605.98
6	(% AV-7.33624)*Climate #	Entered	0.0388	5.53e+15	0.5234	24.893	14	6564.71	6609.27
7	(Age-2.64773)*(shear-0.00025)	Entered	0.0705	4.4e+15	0.5390	23.255	16	6563.75	6613.77
8	(% Binder-0.05286)*(shear-0.00025)	Entered	0.0199	4.39e+15	0.5545	19.634	17	6560.22	6612.93
9	(Age-2.64773)*(Eve-5814.88)	Entered	0.0163	4.54e+15	0.5705	15.824	18	6556.29	6611.65
10	Climate #	Removed	0.2708	2.03e+15	0.5633	14.422	16	6554.2	6604.22
11	(Eve-5814.88)*(b-0.07438)	Entered	0.0469	3.05e+15	0.5741	12.523	17	6552.3	6605.01
12	(shear-0.00025)*(Location #-0.52841)	Entered	0.0532	2.83e+15	0.5841	10.898	18	6550.63	6606
13	Climate #*(Location #-0.52841)	Entered	0.0880	3.62e+15	0.5968	10.269	20	6550.28	6610.86
14	(% Binder-0.05286)*(b-0.07438)	Entered	0.1459	1.55e+15	0.6023	10.28	21	6550.48	6613.62



**FIGURE B- 1 Actual by predicted plot for full two way interactions.**

**TABLE B- 13 Summary of Fit for Full Two Way Interactions**

RSquare	0.602302
RSquare Adj	0.550986
Root Mean Square Error	26967122
Mean of Response	23444113
Observations (or Sum Wgts)	176

**TABLE B- 14 Analysis of Variance for Full Two Way Interactions**

Source	DF	Sum of Squares	Mean Square	F Ratio
Model	20	1.7071e+17	8.536e+15	11.7372
Error	155	1.1272e+17	7.272e+14	<b>Prob &gt; F</b>
C. Total	175	2.8343e+17		<.0001*



**TABLE B- 15 Parameter Estimates for Full Two Way Interactions**

Term	Estimate	Std Error	t Ratio	Prob> t
Intercept	94024310	23342271	4.03	<.0001*
Age	-309885	1050546	-0.29	0.7684
% Binder	184285200	3.235e+8	0.57	0.5697
% AV	-2258837	1335148	-1.69	0.0927
Eve	-8204.546	1218.641	-6.73	<.0001*
b	143980207	41716655	3.45	0.0007*
shear	-1.21e+11	2.14e+10	-5.67	<.0001*
Climate #	1755096.8	1899530	0.92	0.3569
Location #	-6627094	4894679	-1.35	0.1777
(Age-2.64773)*(Eve-5814.88)	1678.9184	546.0321	3.07	0.0025*
(Age-2.64773)*(shear-0.00025)	5.163e+10	1.37e+10	3.76	0.0002*
(% Binder-0.05286)*(b-0.07438)	-8.02e+9	5.487e+9	-1.46	0.1459
(% Binder-0.05286)*(shear-0.00025)	2.496e+13	6.12e+12	4.08	<.0001*
(% Binder-0.05286)*(Location #-0.52841)	2.0349e+9	5.782e+8	3.52	0.0006*
(% AV-7.33624)*(Eve-5814.88)	1836.7015	420.3001	4.37	<.0001*
(% AV-7.33624)*(b-0.07438)	-43578362	21242934	-2.05	0.0419*
(% AV-7.33624)*(shear-0.00025)	3.91e+10	1.2e+10	3.25	0.0014*
(Eve-5814.88)*(b-0.07438)	-63327.19	23532.68	-2.69	0.0079*
(Eve-5814.88)*(Location #-0.52841)	4883.1512	2617.327	1.87	0.0640
(shear-0.00025)*(Location #-0.52841)	-1.18e+11	5.61e+10	-2.10	0.0375*
Climate #*(Location #-0.52841)	7908895.4	3402003	2.32	0.0214*

**TABLE B- 16 Sorted Parameter Estimates for Full Two Way Interactions**

Term	Estimate	Std Error	t Ratio	t Ratio	Prob> t
Eve	-8204.546	1218.641	-6.73		<.0001*
shear	-1.21e+11	2.14e+10	-5.67		<.0001*
(% AV-7.33624)*(Eve-5814.88)	1836.7015	420.3001	4.37		<.0001*
(% Binder-0.05286)*(shear-0.00025)	2.496e+13	6.12e+12	4.08		<.0001*
(Age-2.64773)*(shear-0.00025)	5.163e+10	1.37e+10	3.76		0.0002*
(% Binder-0.05286)*(Location #-0.52841)	2.0349e+9	5.782e+8	3.52		0.0006*
b	143980207	41716655	3.45		0.0007*
(% AV-7.33624)*(shear-0.00025)	3.91e+10	1.2e+10	3.25		0.0014*
(Age-2.64773)*(Eve-5814.88)	1678.9184	546.0321	3.07		0.0025*
(Eve-5814.88)*(b-0.07438)	-63327.19	23532.68	-2.69		0.0079*
Climate #*(Location #-0.52841)	7908895.4	3402003	2.32		0.0214*
(shear-0.00025)*(Location #-0.52841)	-1.18e+11	5.61e+10	-2.10		0.0375*
(% AV-7.33624)*(b-0.07438)	-43578362	21242934	-2.05		0.0419*
(Eve-5814.88)*(Location #-0.52841)	4883.1512	2617.327	1.87		0.0640
% AV	-2258837	1335148	-1.69		0.0927
(% Binder-0.05286)*(b-0.07438)	-8.02e+9	5.487e+9	-1.46		0.1459
Location #	-6627094	4894679	-1.35		0.1777
Climate #	1755096.8	1899530	0.92		0.3569
% Binder	184285200	3.235e+8	0.57		0.5697
Age	-309885	1050546	-0.29		0.7684

## WP Data Set Analysis

This section contains the output for the statistical analysis of the WP testing data set from the JMP statistical analysis program.

### *Stepwise Regression No Interactions*

**TABLE B- 17 Stopping Rule for WP No Interactions**

Prob to Enter	0.25
Prob to Leave	0.25

**TABLE B- 18 Regression Statistics for WP No Interactions**

SSE	DFE	RMSE	RSquare	RSquare Adj	Cp	p	AICc	BIC
7.078e+16	90	28043799	0.3323	0.3101	1.7968536	4	3497.419	3509.454

**TABLE B- 19 Current Estimates for WP No Interactions**

Entered	Parameter	Estimate	nDF	SS	"F Ratio"	"Prob>F"
X	Intercept	88455130.2	1	0	0.000	1
	Age	0	1	7.98e+14	1.015	0.31643
	% Binder	0	1	1.54e+14	0.194	0.66103
X	% AV	-5490944.7	1	1.53e+16	19.462	2.84e-5
X	Eve	-6417.5212	1	1.31e+16	16.630	0.0001
X	b	108911120	1	2.7e+15	3.430	0.06732
	shear	0	1	3.4e+14	0.430	0.51372
	C1000/C0	0	1	6.09e+14	0.773	0.38166
	Climate #	0	1	5.46e+14	0.692	0.40757

**TABLE B- 20 Step History for WP No Interactions**

Step	Parameter	Action	"Sig Prob"	Seq SS	RSquare	Cp	p	AICc	BIC
1	% AV	Entered	0.0000	2.13e+16	0.2006	15.125	2	3509.94	3517.3
2	Eve	Entered	0.0003	1.13e+16	0.3069	3.1424	3	3498.7	3508.43
3	b	Entered	0.0673	2.7e+15	0.3323	1.7969	4	3497.42	3509.45

**TABLE B- 21 Summary of Fit for WP No Interactions**

RSquare	0.328045
RSquare Adj	0.306369
Root Mean Square Error	27893276
Mean of Response	20389014
Observations (or Sum Wgts)	97


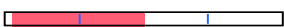

**TABLE B- 22 Analysis of Variance for WP No Interactions**

Source	DF	Sum of Squares	Mean Square	F Ratio
Model	3	3.5324e+16	1.177e+16	15.1340
Error	93	7.2357e+16	7.78e+14	<b>Prob &gt; F</b>
C. Total	96	1.0768e+17		<.0001*

**TABLE B- 23 Parameter Estimates for WP No Interactions**

Term	Estimate	Std Error	t Ratio	Prob> t
Intercept	86557423	12128970	7.14	<.0001*
% AV	-5376032	1229782	-4.37	<.0001*
Eve	-6385.203	1561.699	-4.09	<.0001*
b	125010964	57280946	2.18	0.0316*

**TABLE B- 24 Sorted Parameter Estimates for WP No Interactions**

Term	Estimate	Std Error	t Ratio	t Ratio	Prob> t
% AV	-5376032	1229782	-4.37		<.0001*
Eve	-6385.203	1561.699	-4.09		<.0001*
b	125010964	57280946	2.18		0.0316*

*Stepwise Regression Two Way Interactions*

**TABLE B- 25 Stopping Rule for WP Two Way Interactions**

Prob to Enter	0.25
Prob to Leave	0.25

**TABLE B- 26 Regression Statistics for WP Two Way Interactions**

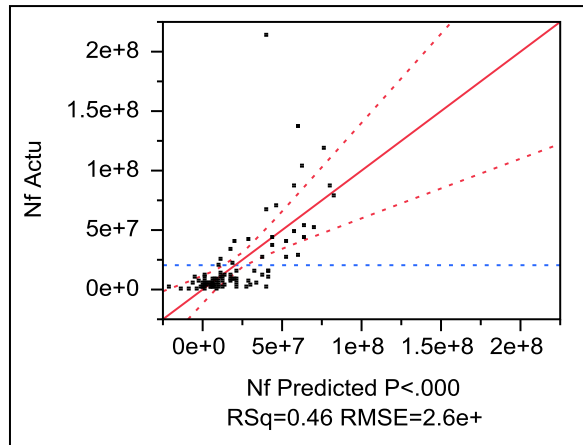
SSE	DFE	RMSE	RSquare	RSquare Adj	Cp	p	AICc	BIC
5.718e+16	84	26091154	0.4606	0.4028	-6.464288	10	3491.903	3516.66

**TABLE B- 27 Current Estimates for WP Two Way Interactions**

Entered	Parameter	Estimate	nDF	SS	"F Ratio"	"Prob>F"
X	Intercept	6961705.26	1	0	0.000	1
	Age	0	1	5.98e+14	0.878	0.3515
X	% Binder	884595663	2	6.01e+15	4.415	0.01503
X	% AV	4238329.9	3	1.45e+16	7.085	0.00027
X	Eve	-6450.5419	2	1.91e+16	14.053	5.44e-6
X	b	94926079.7	1	1.89e+15	2.778	0.09931
X	shear	-1.25e+11	2	4.12e+15	3.029	0.05368
	C1000/C0	0	1	1.99e+14	0.289	0.59219
X	Climate #	5799546.83	2	7.57e+15	5.561	0.00539
	(Age-2.59574)*(% Binder-0.05247)	0	2	1.22e+15	0.897	0.41177
	(Age-2.59574)*(% AV-6.75847)	0	2	6.33e+14	0.459	0.63345
	(Age-2.59574)*(Eve-5967.98)	0	2	6.1e+14	0.442	0.64433
	(Age-2.59574)*(b-0.06807)	0	2	6.65e+14	0.482	0.61919
	(Age-2.59574)*(shear-0.00063)	0	2	6.76e+14	0.491	0.61406
	(Age-2.59574)*(C1000/C0-59190.7)	0	3	8.76e+14	0.420	0.73899
	(Age-2.59574)*Climate #	0	2	6.28e+14	0.455	0.63606
	(% Binder-0.05247)*(% AV-6.75847)	0	1	4.82e+14	0.706	0.40324
	(% Binder-0.05247)*(Eve-5967.98)	0	1	1.88e+14	0.274	0.60204
	(% Binder-0.05247)*(b-0.06807)	0	1	2.16e+14	0.314	0.57674
	(% Binder-0.05247)*(shear-0.00063)	0	1	1.09e+14	0.159	0.69124
	(% Binder-0.05247)*(C1000/C0-59190.7)	0	2	2.13e+14	0.153	0.85811
X	(% Binder-0.05247)*Climate #	938037143	1	4.65e+15	6.833	0.0106
X	(% AV-6.75847)*(Eve-5967.98)	1717.36382	1	3.58e+15	5.257	0.02436
	(% AV-6.75847)*(b-0.06807)	0	1	3.64e+13	0.053	0.81862
X	(% AV-6.75847)*(shear-0.00063)	1.8576e+10	1	3.32e+15	4.878	0.02992
	(% AV-6.75847)*(C1000/C0-59190.7)	0	2	1.99e+14	0.143	0.8671
	(% AV-6.75847)*Climate #	0	1	4.88e+13	0.071	0.79078
	(Eve-5967.98)*(b-0.06807)	0	1	4.39e+14	0.642	0.4253
	(Eve-5967.98)*(shear-0.00063)	0	1	1.88e+14	0.274	0.6022
	(Eve-5967.98)*(C1000/C0-59190.7)	0	2	7.71e+14	0.561	0.57297
	(Eve-5967.98)*Climate #	0	1	1.84e+13	0.027	0.87062
	(b-0.06807)*(shear-0.00063)	0	1	1.67e+14	0.243	0.6235
	(b-0.06807)*(C1000/C0-59190.7)	0	2	1.99e+14	0.143	0.86695
	(b-0.06807)*Climate #	0	1	1.39e+14	0.203	0.65361
	(shear-0.00063)*(C1000/C0-59190.7)	0	2	4e+14	0.289	0.74967
	(shear-0.00063)*Climate #	0	1	1.37e+13	0.020	0.88834
	(C1000/C0-59190.7)*Climate #	0	2	4.89e+14	0.353	0.70331

**TABLE B- 28 Step History for WP Two Way Interactions**

Step	Parameter	Action	"Sig Prob"	Seq SS	RSquare	Cp	p	AICc	BIC
1	(% AV-6.75847)*(Eve-5967.98)	Entered	0.0000	3.58e+16	0.3379	-3.106	4	3496.63	3508.66
2	(% Binder-0.05247)*Climate #	Entered	0.0216	7.35e+15	0.4072	-5.783	7	3493.25	3511.9
3	(% AV-6.75847)*(shear-0.00063)	Entered	0.0723	3.77e+15	0.4428	-6.231	9	3492.39	3515.17
4	b	Entered	0.0993	1.89e+15	0.4606	-6.464	10	3491.9	3516.66



**FIGURE B- 2 Actual by predicted plot for WP two way interactions.**

**TABLE B- 29 Summary of Fit for WP Two Way Interactions**

RSquare	0.460609
RSquare Adj	0.402817
Root Mean Square Error	26091154
Mean of Response	20459172
Observations (or Sum Wgts)	94










**TABLE B- 30 Analysis of Variance for WP Two Way Interactions**

Source	DF	Sum of Squares	Mean Square	F Ratio
Model	9	4.8831e+16	5.426e+15	7.9701
Error	84	5.7183e+16	6.807e+14	<b>Prob &gt; F</b>
C. Total	93	1.0601e+17		<.0001*

**TABLE B- 31 Parameter Estimates for WP Two Way Interactions**

Term	Estimate	Std Error	t Ratio	Prob> t
Intercept	6961705.3	33304712	0.21	0.8349
% AV	4238329.9	4260034	0.99	0.3226
Eve	-6450.542	1595.823	-4.04	0.0001*
b	94926080	56955685	1.67	0.0993
% Binder	884595663	4.33e+8	2.04	0.0442*
shear	-1.25e+11	5.72e+10	-2.19	0.0316*
Climate #	5799546.8	2414719	2.40	0.0185*
(% Binder-0.05247)*Climate #	938037143	3.589e+8	2.61	0.0106*
(% AV-6.75847)*(Eve-5967.98)	1717.3638	749.0205	2.29	0.0244*
(% AV-6.75847)*(shear-0.00063)	1.858e+10	8.41e+9	2.21	0.0299*

**TABLE B- 32 Sorted Parameter Estimates for WP Two Way Interactions**

Term	Estimate	Std Error	t Ratio	t Ratio	Prob> t
Eve	-6450.542	1595.823	-4.04		0.0001*
(% Binder-0.05247)*Climate #	938037143	3.589e+8	2.61		0.0106*
Climate #	5799546.8	2414719	2.40		0.0185*
(% AV-6.75847)*(Eve-5967.98)	1717.3638	749.0205	2.29		0.0244*
(% AV-6.75847)*(shear-0.00063)	1.858e+10	8.41e+9	2.21		0.0299*
shear	-1.25e+11	5.72e+10	-2.19		0.0316*
% Binder	884595663	4.33e+8	2.04		0.0442*
b	94926080	56955685	1.67		0.0993
% AV	4238329.9	4260034	0.99		0.3226

## SH Data Set Analysis

This section contains the output for the statistical analysis of the WP testing data set from the JMP statistical analysis program.

### *Stepwise Regression No Interactions*

**TABLE B- 33 Stopping Rule for SH No Interactions**

Prob to Enter	0.25
Prob to Leave	0.25

**TABLE B- 34 Regression Statistics for SH No Interactions**

SSE	DFE	RMSE	RSquare	RSquare Adj	Cp	p	AICc	BIC
1.114e+17	79	37550340	0.3692	0.3372	4.3292168	5	3176.438	3189.932

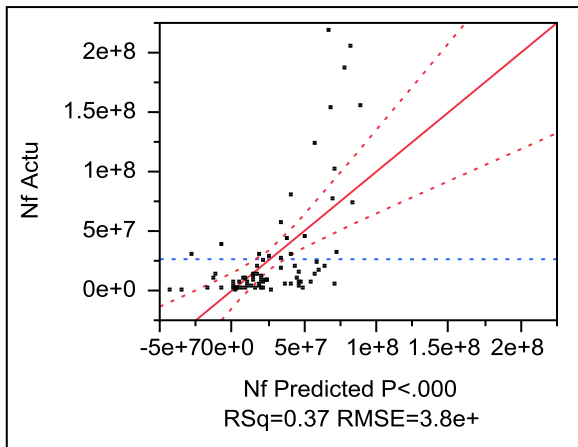
**TABLE B- 35 Current Estimates for SH No Interactions**

Lock	Entered	Parameter	Estimate	nDF	SS	"F Ratio"	"Prob>F"
X	X	Intercept	202789168	1	0	0.000	1
	X	Age	-2405826.9	1	2.75e+15	1.949	0.16661
	X	% Binder	-1.5348e+9	1	1.2e+16	8.541	0.00453
	X	% AV	-6297987.4	1	2.3e+16	16.312	0.00012
	X	Eve	-6611.9024	1	1.13e+16	8.019	0.00587
		b	0	1	1.8e+15	1.279	0.26149
		shear	0	1	1.08e+15	0.762	0.38537
		C1000/C0	0	1	1.3e+12	0.001	0.97604
		Climate #	0	1	5.33e+10	0.000	0.99514



**TABLE B- 36 Step History for SH No Interactions**

Step	Parameter	Action	"Sig Prob"	Seq SS	RSquare	Cp	P	AICc	BIC
1	% AV	Entered	0.0000	3.41e+16	0.1934	20.159	2	3190.3	3197.29
2	Eve	Entered	0.0020	1.59e+16	0.2835	10.963	3	3182.55	3191.76
3	% Binder	Entered	0.0042	1.24e+16	0.3536	4.2616	4	3176.16	3187.55
4	Age	Entered	0.1666	2.75e+15	0.3692	4.3292	5	3176.44	3189.93



**FIGURE B- 3 Actual by predicted plot for SH no interactions.**

**TABLE B- 37 Summary of Fit for SH No Interactions**

RSquare	0.36916
RSquare Adj	0.337219
Root Mean Square Error	37550340
Mean of Response	26344571
Observations (or Sum Wgts)	84





**TABLE B- 38 Analysis of Variance for SH No Interactions**

Source	DF	Sum of Squares	Mean Square	F Ratio
Model	4	6.5185e+16	1.63e+16	11.5575
Error	79	1.1139e+17	1.41e+15	<b>Prob &gt; F</b>
C. Total	83	1.7658e+17		<.0001*

**TABLE B- 39 Parameter Estimates for SH No Interactions**

Term	Estimate	Std Error	t Ratio	Prob> t
Intercept	202789168	34613150	5.86	<.0001*
Age	-2405827	1723308	-1.40	0.1666
% Binder	-1.535e+9	5.252e+8	-2.92	0.0045*
% AV	-6297987	1559368	-4.04	0.0001*
Eve	-6611.902	2334.907	-2.83	0.0059*

**TABLE B- 40 Sorted Parameter Estimates for SH No Interactions**

Term	Estimate	Std Error	t Ratio	t Ratio	Prob> t
% AV	-6297987	1559368	-4.04		0.0001*
% Binder	-1.535e+9	5.252e+8	-2.92		0.0045*
Eve	-6611.902	2334.907	-2.83		0.0059*
Age	-2405827	1723308	-1.40		0.1666

*Stepwise Regression Two Way Interactions*

**TABLE B- 41 Stopping Rule for SH Two Way Interactions**

Prob to Enter	0.25
Prob to Leave	0.25

**TABLE B- 42 Regression Statistics for SH Two Way Interactions**

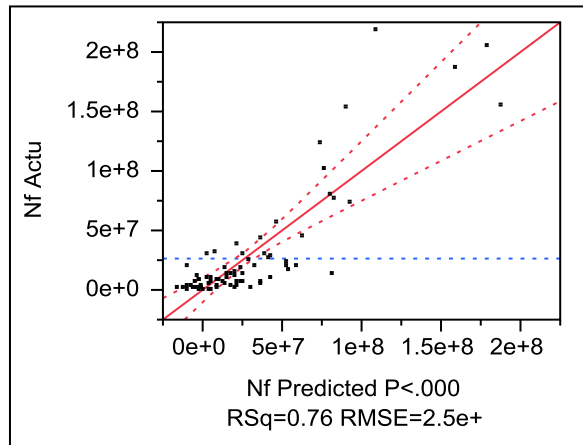
SSE	DFE	RMSE	RSquare	RSquare Adj	Cp	p	AICc	BIC
4.277e+16	70	24719221	0.7578	0.7128	15.712622	14	3120.005	3149.408

**TABLE B- 43 Current Estimates for SH Two Way Interactions**

Entered	Parameter	Estimate	nDF	SS	"F Ratio"	"Prob>F"
X	Intercept	-237676550	1	0	0.000	1
X	Age	19403569.4	4	3.73e+16	15.256	5.12e-9
X	% Binder	5422172743	3	1.4e+16	7.615	0.00018
X	% AV	-5012172.5	4	3.05e+16	12.466	1.04e-7
X	Eve	-6906.3733	3	1.86e+16	10.172	1.21e-5
X	b	134333010	3	8.16e+15	4.453	0.00639
X	shear	-9.692e+10	3	4.83e+16	26.368	1.6e-11
	C1000/C0	0	1	5.44e+13	0.088	0.7678
	Climate #	0	1	1.07e+14	0.174	0.67829
	(Age-2.75)*(% Binder-0.05331)	0	1	3.8e+13	0.061	0.80511
X	(Age-2.75)*(% AV-8.01733)	2008548.59	1	8.74e+15	14.296	0.00033
X	(Age-2.75)*(Eve-5673.72)	2123.38803	1	6.47e+15	10.587	0.00176
	(Age-2.75)*(b-0.08236)	0	1	2.62e+14	0.426	0.5162
X	(Age-2.75)*(shear-0.00047)	1.0434e+11	1	2.93e+16	47.887	1.75e-9
	(Age-2.75)*(C1000/C0-140631)	0	2	9.62e+13	0.077	0.92633
	(Age-2.75)*Climate #	0	2	4.86e+14	0.390	0.67832
	(% Binder-0.05331)*(% AV-8.01733)	0	1	5.67e+14	0.927	0.33911
	(% Binder-0.05331)*(Eve-5673.72)	0	1	6.14e+14	1.005	0.31967
X	(% Binder-0.05331)*(b-0.08236)	-1.086e+10	1	1.75e+15	2.870	0.09467
X	(% Binder-0.05331)*(shear-0.00047)	2.6242e+13	1	1.24e+16	20.237	2.65e-5
	(% Binder-0.05331)*(C1000/C0-140631)	0	2	1.62e+14	0.129	0.87915
	(% Binder-0.05331)*Climate #	0	2	1.11e+14	0.089	0.91518
X	(% AV-8.01733)*(Eve-5673.72)	977.809056	1	2.5e+15	4.094	0.04685
X	(% AV-8.01733)*(b-0.08236)	-48793008	1	2.89e+15	4.727	0.03307
	(% AV-8.01733)*(shear-0.00047)	0	1	8.41e+13	0.136	0.71354
	(% AV-8.01733)*(C1000/C0-140631)	0	2	1.17e+14	0.094	0.91081
	(% AV-8.01733)*Climate #	0	2	7.63e+14	0.618	0.54225
	(Eve-5673.72)*(b-0.08236)	0	1	3.08e+14	0.501	0.48154
	(Eve-5673.72)*(shear-0.00047)	0	1	9.93e+13	0.161	0.68986
	(Eve-5673.72)*(C1000/C0-140631)	0	2	2.02e+14	0.161	0.85152
	(Eve-5673.72)*Climate #	0	2	9.71e+14	0.790	0.45811
	(b-0.08236)*(shear-0.00047)	0	1	5.45e+14	0.891	0.34843
	(b-0.08236)*(C1000/C0-140631)	0	2	5.5e+13	0.044	0.9572
	(b-0.08236)*Climate #	0	2	6.75e+14	0.545	0.58233
	(shear-0.00047)*(C1000/C0-140631)	0	2	1.06e+14	0.084	0.91943
	(shear-0.00047)*Climate #	0	2	8.83e+14	0.716	0.49216
	(C1000/C0-140631)*Climate #	0	3	2.1e+14	0.110	0.95385

**TABLE B- 44 Step History for SH Two Way Interactions**

Step	Parameter	Action	"Sig Prob"	Seq SS	RSquare	Cp	p	AICc	BIC
1	(Age-2.75)*(% AV-8.01733)	Entered	0.0000	6.56e+16	0.3713	110.13	4	3173.83	3185.22
2	(Age-2.75)*(% Binder-0.05331)	Entered	0.0058	1.37e+16	0.4491	91.083	6	3167.43	3182.98
3	(Age-2.75)*(Eve-5673.72)	Entered	0.0126	1.06e+16	0.5091	77.337	8	3162.72	3182.16
4	(b-0.08236)*(shear-0.00047)	Entered	0.0050	1.39e+16	0.5877	60.057	11	3156.01	3180.79
5	(Age-2.75)*(shear-0.00047)	Entered	0.0085	6.71e+15	0.6257	50.799	12	3150.69	3177.09
6	(% Binder-0.05331)*(shear-0.00047)	Entered	0.0000	1.7e+16	0.7222	24.255	13	3128.55	3156.5
7	(Age-2.75)*(% Binder-0.05331)	Removed	0.9658	1.28e+12	0.7222	22.257	12	3125.67	3152.07
8	(% Binder-0.05331)*(b-0.08236)	Entered	0.0785	2.11e+15	0.7341	20.723	13	3124.87	3152.81
9	(b-0.08236)*(shear-0.00047)	Removed	0.5151	2.83e+14	0.7325	19.198	12	3122.49	3148.89
10	(% AV-8.01733)*(b-0.08236)	Entered	0.0837	1.96e+15	0.7436	17.907	13	3121.81	3149.75
11	(% AV-8.01733)*(Eve-5673.72)	Entered	0.0469	2.5e+15	0.7578	15.713	14	3120	3149.41



**FIGURE B- 4 Actual by predicted plot for SH two way interactions.**

**TABLE B- 45 Summary of Fit for SH Two Way Interactions**

RSquare	0.757768
RSquare Adj	0.712782
Root Mean Square Error	24719221
Mean of Response	26344571
Observations (or Sum Wgts)	84

**TABLE B- 46 Analysis of Variance for SH Two Way Interactions**

Source	DF	Sum of Squares	Mean Square	F Ratio
Model	13	1.338e+17	1.029e+16	16.8445
Error	70	4.2773e+16	6.11e+14	<b>Prob &gt; F</b>
C. Total	83	1.7658e+17		<.0001*

**TABLE B- 47 Parameter Estimates for SH Two Way Interactions**

Term	Estimate	Std Error	t Ratio	Prob> t
Intercept	-2.377e+8	90650077	-2.62	0.0107*
Age	19403569	3410622	5.69	<.0001*
% Binder	5.4222e+9	1.36e+9	3.99	0.0002*
% AV	-5012173	1205292	-4.16	<.0001*
Eve	-6906.373	1760.217	-3.92	0.0002*
b	134333010	56795841	2.37	0.0208*
shear	-9.69e+10	2.01e+10	-4.81	<.0001*
(Age-2.75)*(% AV-8.01733)	2008548.6	531229.1	3.78	0.0003*
(Age-2.75)*(Eve-5673.72)	2123.388	652.6022	3.25	0.0018*
(Age-2.75)*(shear-0.00047)	1.043e+11	1.51e+10	6.92	<.0001*
(% Binder-0.05331)*(b-0.08236)	-1.09e+10	6.41e+9	-1.69	0.0947
(% Binder-0.05331)*(shear-0.00047)	2.624e+13	5.83e+12	4.50	<.0001*
(% AV-8.01733)*(Eve-5673.72)	977.80906	483.2552	2.02	0.0469*
(% AV-8.01733)*(b-0.08236)	-48793008	22441187	-2.17	0.0331*

**TABLE B- 48 Sorted Parameter Estimates for SH Two Way Interactions**

Term	Estimate	Std Error	t Ratio	t Ratio	Prob> t
(Age-2.75)*(shear-0.00047)	1.043e+11	1.51e+10	6.92		<.0001*
Age	19403569	3410622	5.69		<.0001*
shear	-9.69e+10	2.01e+10	-4.81		<.0001*
(% Binder-0.05331)*(shear-0.00047)	2.624e+13	5.83e+12	4.50		<.0001*
% AV	-5012173	1205292	-4.16		<.0001*
% Binder	5.4222e+9	1.36e+9	3.99		0.0002*
Eve	-6906.373	1760.217	-3.92		0.0002*
(Age-2.75)*(% AV-8.01733)	2008548.6	531229.1	3.78		0.0003*
(Age-2.75)*(Eve-5673.72)	2123.388	652.6022	3.25		0.0018*
b	134333010	56795841	2.37		0.0208*
(% AV-8.01733)*(b-0.08236)	-48793008	22441187	-2.17		0.0331*
(% AV-8.01733)*(Eve-5673.72)	977.80906	483.2552	2.02		0.0469*
(% Binder-0.05331)*(b-0.08236)	-1.09e+10	6.41e+9	-1.69		0.0947